JN251 74-19

Applicability of Two-Dimensional Shielding Code

August, 1974

POWER REACTOR AND NUCLEAR FUEL DEVELOPMENT CORPORATION

〒319-1184　茨城県那珂郡東海村大字村松4番地49
核燃料サイクル開発機構
技術展開部　技術協力課

Inquiries about copyright and reproduction should be addressed to:
Technical Cooperation Section,
Technology Management Division,
Japan Nuclear Cycle Development Institute
4-49 Muramatsu, Tokai-mura, Naka-gun, Ibaraki, 319-1184
Japan

N251 74-19

August, 1974

Applicability of Two-Dimensional Shielding Code*

Yoshihisa Tanaka**,
Ikunory Suzuki**,
Morio Takemura**, and
Tatsushi Suzuki**.

Abstract

Two-dimensional shielding code RASC-2D has been improved to treat line of sight calculation in annular duct with axial symmetrical geometry.

As the application of the improved RASC-2D code, the analysis of the main shield of the Prototype Fast Reactor "MONJU" has been performed and the effects of neutron streaming along voids and the shielding effects of top shield and the adjacent concrete shield are shown and re-evaluated comparing with previous results. (J213 73 01 report).

It has been made clear that Albedo effects at void surface are small at high energy region and large at low energy region.

This is the translation of the report, No. J213 73-02, issued in November, 1973.

* Work performed by Kawasaki Heavy Industries, Ltd. under contract with Power Reactor and Nuclear Fuel Development Corporation.

** Kawasaki Heavy Industries, Ltd.

C O N T E N T S

Table List

Figure List (1)

Figure List (2)

I. Purpose and Outline

In previous study, two-dimensional diffusion calculation code DIAC was improved to make it possible to analize large two-dimensional shielding system including voids using line of sight and diffusion method, and two-dimensional analysis of "MONJU" main shield including voids was done, and it was shown that voids in shield region gave a considerable effects to neutron flux distribution. In that analysis, however, neutrons entering into voids from void surface were assumed to have cosine angular distribution, so when the void intersected with radial center axis as N_2 gas layer of "MONJU", it was considered to overestimate the neutrons streaming from void surface on radial center axis to upper part of void.

In this study, the code has been improved to estimate exactly the neutron streaming from void surface on radial center axis to upper part of void under condition of axial symmetrical geometry. In this study following works have been performed.

I. Improvement of DIAC Code

i) Addition of axial symmetrical line of sight calculation in void.

ii) Removement of minus neutron current entering into void from void surface at high energy region.

II. Two-dimensional analysis of "MONJU" main shield including void.

From these works, it has been made clear that the analysis including void is necessary and streaming neutrons in void affect to neutron flux distribution as far as energy is high. These results are reported.

II. Improvement of RASC-2D Code

(II-1) Addition of Axial Symmetrical Line of sight Calculation

1) Calculation method of axial symmetric void

According to the assumption of axial symmetric geometry to the void intersecting with radial center axis, space meshes around void are assumed to be axial symmetric.

Neutron current J_i^- entering into an element i on the void surface can be obtained from neutron current J_0^+ flowing out from other surface element 0, as follows. (Previous report J213 73 01)

$$J_i^- = \frac{1}{F_i} \sum_{0=1}^{n} F_0 P_{0\to i} J_0^+ \qquad (1)$$

At axial symmetrical void, neutron current J_i^- entering to the upper element than radial center axis, which is necessary to diffusion calculation, can be devided to two contributions from upper and lower part. That is

$$J_i^- = \frac{1}{F_i} \sum_{0=1}^{n} F_0 P_{0\to i} J_0^+ + \frac{1}{F_i} \sum_{0'=1}^{n} F_{0'} P_{0'\to i} J_{0'}^+ . \qquad (2)$$

$\sum_{0=1}^{n}$: Sum of upper element

$\sum_{0=1}^{n}$: Sum of lower element

$P_{0\to i}$ Probability entering from upper element 0 to i

$P_{0'\to i}$ Probability entering from lower element 0' to i

Here, if lower element 0' is assumed to exist at symmetric position with upper element 0, neutron current $J_{0'}^{+}$ and surface cross-section $F_{0'}$ equal to J_0^{+} and F_0. So equation (2) can be represented as follows;

$$J_i^{-} = \frac{1}{F_i} \sum_{0=1}^{n} F_0 (P_{0\to i} + P_{0'\to i}) J_0^{+}. \qquad (3)$$

And if

$$P_{0\to i} = P_{0\to i} + P_{0'\to i}, \qquad (4)$$

equation (3) and equation (1) are same.

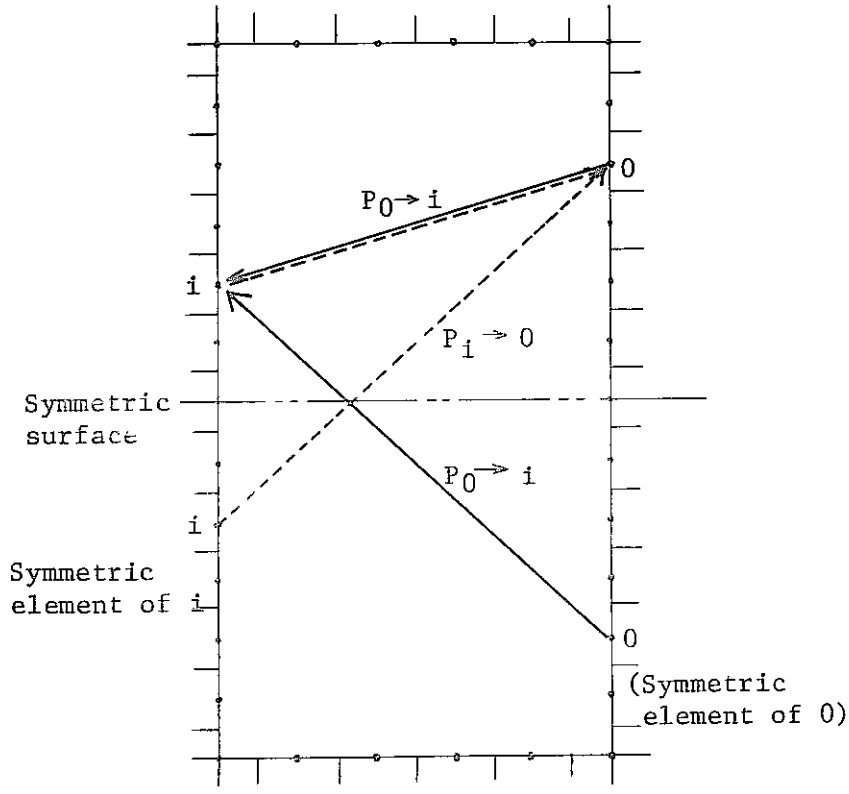

Fig. (II-1) Geometry of Probability Calculation

Consequently, neutron current entering from lower element (accordingly from all element) can be obtained by using as $P_{0\to i}$ outward probability obtained from summation of true probability $P_{0\to i}$ and $P_{0'\to i}$ when neutron current $\bar{J}_i$ entering from upper element is calculated by equation (1).

As true probability $P_{0\to i}$ and $P_{0'\to i}$ are

$$P_{0\to i} = \frac{F_i}{F_0} P_{i\to 0'} \quad P_{0'\to i} = \frac{F_i}{F_0} P_{i\to 0''}$$

outward probability $P_{0\to i}$ from element 0 to i is represented as follows by equation (4).

$$P_{0\to i} = \frac{F_i}{F_0}(P_{i\to 0} + P_{i\to 0'})$$

Here $P_{i\to 0'}$ equals to $P_{i'\to 0}$ because of symmetry of void, then $P_{0\to i}$ is same as true probability, that is

$$P_{0\to i} = \frac{F_i}{F_0}(P_{i\to 0} + P_{i'\to 0}),$$

and

$$P_{0\to i} = \frac{F_i}{F_0} P_{i\to 0}.$$

Finally, outward probability $P_{0\to i}$ and $P_{i\to 0}$ are sufficient by calculating either of the two.

2) Modification of Code

Modification has been done mainly in subroutine PROFAC, and other elemental modification has been

unnecessary.

Fig. (II-2) shows subroutine PRØFAC's frow diagram after modification, and right-hand parts have been newly added.

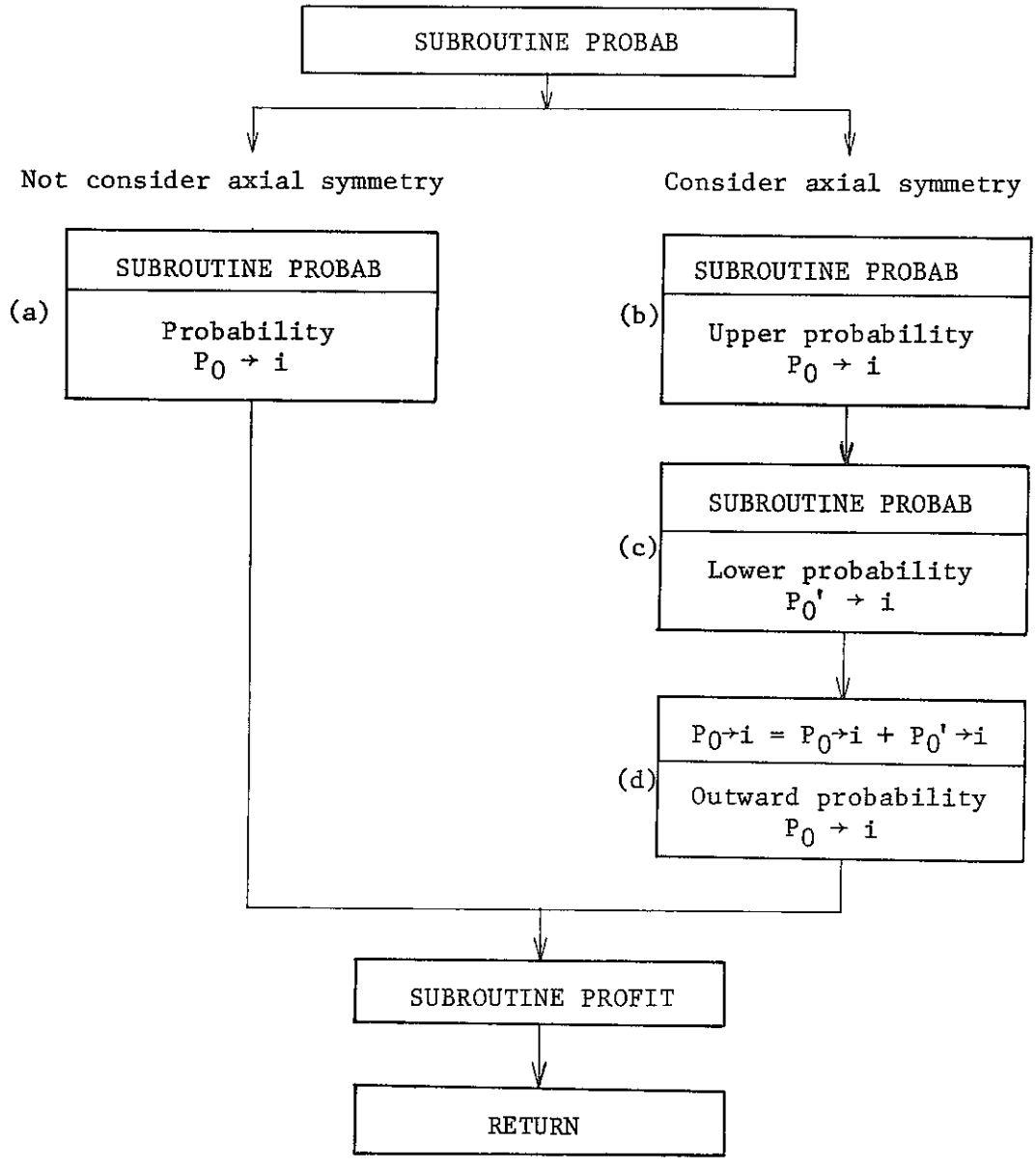

Fig. (II-2) Flow Diagram of Subroutine PROFAC

3) Test calculation of probability

Test calculation has been done to examine whether the probability between lower element and upper one of axial symmetrical void is calculated exactly or not. Fig. (II-3) shows the Test Calculation configulation same as previous one.

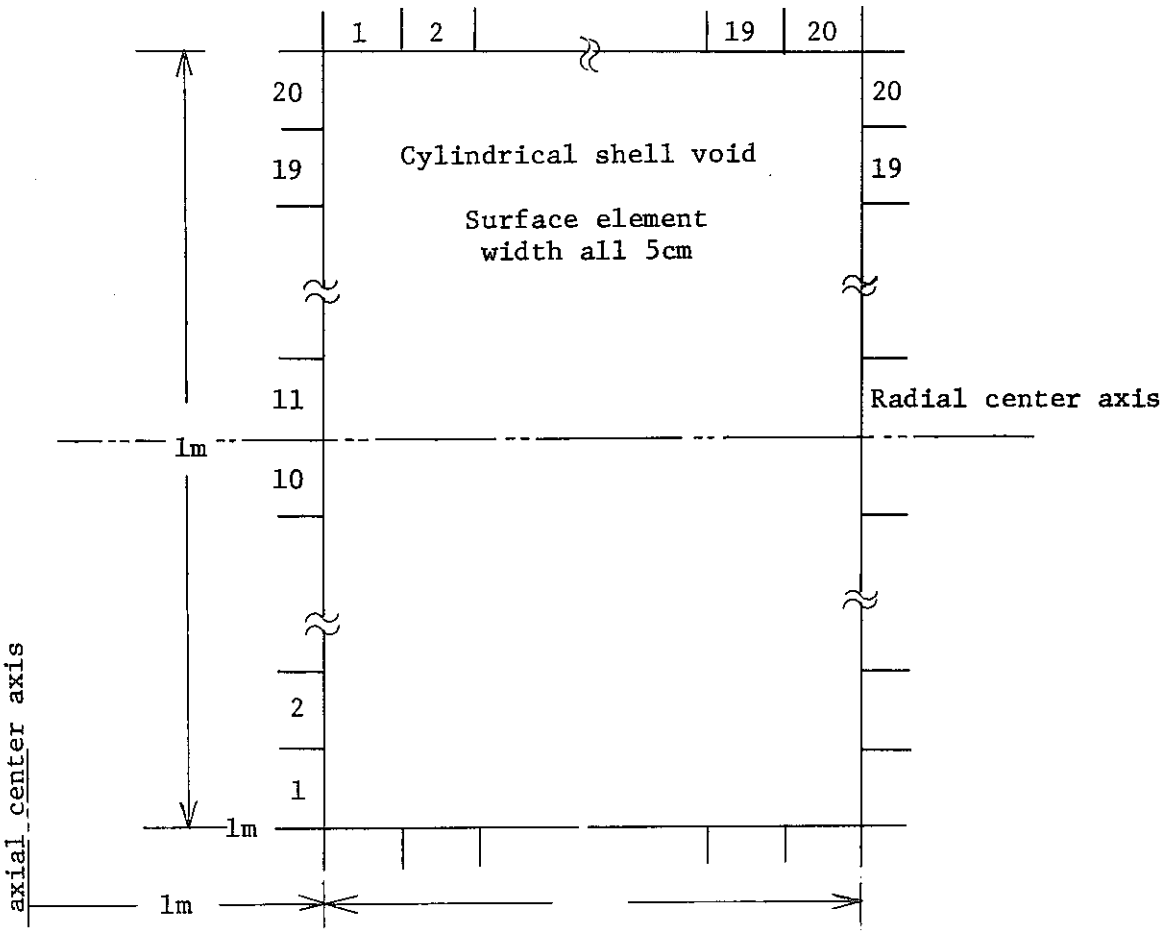

Fig. (II-3) Geometry of Probability Test Calculation

(i) The probability calculation result has agreed with previous calculation using ordinary method ((a) of Fig. (II-2)) when it has been assumed that this void exists above radial center axis.

(ii) Probability has been calculated on the assumption that the upper harf of the void exists above radial center axis. The results of upper probability given by (b) in Fig. (II-2) and the results of lower one given by (c) in Fig. (II-2) have agreed each corresponding results of (i).

(iii) And in (ii), total sum of outward probabilities given by (b) in Fig. (II-2) and outward probabilities between upper element lower one has been equal to 1.00.

Fig. (II-4) shows examples of calculated probabilities. The symbol of (a), (b), (c) and (d) represents each of the results of (a), (b), (c) and (d) in Fig. (II-2).

From (i), (ii) and (iii), it is understood that modification based on the chapter (II-1) is done exactly.

(II-2) Removement of Minus Neutron Current

In high energy region, minus neutron current entering into void from void surface appears sometimes on the calculation procedure. Albedo β calculated according to the approximate formula $\beta = \frac{1-2D/L}{1+2D/L}$ using the constant of "MONJU" main shield is shown in Table (II-1). Albedo of first energy group is minus. That the neutron current entering into void from void surface is minus is consistent with minus albedo. Actually J^+ (or β) is determined by a diffusion constant and the gradient of neutron flux, so in some cases neutron current entering into void from some space meshes on the void surface becomes minus number. Physically minus neutron current can not exist, and in this energy region diffusion approximation does not formed because forward scattering is much greater than back scattering. In this code, however, minus neutron current J^+ is considered to be the diffusion approximation expression that the neutrons entering into void are almost negligible, and when the minus current appears it is put into zero.

Before this modification of the code, neutron current is put into zero when the current entering into some mesh becomes minus after suming up all mesh of void surface. This method ignores the contribution of all other mesh when the minus contribution of some mesh is large, so sometimes distorted neutron flux distribution is calculated under opposite boundary conditions that the gradient of neutron flux in some mesh is minus and in adjacent mesh is plus (see Fig. (II-5)).

From above reason, DIAC code has been modified to put zero the minus current entering into void immediately after the current is calculated. From this, the distortion of neutron flux is removed as is shown in Fig. (II-6).

Table(II-1) Neutron Albedo

$$\beta = \frac{1-2\kappa D}{1+2\kappa D} \qquad \kappa = \frac{1}{L} = \sqrt{\frac{\Sigma_a}{D}}$$

Energy Group No.	Albedo β			
	SUS	Fe	Na	C
1	-0.02	-0.03	-0.02	-0.16
2	0.10	0.10	0.13	0.20
3	0.39	0.38	0.31	0.29
4	0.60	0.68	0.49	0.47
5	0.68	0.61	0.58	0.47
6	0.66	0.68	0.54	0.49
7	0.68	0.66	0.61	0.51
8	0.61	0.57	0.69	0.52
9	0.37	0.23	0.47	0.94

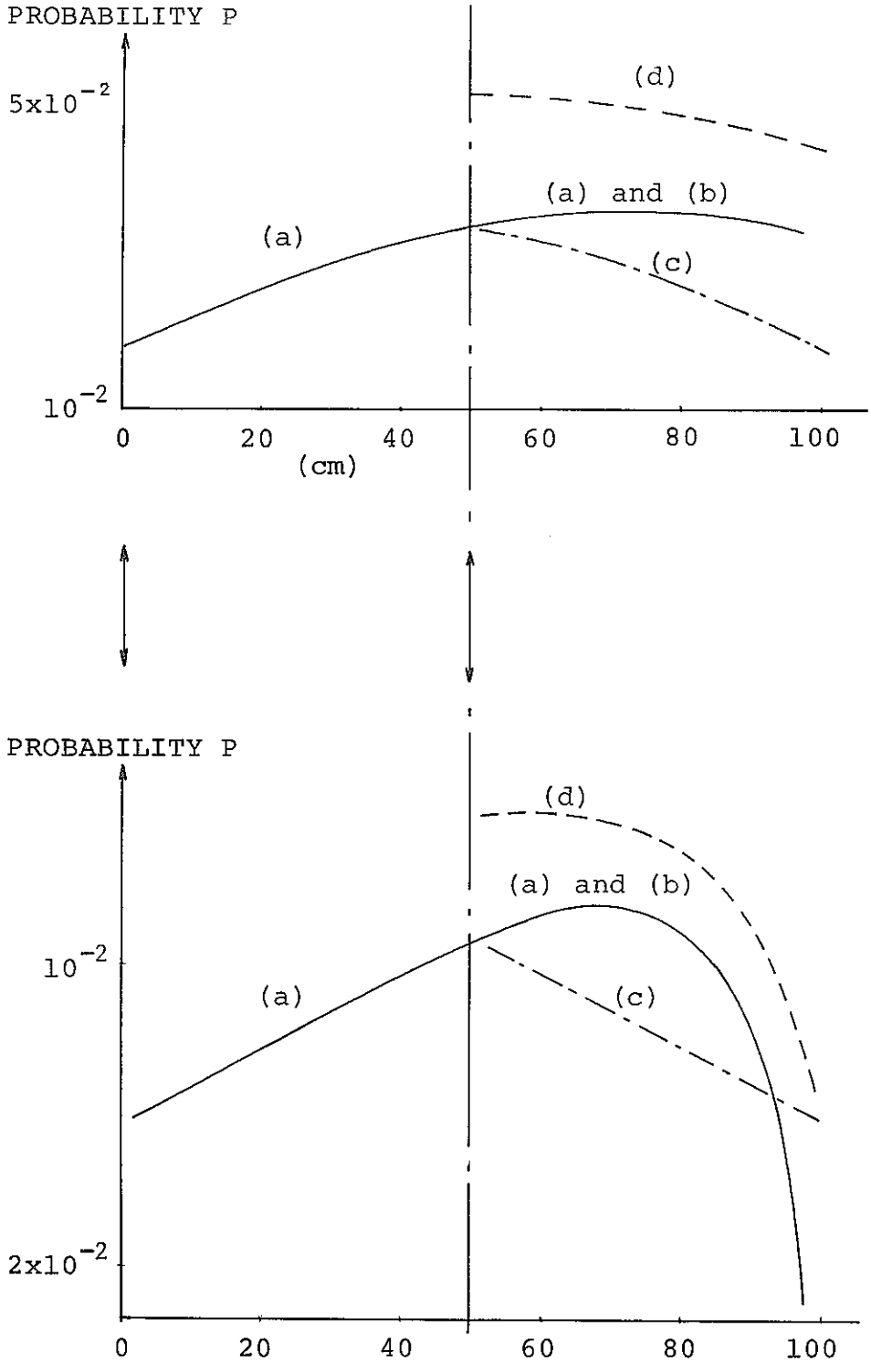

Fig.II-4 Test Calculation of Probability

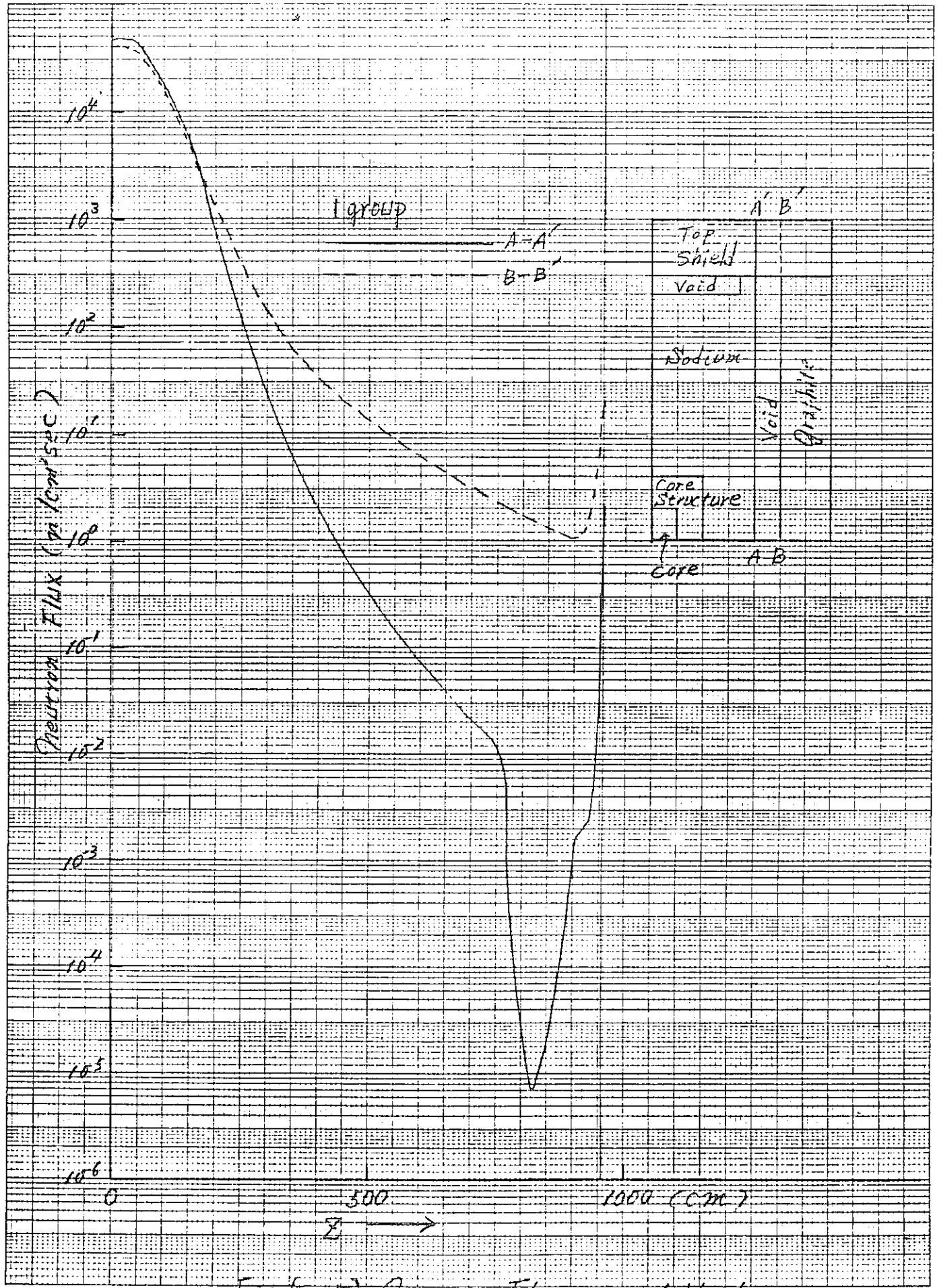

Fig.(II-5) Neutron Flux around Void before Modification of Code

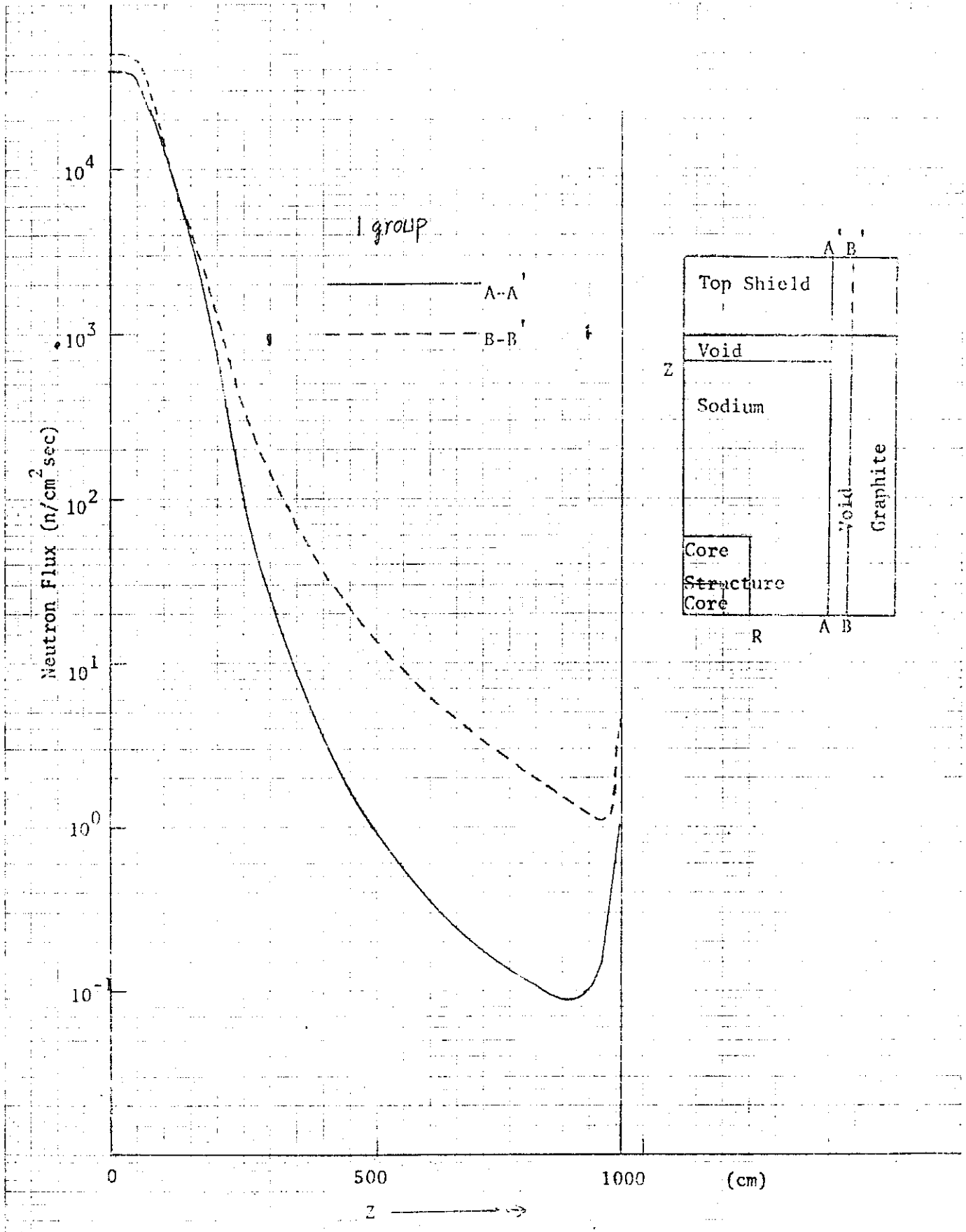

Fig.(II-6) Neutron Flux around Void after Modification of Code

III. Evaluation of Void Effect of Prototype Fast Reactor "MONJU" Main Shield

(III-1) Outline

By using the RASC-2D (DIAC) code as described in the previous chapter, two-dimensional neutron flux distribution in the main shield of the fast prototype reactor "MONJU" has been calculated under condition that in N_2 gas void between reactor vessel and graphite shield, neutrons streaming from lower part below radial central axis are calculated according axial symmetrical geometry.

The following two points has been the main concern in this study.

1) Comparison between calculation of not including void (J213 72-03-01 before previous calculation) and this calculation. Comparing before previous analysis, this analysis containes following newly added four layers.

i) Top shield plug.

ii) Concrete shield adjacent to above plug.

iii) Ar gas void layer on the sodium liquid surface inside reactor vessel.

iv) N_2 gas void layer between the reactor vessel and graphite shield.

The problems have been that what extent the neutron flux disturbance occurs by the newly added layers, and especially that whether the neutrons streaming in the N_2 gas void raise the flux level at the top shield plug or not.

2) Comparison between this calculation and the calculation under condition that the neutrons enter into N_2 gas void from the void surface intersecting with radial center axis. (J213 73-01, previous calculation). The problem has been that to what extent overestimate the neutron streaming to upper part, and that whether the neutron flux distribution in shields will be affected or not.

(III-2) Calculation Method

1) Calculation Configulation

Fig. (III-1) shows the calculation configulation of prototype fast reactor "MONJU" main shield. Analysis has been done covering radial direction up to the graphite shield outside of the reactor vessel and axial direction up to the top-side of the upper shield plug. As the voids, N_2 gas layer between reactor vessel and graphite shield, and Ar gas layer on the sodium liquid surface have been taken into account. As the analysable forms of voids in RASC-2D code are limited to only the cylindrical shape and cylindrical shell shape, a symplification of actual void configuration has been done.

2) Energy Group Structure

It has been analysed entirely under the identical energy structure as before previous and previous calculations. It has been with seven groups of removal

neutrons and nine groups of diffusion neutrons of which energy structures are shown in Table (III-1) and (III-2) respectively.

3) Group Constant

The densities of atomic elements composing each layer are given in Table (III-3).

i) Removal Cross Section

For the removal cross section in each layer below the dip-plate, those which have been prepared in the before previous calculation as the previous calculation have been employed. These have been prepared so as to adjust the removal-diffusion calculation result to the result of one dimensional transport calculation code ANISN. The removal cross sections of the top shield layers have not been adjusted other than these have been collapsed from the basic constants of 25-group to 7-group. Table (III-4) shows the removal cross sections employed for the analysis.

ii) Diffusion Group Constant

For the diffusion group constant at each layer below the dip-plate, those which have been prepared in the before previous calculation as previous calculation have been used the same as in the case of removal cross section. That is, for the core and blanket regions, the 9-group collapsed constants produced as an output from one dimensional core calculation code EXPANDA-2 have been obtained by converting into a

continuous slowing-down type from a matrix type. For other shield regions, 31-group one-dimensional calculations have been done in both r-direction and z-direction, and with these 31 group spectrums as a weight, 31-group constants have been collapsed into 9 groups, and the slowing down model has been converted into continuous type from the matrix one. The constants of the upper shield have been newly prepared by the above mentioned procedures. Table (III-5) shows the diffusion parameters.

4) Calculation Input

i) Removal source calculation input

For the removal source, power distributions of the core calculation result in the core and blanket region have been inputed as an external source, and for the shield regions, the removal sources have been calculated by the removal source calculation code REAC. Fig. (III-2) shows the power distributions of the core and blanket regions, while Table (III-6) shows the total power. Fig. (III-3) shows the removal source calculation points. The gauss integral division points have been taken as Z4 x R4 x Q4 in the four source regions (core 1, core 2 and two axial blanket regions), and as Z4 x R4 x Q6 in the two radial blanket regions.

ii) Diffusion calculation input

The material distribution for diffusion calculation is shown in Fig. (III-4), and at the same time space meshes are also shown. The space meshes have been determined from the results of one dimensional calculation along both radial and axial center axis. Fig. (III-5) and (III-6) show the comparison between the finely cut mesh and roughly cut mesh respectively. There is seen an error of about ∿30%. Finally, a space mesh having the size of 130 maximum along axial direction and 78 maximum to radial direction has been selected considering the capacity of the code as shown in Fig. (III-4).

iii) Input for line of sight calculation in void

a) Void Condition

Line of sight calculation in N_2 gas void layer outside reactor vessel has been done using the option of axial symmetrical condition, and it differs from previous calculation.

b) Gauss integral division point number

16 points have been taken the same as previous calculation.

c) Order of multinomial fitting of the neutron transition probability in voids

The orders of multinomial fitting of probabilities obtained at each diffusion mesh have been selected as follows, the same as previous calculation:

	N_2 Gas Void	Air Gas Void
(1) Inner Circle⟷Outer Circle	14	
(2) " ⟷Upper(Lower) End	12	
(3) Outer Circle⟷ "	12	9
(4) " ⟷Outer Circle	9	12
(5) Upper(Lower)⟷Lower(Upper) End	9	12

The fitting error has been largest in the case of N_2 gas void "Inner circle → Outer circle", and has been as much as 30% at a certain location. This might be because of the extremely long shape to axial direction. But as a whole, it is considered the error will not be too large because the neutron current is calculated as the total sum of the contribution from other area, and because noted neutron streming will come from the lower part of void which is high neutron flux level. In other cases, the errors have been below ∿ 10%. The degree of the errors does not differ between this calculation and previous one.

d) Frequency of line of sight calculation during line iteration

The calculation performed this time has been such a large geometry that it has been assumed that the neutron flux attenuation might be more than 25 figures at the maximum, and in addition, the neutron flux variation would be great due to void effect, which would make convergency extremely difficult and would require

so many repeated calculation iteration (line iteration). There has been a possibility that any recalculation made by line of sight method for incident neutrons at the void surface at each line iteration would invite a larger neutron flux variation, and would not make the calculation convergence. For this reason, this time the following convergency calculation method has been adopted:

Line Iteration No.	Line of Sight Calculation in Void	Energy Group
1		
	Every time	
5		1st group
	Every 5 times	
50		8th group
	None	
100		
1		
	None	
30		
	Every time	
35		9th group (thermal)
	Every 10 times	
100		
	None	
150		

In 1 group to 8 group, line of sight calculation has been inserted to every five times of line iteration from the experience of previous calculation that neutron flux around void converges in about five line

iterations. The reason of stopping line of sight calculation in 50 line iterations has been that the neutron flux below void region converges.

In 9 group (thermal), the method of inserting line of sight calculation has differed from above 8 groups.

Line of sight calculation of 9 group has been inserted after neutron flux has converged, because as the neutron flux distributions of those above 8th group are relatively resembled to the removal neutron source distribution or the slowing-down neutron source distribution, those neutron fluxes in the neighbourhood of void surface have converged at the early stage of the line iteration while those of the ninth group seemed not like that. The final convergence accuracy has been 1% and each group needed 120 - 140 times of iterations. Particularly it has been difficult to have the neutron flux convergence inside top shield, and it has been the cause of so many iterations. The reason for this has been assumed to be the large neutron flux attenuation inside upper shield and the relatively rough space meshes.

5) Computing time

For this calculation, it took about one hour by CDC-6600.

(III-3) Calculation Result

Fig. (III-7) to Fig. (III-33) show the results.

1) Contour distribution of neutron flux

Nine groups neutron flux contour distribution mappings are shown in Fig. (III-7) ∿ Fig. (III-15). Three groups neutron flux contour distribution mappings combined into fast, intermediate and thermal neutron groups are shown in Fig. (III-16) ∿ Fig. (III-18).

In above 8 groups (fast and intermediate neutrons), neutrons streaming through N_2 gas void outside reactor vessel from bottom to top raise the neutron flux level at both side surface of void and lower part of top shield. From the part of high neutron flux level, neutrons enter into the adjacent Ar gas void above sodium surface, then on the axial center axis, neutron flux level in Ar gas void becomes higher than that in sodium liquid. Neutron flux contour distribution having peak point at the entrance surface of the streaming neutron is newly formed. The decay rate of neutron flux in sodium is largest in energy group 4, so the streaming neutrons give the greatest effect to the neutron flux in sodium.

In 9 group (thermal neutron), streaming neutrons are very little because as the N_2 gas void surface is composed by stainless steel many thermal neutrons are absorbed, so thermal neutron flux distribution is

formed from the slowing down neutrons caused by the streaming neutron distribution above 8 groups. Peak of thermal neutron flux formed at the position near the carbon shield.

Fig. (III-19) shows the neutron fluxes at both N_2 gas void surface on radial center axis and the top of N_2 gas void, and at the same time decay rate of neutron flux along void is shown. It seems that the decay rate becomes smaller as energy becomes lower. Streaming neutrons entering into the top of the void come mostly from the part of high neutron flux at lower side surface of void, while streaming effects are decreased as energy becomes lower because the contribution of slowing down neutron increases. This is considered the spectrum softening seen in Fig. (III-19).

2) Decay distribution of neutron flux

In Fig. (III-20) ∿ Fig. (III-29), neutron flux decay distributions on the surface parallel to r, z axis are shown comparing between calculation including void and that not including void. On the r-axis, almost no difference exists between both calculations, and also on the z-axis there seemes only little difference at the neighbourhood of Ar gas void. Decay distribution on the surface parallel to r-axis, the difference becomes greater from the neighbourhood of N_2 gas void to whole part as it remoted from r-axis

and energy become lower. This is because the effects of streaming are greater as energy becomes higher. This is same as on the surface parallel to z axis.

3) Comparison between this calculation and before previous one

Fig. (III-30) shows the comparison at the top of N_2 gas void between the calculation including void and that not including void. There seems that the streaming neutrons raise the neutron flux level at the top of N_2 gas void by maximum 5 figures at high energy region and 3 figures at low energy region. However, the increased neutron flux is fully shielded by the top shield and adjacent concrete shield, and it seems that there exists any shield design problem, within the assumption of simplified void geometry.

4) Comparison between this calculation and previous one

Fig. (III-31) shows the comparison between the calculation using axial symmetric void option and the calculation under condition that neutron streams to upper part from the surface of N_2 gas void intersected radial center axis with cosine distribution. Neutron flux is compared at the top of N_2 gas void. It seems that over whole energy groups previous calculation is greater by about 1 figure than this one. Previous calculation evidently overestimates the neutron flux

in long narrow N_2 gas void because the neutron transition probability becomes larger between upper part and lower one.

5) Neutron flux around N_2 gas void

As is shown in Fig. (III-32) ∿ Fig. (III-33), the neutron flux level at inner surface of N_2 gas void becomes lower than that at outer surface as going to upper part. Table (III-7) represents ratio of neutron flux at inner surface to that of outer surface of 60th mesh (703.7 cm). The ratio becomes 10 to 2 according to high to low energy. The reason is that neutron flux distribution at upper part of void is determined by the neutron streaming from lower part of void which is high flux level. As is shown in Table (III-8), the neutron transition probability from the lower part of the inner void surface to the upper part of void is greater by maximum 9 times than that from lower part of outer void surface, and this comes from the difference between both solid angles. Further, as is shown Table (III-9), neutrons entering into void from inner surface are more by about 10 times at high energy than those from the outer surface. Consequently, at high energy region the difference between neutron currents entering into outer surface and into inner surface is more than ten times and the difference of neutron fluxes is caused. As going to lower energy region, the difference of neutron flux between inner

surface and outer one becomes small because the difference between these neutron currents entering into the void becomes little and because the neutron flux in shields does not decay largely and because the exchange of neutrons between inner surface and outer one increases.

Table(III-1) Energy Structure of Removal Calculation

No.	Original Energy Structure (Mev)	No.	Collapsed Energy Structure (mev)
1	18.00-13.74	1	18.00- 8.25
2	13.74-10.50		
3	10.50- 9.30		
4	9.30- 8.25		
5	8.25- 7.32	2	8.25- 6.50
6	7.32- 6.50		
7	6.50- 5.75	3	6.50- 5.10
8	5.75- 5.10		
9	5.10- 4.52	4	5.10- 4.00
10	4.52- 4.00		
11	4.00- 3.55	5	4.00- 2.50
12	3.55- 3.16		
13	3.16- 2.81		
14	2.81- 2.50		
15	2.50- 2.16	6	2.50- 1.40
16	2.16- 1.87		
17	1.87- 1.61		
18	1.61- 1.40		
19	1.40- 1.21	7	1.40- 0.05
20	1.21- 1.05		
21	1.05- 0.92		
22	0.92- 0.80		
23	0.80- 0.57		
24	0.57- 0.40		
25	0.40- 0.05		

Table (III-2) Energy Structure of Diffusion Calculation

Gr.	Eneregy Range (Mev)	Lethogy
1	1.0 5 (+1)−8.2 5 (+1)	0.2 4 1
2	8.2 5 (+1)−6.5 0 (+0)	0.2 3 4
3	6.5 0 (+0)−5.1 0 (+0)	0.2 4 3
4	5.1 0 (+0)−4.0 0 (+0)	0.2 4 3
5	4.00 (+0)−3.1 6 (+0)	0.2 3 5
6	3.1 6 (+0)−2.5 0 (+0)	0.2 3 5
7	2.5 0 (+0)−1.8 7 (+0)	0.2 8 1
8	1.3 7 (+0)−1.4 0 (+0)	0.2 9 0
9	1.4 0 (+0)−1.0 5 (+0)	0.2 8 7
10	1.0 5 (+0)−8.0 0 (−1)	0.2 7 2
11	8.0 0 (−1)−4.0 0 (−1)	0.6 9 3
12	4.0 0 (−1)−2.0 0 (−1)	0.6 9 3
13	2.0 0 (−1)−1.0 0 (−1)	0.6 9 4
14	1.0 0 (−1)−4.6 5 (−2)	0.7 6 5
15	4.6 5 (−2)−2.1 5 (−2)	0.7 7 2
16	2.1 5 (−2)−1.0 0 (−2)	0.7 6 5
17	1.0 0 (−2)−4.6 5 (−3)	0.7 7 1
18	4.6 5 (−3)−2.1 5 (−3)	0.7 6 6
19	2.1 5 (−3)−1.0 0 (−3)	0.7 6 3
20	1.0 0 (−3)−4.6 5 (−4)	0.7 7 0
21	4.6 5 (−4)−2.1 5 (−4)	0.7 7 0
22	2.1 5 (−4)−1.0 0 (−4)	0.7 7 0
23	1.0 0 (−4)−4.6 5 (−5)	0.7 7 0
24	4.6 5 (−5)−2.1 5 (−5)	0.7 7 0
25	2.1 5 (−5)−1.0 0 (−5)	0.7 6 0
26	1.0 0 (−5)−4.6 5 (−6)	0.7 7 0
27	4.6 5 (−6)−2.1 5 (−6)	0.7 7 0
28	2.1 5 (−6)−1.0 0 (−6)	0.7 6 0
29	1.0 0 (−6)−4.6 5 (−7)	0.7 7 0
30	4.6 5 (−7)−2.1 5 (−7)	0.7 7 0
31	2.1 5 (−7)−0.0 0	

Gr	Energy Range (Mev)	Lethagy
1	1.0 5 (+1)−6.5 0 (+0)	0.4 7 5
2	6.5 0 (+0)−2.5 0 (+0)	0.9 5 6
3	2.5 0 (+0)−8.0 0 (−1)	1.1 3 0
4	8.0 0 (−1)−4.6 5 (−2)	2.8 4 5
5	4.6 5 (−2)−2.1 5 (−3)	3.0 7 4
6	2.1 5 (−3)−1.0 0 (−4)	3.0 7 3
7	1.0 0 (−4)−4.6 5 (−6)	3.0 7 0
8	4.6 5 (−6)−2.1 5 (−7)	3.0 7 0
9	2.1 5 (−7)−0.0 0	

Table (III-3)·(1) Composition of Core, Blanket Materials

Materials / Element	Core		Radial Blanket	Axial Blanket
	I	II		
U 235	9.8615 (-6)	1.0816 (-5)	2.0785 (-5)	1.3920 (-5)
U 238	4.9209 (-3)	5.3972 (-3)	1.0372 (-2)	6.9460 (-3)
Pu239	8.6042 (-4)	1.3883 (-3)		
Pu240	2.2945 (-4)	3.7021 (-4)		
Pu241	5.7362 (-5)	9.2552 (-5)		
Na	1.0806 (-2)	9.3071 (-3)	7.6948 (-3)	8.7460 (-3)
Fe	1.2160 (-2)	1.2841 (-2)	1.0839 (-2)	1.4770 (-2)
Cr	3.1293 (-3)	3.3048 (-3)	2.7895 (-3)	4.1810 (-3)
Ni	2.2352 (-3)	2.3606 (-3)	1.9925 (-3)	2.2060 (-3)
Mo	3.5763 (-4)	3.7769 (-4)	3.1880 (-4)	
O	1.2156 (-2)	1.4518 (-2)	2.0785 (-2)	1.3890 (-2)

Table (III-3) (2) Composition of Shielding Materials

($\times 10^{-4}$ CC)

Material / Element	Nickel Shield	Graphit Shield	Core Barrel	Gas Plenum	Fuel Elempent Hold Down Part	Hanalings Head	Guid Tobe and Thermo couple
Ni	62340	00925	09346	02370	33120	01869	00935
Fe	05102	05128	51800	15100	21109	10360	05180
Cr	01457	01465	14800	03970	05950	02960	01480
Mo	00191	00192	01947			00987	00195
Na	01838	01806		03140	03409	00954	07834
C		14090					
Total	70928	20606	77893	24789	32670	22540	15624

Material / Element	Solium	Dip Plate	Graphite	Thermal Shield	Cove Vessel and Thermal Shield	Carbon Steel
Ni		05608		05607	09346	
Fe		31080		31080	51800	77790
Cr		08881		08889	14800	
Mo		01168		01168	01947	
Na	04705	03482		03482		
C			16000			00785
Total	08705	50219	16000	50217	77893	78485

Table (III-3) (3) Composition of Shielding Materials

	121 Fe	122,123 Graphite, Ar Gas Fe	124 N_2 Gas, Fe	125 Ar Gas, Fe
Ni	0.4226	0.1797		
Fe	2.3423	0.9962	4.3917	7.0528
Cr	0.7573	0.3221		
Mo				
C		1.2308	0.0044	0.0071

	126 Ordinary Concrete
Fe	0.0620
C	0.0065
O	1.2040
Na	0.0268
H	0.0117
Si	0.8610
S	0.0039
K	0.0194
Ca	0.2000
Mn	0.0060

Table (III-4) (1) Removal Cross-section for "MONJU"

101 Core 1		
Gr.	(A)	(B)
1	0.08478	0.08478
2	0.08862	0.08862
3	0.09514	0.09514
4	0.10230	0.10230
5	0.11300	
6	0.11640	
7	0.14940	

102 Core2		
Gr.	(A)	(B)
1	0.08478	0.08478
2	0.08862	0.08862
3	0.09514	0.09514
4	0.10230	0.10230
5	0.11300	
6	0.11640	
7	0.14940	

103 Radial Blanket		
Gr.	(A)	(B)
1	0.09490	0.09490
2	0.09941	0.09941
3	0.10680	0.10680
4	0.11480	0.11480
5	0.12870	
6	0.12970	
7	0.18050	

104 Axial Blanket		
Gr.	(A)	(B)
1	0.08471	0.08471
2	0.08853	0.08853
3	0.09504	0.09504
4	0.10220	0.10220
5	0.11300	
6	0.11630	
7	0.14930	

105 Nickel Shield		
Gr.	(A)	(B)
1	0.15680	0.13260
2	0.17080	0.14230
3	0.18030	0.15030
4	0.19340	0.16120
5	0.17060	
6	0.18510	
7	0.20200	

106 Carbon Shield		
Gr.	(A)	(B)
1	0.05798	0.06772
2	0.08031	0.07295
3	0.08807	0.07809
4	0.11380	0.09484
5	0.13640	
6	0.12270	
7	0.15490	

107 Gas Plenum		
Gr.	(A)	(B)
1	0.06270	0.05225
2	0.06515	0.05429
3	0.06986	0.05821
4	0.07518	0.06265
5	0.06664	
6	0.07247	
7	0.07255	

108 Fuel Hold-down Mecanism		
	(A)	(B)
1	0.08133	0.06778
2	0.08466	0.07055
3	0.09087	0.07573
4	0.08755	0.08154
5	0.08665	
6	0.09346	
7	0.09141	

(A) After Adjust

(B) Before Adjust

Table (III-4) (2) Removal Cross-section for "MONJU"

109 Sodium 1		
Gr.	(A)	(B)
1	0.03380	0.02816
2	0.03499	0.02916
3	0.03811	0.03176
4	0.04088	0.03460
5	0.03556	
6	0.04458	
7	0.05974	

110 Core Barrel		
Gr.	(A)	(B)
1	0.18200	0.15160
2	0.14630	0.15710
3	0.13340	0.16680
4	0.14360	0.17950
5	0.19290	
6	0.20150	
7	0.18180	

111 Handlings Head		
Gr.	(A)	(B)
1	0.05853	0.05198
2	0.05931	0.05384
3	0.06083	0.05771
4	0.06070	0.06210
5	0.06592	
6	0.07457	
7	0.08230	

112 Sodium 2		
Gr.	(A)	(B)
1	0.03380	0.02816
2	0.03499	0.02916
3	0.03811	0.03176
4	0.04088	0.03406
5	0.03556	
6	0.04458	
7	0.05974	

113 Sodium 3		
Gr.	(A)	(B)
1	0.03237	0.02816
2	0.03301	0.02916
3	0.03495	0.03176
4	0.03658	0.03406
5	0.03556	
6	0.04458	
7	0.05973	

114 Sodium 4		
Gr.	(A)	(B)
1	0.03237	0.02816
2	0.03301	0.02916
3	0.03495	0.03176
4	0.03658	0.03406
5	0.03556	
6	0.04458	
7	0.05973	

115 Dip Plate		
Gr.	(A)	(B)
1	0.11640	0.10220
2	0.11630	0.10590
3	0.13530	0.11280
4	0.09707	0.12130
5	0.13000	
6	0.13870	
7	0.13300	

116 Thermal Shield		
Gr.	(A)	(B)
1	0.12270	0.10220
2	0.12710	0.10590
3	0.13530	0.11280
4	0.14560	0.12130
5	0.13000	
6	0.13870	
7	0.13300	

(A) After Adjust

(B) Before Adjust

Table(III-4) (3) Removal Cross-section for "MONJU"

117 Core Vessel		
Gr.	(A)	(B)
1	0.12130	0.15170
2	0.12570	0.15710
3	0.13350	0.16680
4	0.14360	0.17960
5	0.19300	
6	0.20150	
7	0.18180	

118 Graphite		
Gr.	(A)	(B)
1	0.06970	0.06762
2	0.06878	0.07408
3	0.07996	0.07930
4	0.12120	
5	0.15620	
6	0.13480	
7	0.17960	

119 Carbon Steel		
Gr.	(A)	(B)
1	0.15250	0.14710
2	0.12550	0.15690
3	0.20880	0.17400
4	0.15130	0.18910
5	0.19810	
6	0.20560	
7	0.17680	

120 Guid Tube and Thermo Couple		
Gr.	(A)	(B)
1	0.04861	0.04051
2	0.05031	0.04195
3	0.05353	0.04526
4	0.05821	0.04861
5	0.05129	
6	0.06026	
7	0.07194	

(A) After Adjust

(B) Before Adjust

Table (III-4) (4) Removal Cross-section for "MONJU" Shield

121 Fe	
Gr.	
1	0.0686
2	0.0710
3	0.0754
4	0.0812
5	0.0873
6	0.0911
7	0.0941

122 Graphite, Ar Gas Fe (1)	
Gr.	
1	0.0812
2	0.0872
3	0.0931
4	0.1120
5	0.1560
6	0.1420
7	0.2030

123 Graphite,Ar Gas Fe (2)	
Gr.	
1	0.0812
2	0.0872
3	0.0931
4	0.1120
5	0.1560
6	0.1420
7	0.2030

124 N_2 Gas, Fe	
Gr.	
1	0.0832
2	0.0887
3	0.0983
4	0.1070
5	0.1120
6	0.1160
7	0.1200

125 Ar Gas,Fe	
Gr.	
1	0.1340
2	0.1420
3	0.1580
4	0.1720
5	0.1870
6	0.1870
7	0.1920

126 Ordinary Concrete	
Gr.	
1	0.0807
2	0.0813
3	0.0875
4	0.0963
5	0.1260
6	0.1370
7	0.2650

Table (III-5) (1) Diffusion Constant of Core and Blanket

101 Core I

Gr.	D.C.	Σ_R	Σ_{SL}
1	4.34151400E+00	5.28422570E-02	1.44427370E-02
2	3.29080530E+00	5.11417871E-02	2.99233731E-02
3	2.56049230E+00	4.11801304E-02	2.82841187E-02
4	1.71327300E+00	1.16580028E-02	3.79478048E-03
5	1.17117590E+00	1.71133778E-02	3.72681100E-03
6	9.87421930E-01	3.74824992E-02	8.00886200E-04
7	8.79196080E-01	1.43969511E-01	8.96853070E-05
8	9.15573640E-01	9.00087097E-02	3.51126900E-05
9	1.91600543E-01	9.39315201E-01	0.

102 Core II

Gr.	D.C.	Σ_R	Σ_{SL}
1	4.03343250E+00	6.32500620E-02	1.48988360E-02
2	3.05560030E+00	5.96577370E-02	3.16285804E-02
3	2.37379110E+00	4.93574833E-02	3.08423923E-02
4	1.58169040E+00	1.59941386E-02	3.94916381E-03
5	1.08127180E+00	2.34918294E-02	3.60319550E-03
6	9.06313410E-01	5.40538393E-02	8.32760260E-04
7	7.82691510E-01	2.02161530E-01	1.91617740E-04
8	7.81381780E-01	2.32994905E-01	7.46753490E-05
9	1.91600543E-01	9.39315201E-01	0.

103 Radial Blanket

Gr.	D.C.	Σ_R	Σ_{SL}
1	3.66649810E+00	6.81142330E-02	1.54966880E-02
2	2.76686130E+00	5.91926863E-02	3.44163682E-02
3	2.06548020E+00	4.65613751E-02	3.75936515E-02
4	1.33074740E+00	8.37906258E-03	5.85415010E-03
5	9.35450390E-01	1.10742136E-02	4.58728740E-03
6	8.77312220E-01	1.56977931E-02	2.43057420E-03
7	8.55837570E-01	2.60847922E-02	8.57823070E-04
8	8.88159250E-01	1.76263634E-02	3.77768760E-04
9	7.80448860E-01	5.53614268E-02	0.

104 Axial Blanket

	D.C.	Σ_R	Σ_{SL}
1	3.97363500E+00	5.14545630E-02	1.54472690E-02
2	3.00161140E+00	5.05679339E-02	3.38299332E-02
3	2.34868700E+00	3.68787647E-02	3.10459921E-02
4	1.54968280E+00	7.03434887E-03	5.27241388E-03
5	1.06791370E+00	9.16044686E-03	4.67134590E-03
6	9.17734710E-01	1.26225632E-02	2.59848470E-03
7	8.72060800E-01	1.97228522E-02	8.75877690E-04
8	8.90243940E-01	1.64938592E-02	4.33910680E-04
9	7.90251150E-01	5.74612536E-02	0.

Table(III-5) (2) Diffusion Constant of Shield Region

105 Nickel Shield

Gr.	D.C.	Σ_R	Σ_{SL}
1	2.38747058E+00	1.16745337E-01	2.55200000E-02
2	1.99234000E+00	8.98452500E-02	6.10447510E-02
3	1.72897346E+00	1.64599132E-02	1.67061775E-02
4	1.26999581E+00	9.55769814E-03	8.88603782E-03
5	4.07557190E-01	1.95443190E-02	1.80200180E-02
6	3.05623952E-01	1.63637142E-02	1.30700007E-02
7	2.82202824E-01	2.12299374E-02	1.02700001E-02
8	2.74492109E-01	4.45399017E-02	4.35342818E-03
9	2.28333924E-01	2.16104981E-01	0.

106 Carbon Shield

Gr.	D.C.	Σ_R	Σ_{SL}
1	4.97508233E+00	8.38697667E-02	4.71200000E-02
2	3.07061243E+00	4.73717190E-02	4.37827622E-02
3	2.28918270E+00	4.15597084E-02	4.16865009E-02
4	1.29274152E+00	2.41400582E-02	2.40716201E-02
5	9.71623360E-01	1.86352036E-02	1.82800006E-02
6	9.52025099E-01	1.66178431E-02	1.60400000E-02
7	9.37031637E-01	1.56133866E-02	1.45300000E-02
8	9.29751785E-01	1.59706589E-02	1.17220461E-02
9	8.81803682E-01	1.85260932E-02	0.

107 Gas Plenum

Gr.	D.C.	Σ_R	Σ_{SL}
1	6.20847211E+00	4.37507863E-02	1.33500000E-02
2	5.12053374E+00	3.16896153E-02	2.53032446E-02
3	4.70413520E+00	1.26434920E-02	1.29876798E-02
4	3.29913121E+00	4.49298783E-03	4.34710533E-03
5	2.24072822E+00	6.25570993E-03	5.50200194E-03
6	1.32567185E+00	5.21979666E-03	3.73300007E-03
7	1.22763955E+00	5.72295956E-03	3.00700000E-03
8	1.20394801E+00	1.05038786E-02	1.37651274E-03
9	1.01551201E+00	4.59207150E-02	0.

109 Fuel Hold-down Mecanism

Gr.	D.C.	Σ_R	Σ_{SL}
1	4.78371801E+00	5.67437432E-02	1.66100000E-02
2	3.91973355E+00	4.20132600E-02	3.40800288E-02
3	3.73992607E+00	1.70823001E-02	1.70281610E-02
4	2.58667043E+00	5.91835961E-03	5.71533857E-03
5	1.77748564E+00	7.35281527E-03	6.33200042E-03
6	9.87016629E-01	7.25535041E-03	5.29600001E-03
7	9.07871096E-01	7.94835589E-03	4.24700007E-03
8	8.91215589E-01	1.44041293E-02	1.86865538E-03
9	7.53706911E-01	6.59595974E-02	0.

Table (III-5) (3) Diffusion Constant of Shield Region

109 Sodium 1

Gr.	D.C.	Σ_R	Σ_{SL}
1	1.15252049E+01	2.41373468E-02	1.18600000E-02
2	9.65392945E+00	1.54209104E-02	1.36195407E-02
3	6.28270084E+00	1.29068509E-02	1.30967404E-02
4	4.01357230E+00	5.53060085E-03	5.51401108E-03
5	2.82168396E+00	7.30579694E-03	7.22900001E-03
6	4.44869886E+00	2.16295238E-03	2.00500000E-03
7	4.91194610E+00	2.02456329E-03	1.61900000E-03
8	4.59936778E+00	3.28852880E-03	1.39930500E-03
9	3.89004144E+00	8.30051767E-03	0.

110 Core Barrel

Gr.	D.C.	Σ_R	Σ_{SL}
1	2.14509376E+00	1.25334839E-01	3.19100000E-02
2	1.79097699E+00	9.43071508E-02	7.53789173E-02
3	1.81602760E+00	2.50916485E-02	2.63204249E-02
4	1.31663510E+00	9.91423275E-03	9.40621387E-03
5	8.91632821E-01	4.56948462E-03	1.80200594E-03
6	4.18987456E-01	1.70673318E-02	1.18400001E-02
7	3.78995126E-01	1.76223149E-02	8.17600001E-03
8	3.73241357E-01	3.57650613E-02	3.70324655E-03
9	3.12810154E-01	1.63477156E-01	0.

111 Handlings Head

Gr.	D.C.	Σ_R	Σ_{SL}
1	6.25638900E+00	4.34597249E-02	1.53500000E-02
2	5.14598976E+00	3.15565159E-02	2.61744495E-02
3	4.21539273E+00	1.85655366E-02	1.85534391E-02
4	2.89538178E+00	6.37214397E-03	6.25479661E-03
5	1.97318086E+00	7.25998443E-03	6.67600012E-03
6	1.50556721E+00	5.23132050E-03	4.05900000E-03
7	1.46131019E+00	5.48536677E-03	3.22200000E-03
8	1.42281471E+00	9.36497076E-03	1.50443199E-03
9	1.19473237E+00	4.00753984E-02	0.

112 Sodium 2

Gr.	D.C.	Σ_R	Σ_{SL}
1	1.15441121E+01	2.38844755E-02	1.16400000E-02
2	9.61498549E+00	1.55153032E-02	1.36952260E-02
3	6.39273032E+00	1.17435086E-02	1.19787631E-02
4	4.03874602E+00	5.22701397E-03	5.21000847E-03
5	2.90866657E+00	5.47713496E-03	5.41300001E-03
6	4.73168910E+00	2.70441093E-03	2.55600000E-03
7	4.91350824E+00	2.03713691E-03	1.63400000E-03
8	4.61573935E+00	2.76733346E-03	1.01349553E-03
9	3.89004144E+00	8.30052767E-03	0.

Table(III-5) (4) Diffusion Constant of Shield Region

113 Sodium 3

Gr.	D.C.	Σ_R	Σ_{SL}
1	1.15473800E+01	2.38407688E-02	1.16000000E-02
2	9.50711257E+00	1.65017711E-02	1.43554125E-02
3	6.41049797E+00	1.14668375E-02	1.16761848E-02
4	3.91433686E+00	7.43997730E-03	7.42100028E-03
5	2.84256529E+00	6.16659366E-03	6.09700000E-03
6	4.98574789E+00	4.73108706E-03	4.58100000E-03
7	4.88235694E+00	3.25394664E-03	2.77900000E-03
8	4.58444559E+00	3.69470716E-03	1.67376269E-03
9	3.89004144E+00	8.30051757E-03	0.

114 Sodium 4

Gr.	D.C.	Σ_R	Σ_{SL}
1	1.15593923E+01	2.36801124E-02	1.14500000E-02
2	9.53490127E+00	1.66747476E-02	1.51242955E-02
3	6.43780700E+00	1.11118593E-02	1.13260372E-02
4	3.90130125E+00	7.64200108E-03	7.62300155E-03
5	2.80911691E+00	6.52747426E-03	6.45500000E-03
6	5.04771401E+00	6.29127457E-03	6.13500000E-03
7	4.85632007E+00	4.53335091E-03	3.99600000E-03
8	4.56178951E+00	4.44369691E-03	2.23291792E-03
9	3.89004144E+00	8.30051757E-03	0.

115 Dip Plate

Gr.	D.C.	Σ_R	Σ_{SL}
1	3.19248051E+00	8.38123083E-02	2.28000000E-02
2	2.62317037E+00	6.35396732E-02	5.85084136E-02
3	2.53168118E+00	2.06357153E-02	2.11148029E-02
4	1.71806681E+00	1.12454171E-02	1.09127687E-02
5	1.08488620E+00	1.30136456E-02	1.12700004E-02
6	6.05977838E-01	2.89275505E-02	2.55400000E-02
7	6.00433243E-01	2.43580248E-02	1.67600000E-02
8	5.86417635E-01	3.23505551E-02	6.52424906E-03
9	4.94817017E-01	1.04407709E-01	0.

116 Thermal Shield and Vessel

Gr.	D.C.	Σ_R	Σ_{SL}
1	3.18708002E+00	8.42733632E-02	2.32900000E-02
2	2.62087097E+00	6.30319297E-02	5.11103841E-02
3	2.52383784E+00	1.99147573E-02	2.06281511E-02
4	1.75994796E+00	9.26780943E-03	8.94143046E-03
5	1.11556680E+00	1.22381278E-02	1.05200017E-02
6	6.25547423E-01	1.79069320E-02	1.47700000E-02
7	6.00707298E-01	1.44118144E-02	8.09400000E-03
8	5.88881359E-01	2.53657693E-02	3.65990977E-03
9	4.94833005E-01	1.04404549E-01	0.

Table (III-5) (5) Diffusion Constant of Shield Region

117 Reactor Vessel

Gr.	D.C.	Σ_R	Σ_{SL}
1	2.14914958E+00	1.24589214E-01	3.10700000E-02
2	1.76346877E+00	9.49156726E-02	7.70876094E-02
3	1.82884111E+00	2.60063498E-02	2.62773287E-02
4	1.28086736E+00	1.19525266E-02	1.14275932E-02
5	8.00231794E-01	1.14910929E-02	8.61300146E-03
6	4.01307956E-01	2.68418757E-02	2.15700000E-02
7	3.78984736E-01	2.35220532E-02	1.30800000E-02
8	3.72496761E-01	3.88782623E-02	4.71863068E-03
9	3.12761575E-01	1.68526130E-01	0.

118 Graphite

Gr.	D.C.	Σ_R	Σ_{SL}
1	5.07131099E+00	9.71886482E-02	6.12100000E-02
2	3.07837207E+00	3.77704635E-02	3.49194028E-02
3	2.07970527E+00	4.00325854E-02	4.01760649E-02
4	1.07791991E+00	3.23138954E-02	3.23000000E-02
5	9.17633811E-01	3.50511767E-02	3.50500000E-02
6	9.08217738E-01	3.11205685E-02	3.11200000E-02
7	9.07551687E-01	2.87365252E-02	2.87100000E-02
8	9.07442894E-01	2.81019784E-02	2.80550512E-02
9	9.06903419E-01	2.94331045E-04	0.

119 Carbon Steel

Gr.	D.C.	Σ_R	Σ_{SL}
1	2.18299169E+00	1.29125073E-01	3.48000000E-02
2	1.77626315E+00	9.32236874E-02	8.90801204E-02
3	1.80222272E+00	2.93862924E-02	3.83565424E-02
4	1.32074609E+00	7.54363909E-03	7.21359936E-03
5	1.12541840E+00	1.32337247E-02	1.12201415E-02
6	3.82109352E-01	2.46613852E-02	2.13500019E-02
7	3.46576930E-01	2.97350483E-02	2.06600000E-02
8	3.42217006E-01	5.51223859E-02	1.60862708E-02
9	3.02098843E-01	3.26603748E-01	0.

120 Guid Tube and Thermo Couple

Gr.	D.C.	Σ_R	Σ_{SL}
1	8.02774062E+00	3.40445703E-02	1.36700000E-02
2	6.60642142E+00	2.42794530E-02	2.05109630E-02
3	4.90093922E+00	1.75199550E-02	1.75541653E-02
4	3.29580574E+00	6.54964325E-03	6.48118114E-03
5	2.29725103E+00	6.48182283E-03	6.15600002E-03
6	2.24342799E+00	4.34292801E-03	3.69400000E-03
7	2.23565541E+00	4.06529601E-03	2.70000000E-03
8	2.15742167E+00	6.42984678E-03	1.40314005E-03
9	1.81478996E+00	2.43177048E-02	0.

Table (III-5) (6) Diffusion Constant of Shield Region

121 Fe			
Gr.	D.C.	Σ_R	Σ_{SL}
1	.4775E+01	.5562E-01	.1328E-01
2	.3964E+01	.4254E-01	.5104E-01
3	.4057E+01	.1180E-01	.1242E-01
4	.2867E+01	.5217E-02	.4985E-02
5	.1724E+01	.5417E-02	.4103E-02
6	.3467E+00	.1955E-01	.1705E-01
7	.8383E+00	.1714E-01	.1154E-01
8	.3213E+00	.2149E-01	.3553E-02
9	.6913E+00	.7832E-01	0.

122 Graphite , Ar Gas , Fe (1)			
Gr.	D.C.	Σ_R	Σ_{SL}
1	.4151E+01	.1029E+00	.5735E-01
2	.2933E+01	.4437E-01	.4098E-01
3	.1897E+01	.7887E-01	.7916E-01
4	.1162E+01	.2652E-01	.2645E-01
5	.8503E+00	.2605E-01	.2541E-01
6	.7614E+00	.2531E-01	.2427E-01
7	.7380E+00	.4576E-01	.4332E-01
8	.7300E+00	.4153E-01	.3148E-01
9	.6835E+00	.3346E-01	0.

123 Graphite , Ar Gas, Fe (2)			
Gr.	D.C.	Σ_R	Σ_{SL}
1	.4147E+01	.1014E+00	.5583E-01
2	.2893E+01	.4455E-01	.4239E-01
3	.2120E+01	.3813E-01	.3295E-01
4	.1217E+01	.1821E-01	.1812E-01
5	.8701E+00	.2042E-01	.1982E-01
6	.7655E+00	.2131E-01	.2125E-01
7	.7383E+00	.2263E-01	.2161E-01
8	.7317E+00	.2642E-01	.1849E-01
9	.6835E+00	.3346E-01	0.

Table (III-5) (7) Diffusion Constant of Shield Region

124 N_2 Gas , Fe			
Gr.	D.C.	Σ_R	Σ_{SL}
1	.3855E+01	.7313E-01	.1984E-01
2	.3136E+01	.5279E-01	.7032E-01
3	.3243E+01	.1755E-01	.2210E-01
4	.2342E+01	.4079E-02	.3863E-02
5	.2117E+01	.6034E-02	.4910E-02
6	.7124E+00	.9985E-02	.7868E-02
7	.6129E+00	.1182E-01	.7350E-02
8	.5066E+00	.2176E-01	.4354E-02
9	.5345E+00	.8488E-01	0.

125 Ar Gas,Fe			
Gr.	D.C.	Σ_R	Σ_{SL}
1	.2416E+01	.1166E+00	.3093E-01
2	.1931E+01	.9563E-01	.1502E+00
3	.2131E+01	.3209E-01	.3304E-01
4	.1427E+01	.7803E-02	.7382E-02
5	.1261E+01	.9324E-02	.7553E-02
6	.4543E+00	.1383E-01	.1020E-01
7	.3816E+00	.1633E-01	.9539E-02
8	.3780E+00	.2947E-01	.4838E-02
9	.3328E+00	.1363E+00	0.

126 Ordinary Concrete			
Gr.	D.C.	Σ_R	Σ_{SL}
1	.4623E+01	.3671E-01	.2277E-01
2	.3636E+01	.2225E-01	.1866E-01
3	.2678E+01	.2545E-01	.2712E-01
4	.1379E+01	.2951E-01	.2911E-01
5	.1287E+01	.4878E-01	.4844E-01
6	.1201E+01	.5173E-01	.5134E-01
7	.1223E+01	.5266E-01	.5204E-01
8	.1218E+01	.5364E-01	.5375E-01
9	.4619E+00	.7132E-02	0.

Table (III-6) Power of "MONJU"

Name of Region	Power(Mw)
Core I	391.40
Core II	296.40
Radial Blanket (Upper half)	14.79
Axial Blanket (Upper half)	5.67

Table (III-7) Neutron Flux Ratio between Inside and Outside of Void

Z=703.76cm(57mesh)

Energy Group	Outside Flux / Inside Flux
1	17.74
2	6.31
3	1.91
4	1.69
5	1.70
6	1.58
7	1.57
8	1.56
9	1.66

Table(III-8) Neutron Transition Probability Inside N_2 Gas Void

Inner Side $\leftrightarrow$ Outer Side $P_i = \dfrac{F_i P_{i\to o}}{F_i F_o}$

Outer Side $\leftrightarrow$ Outer Side $P_o = \dfrac{F_o P_{o\to o}}{F_o F_o}$

$J_{(i\to o)} = P_i J_i \; {}_o F_i$

$J_{(o\to o)} = P_o J_{o\to o} F_o$

P_i or P_o						
Mesh No.	1		10		20	
	Inner Side ↕ Outer Side	Outer Side ↕ Outer Side	Inner Side ↕ Outer Side	Outer Side ↕ Outer Side	Inner Side ↕ Outer Side	Inner Side ↕ Outer Side
1	1.67×10^{-5}	3.38×10^{-7}				
10			8.29×10^{-6}	2.51×10^{-7}		
20	1.13×10^{-7}	1.02×10^{-7}	2.50×10^{-7}	1.13×10^{-7}	7.51×10^{-6}	1.86×10^{-7}
40	2.79×10^{-10}	9.24×10^{-9}	2.28×10^{-8}	1.02×10^{-9}	5.47×10^{-9}	1.52×10^{-8}
60	1.53×10^{-10}	1.02×10^{-9}	1.53×10^{-10}	8.38×10^{-10}	2.07×10^{-10}	1.25×10^{-9}
80	6.22×10^{-11}	4.16×10^{-10}	6.22×10^{-11}	4.60×10^{-10}	7.60×10^{-11}	5.08×10^{-10}

Table(III-9) Neutron Current Around N_2 Gas Void (1 Group)

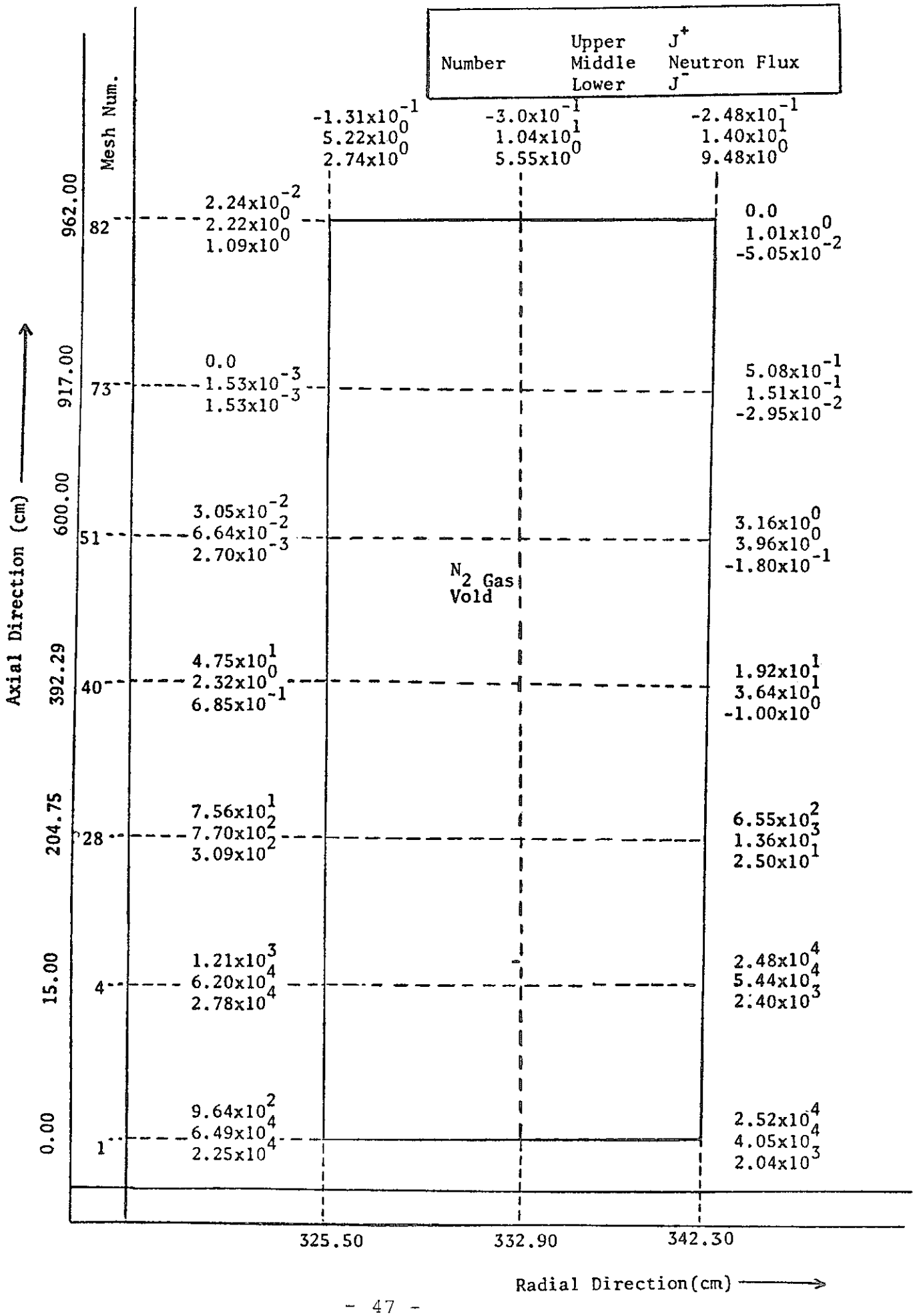

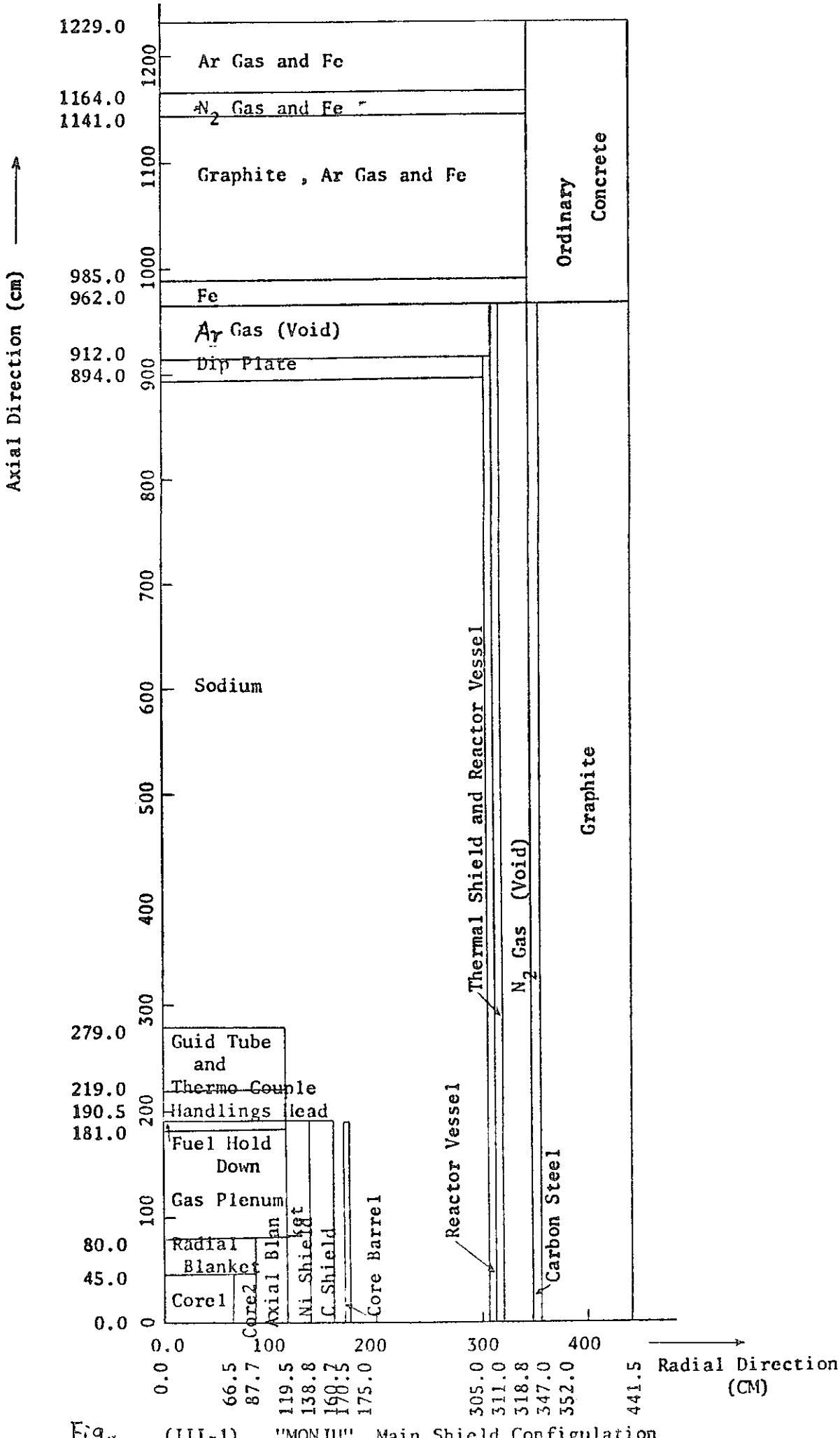

Fig. (III-1) "MONJU" Main Shield Configulation

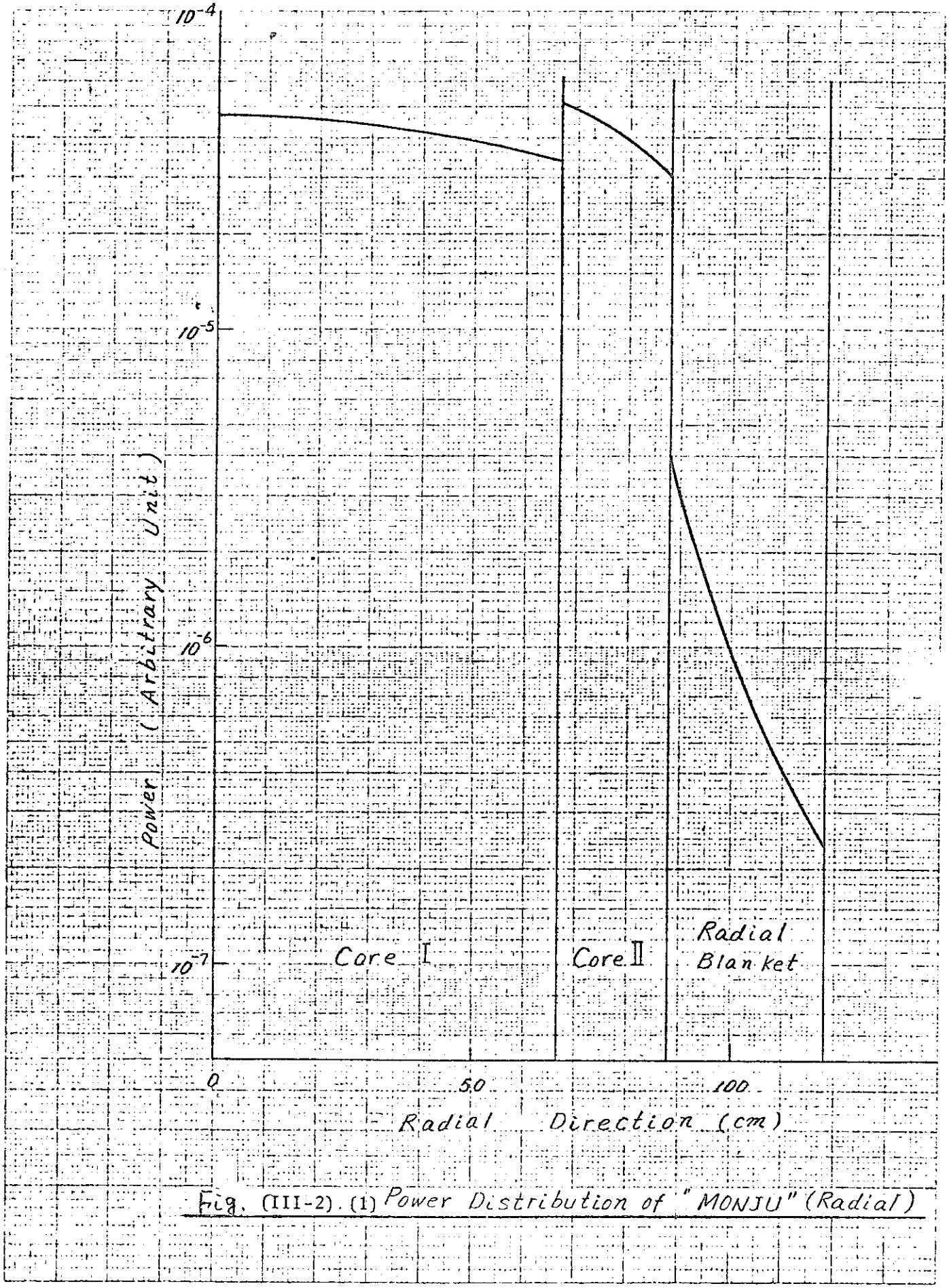

Fig. (III-2). (1) Power Distribution of "MONJU" (Radial)

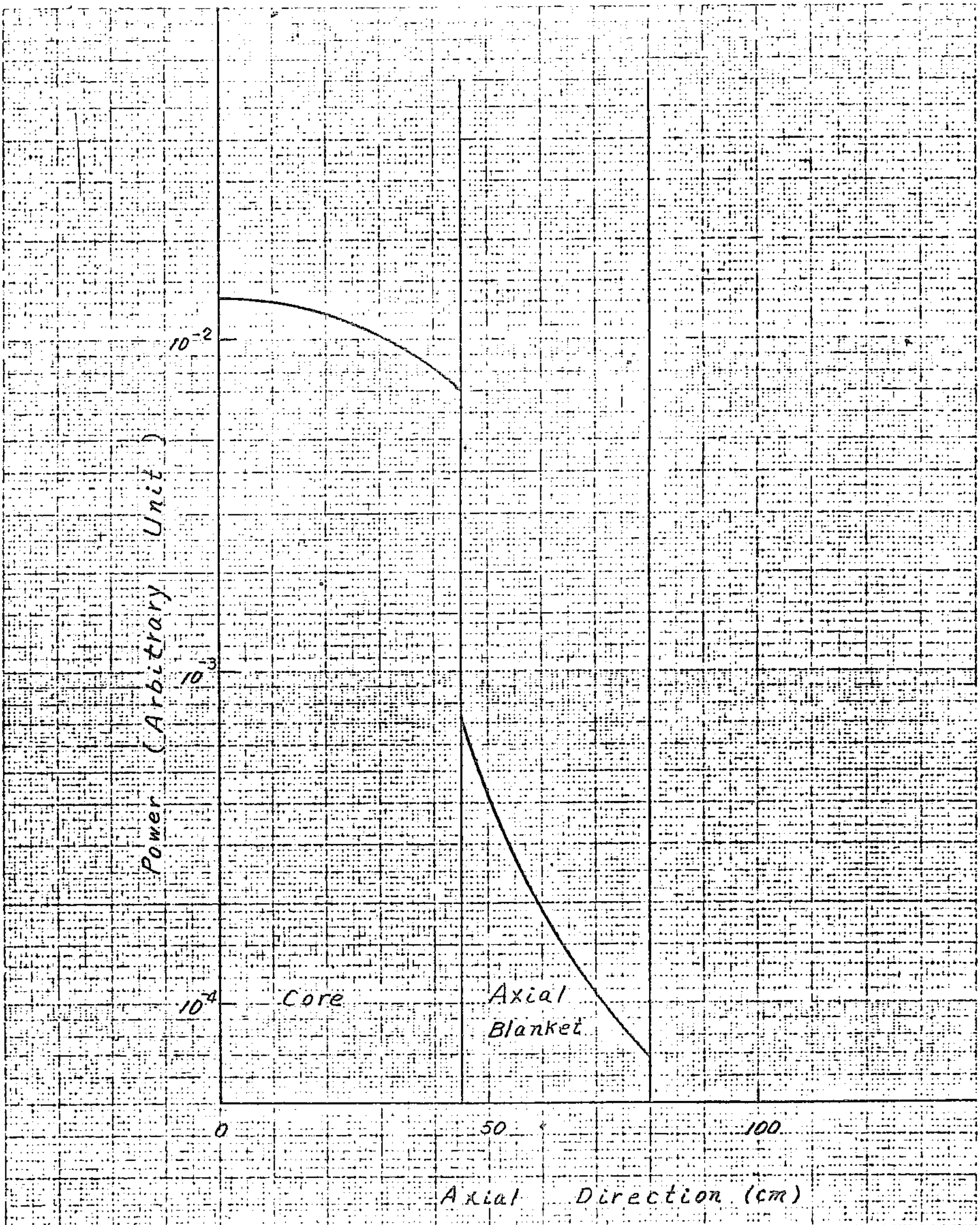

Fig. (III-2) (2) Power Distribution of "MONJU" (Axial)

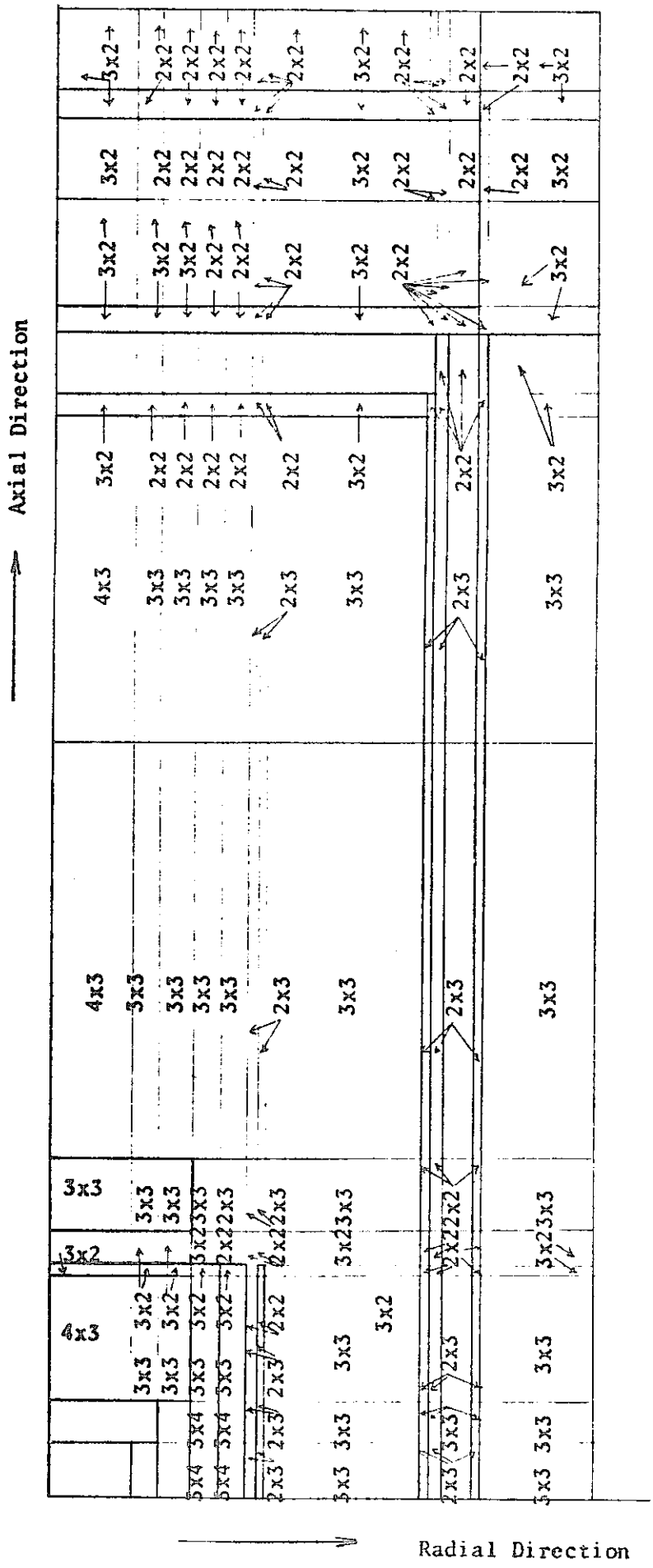

Fig. (III-3) Calculation Point of Removal Sources

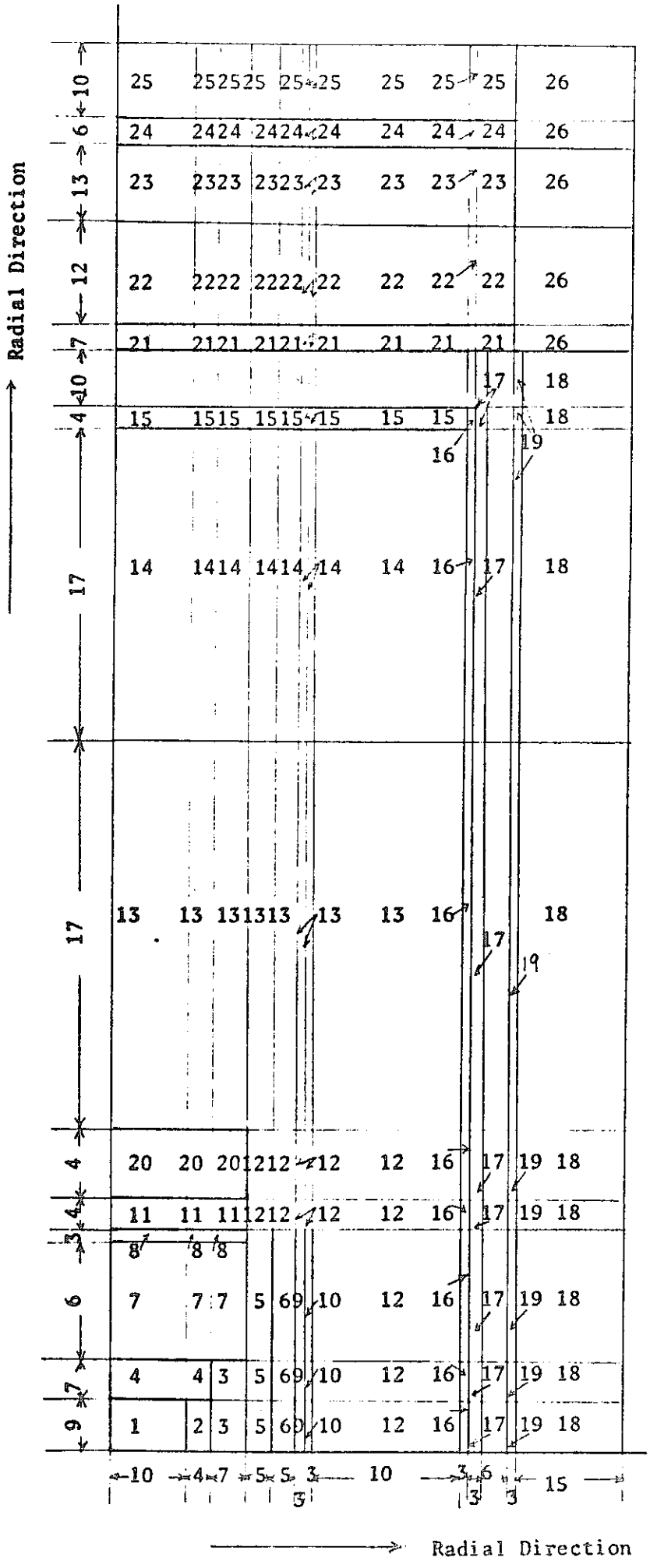

Fig. (III-4) Input of Diffusion Calculation

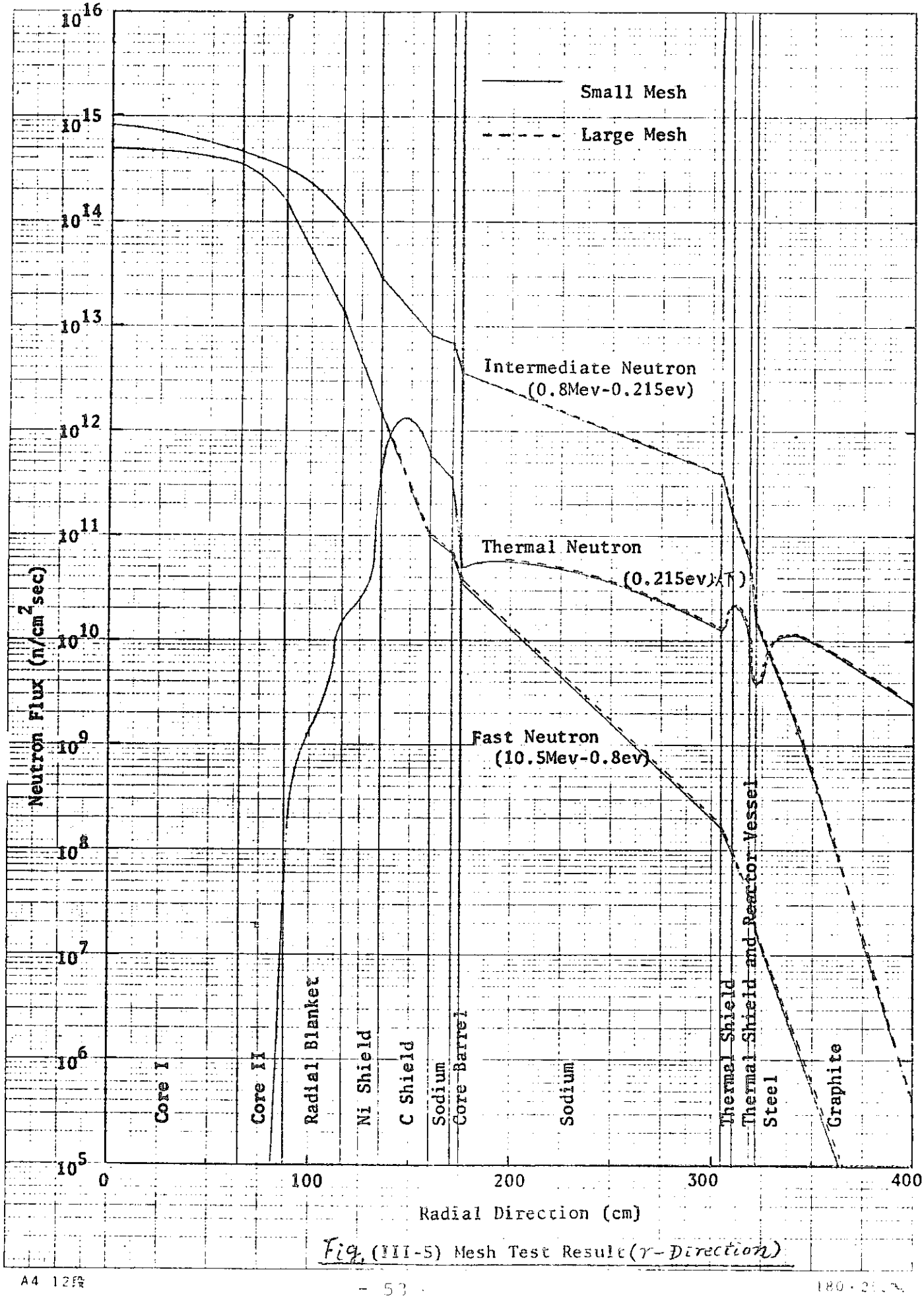

Fig. (III-5) Mesh Test Result (γ-Direction)

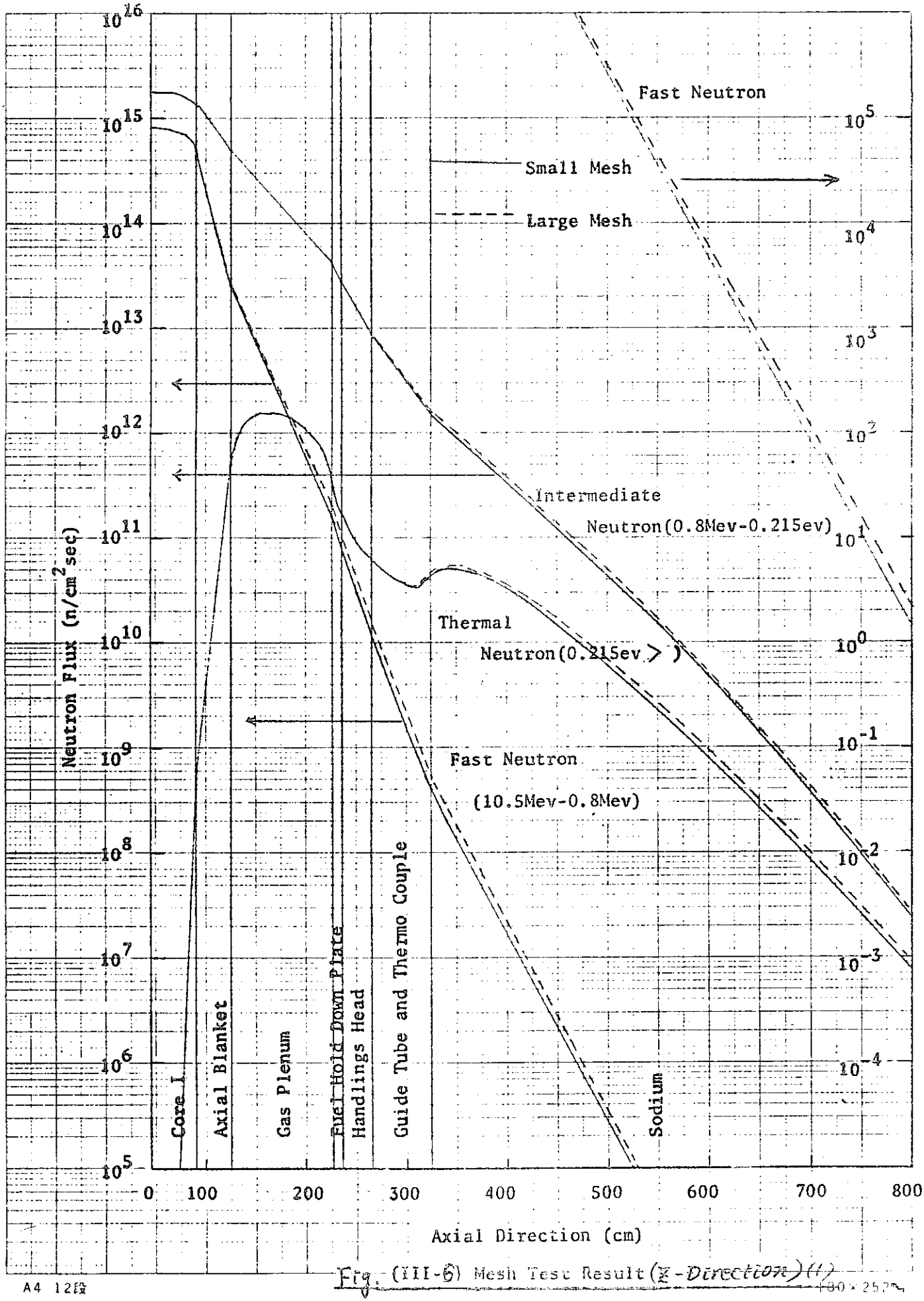

Fig. (III-6) Mesh Test Result (Z-Direction) (1)

A4 12段

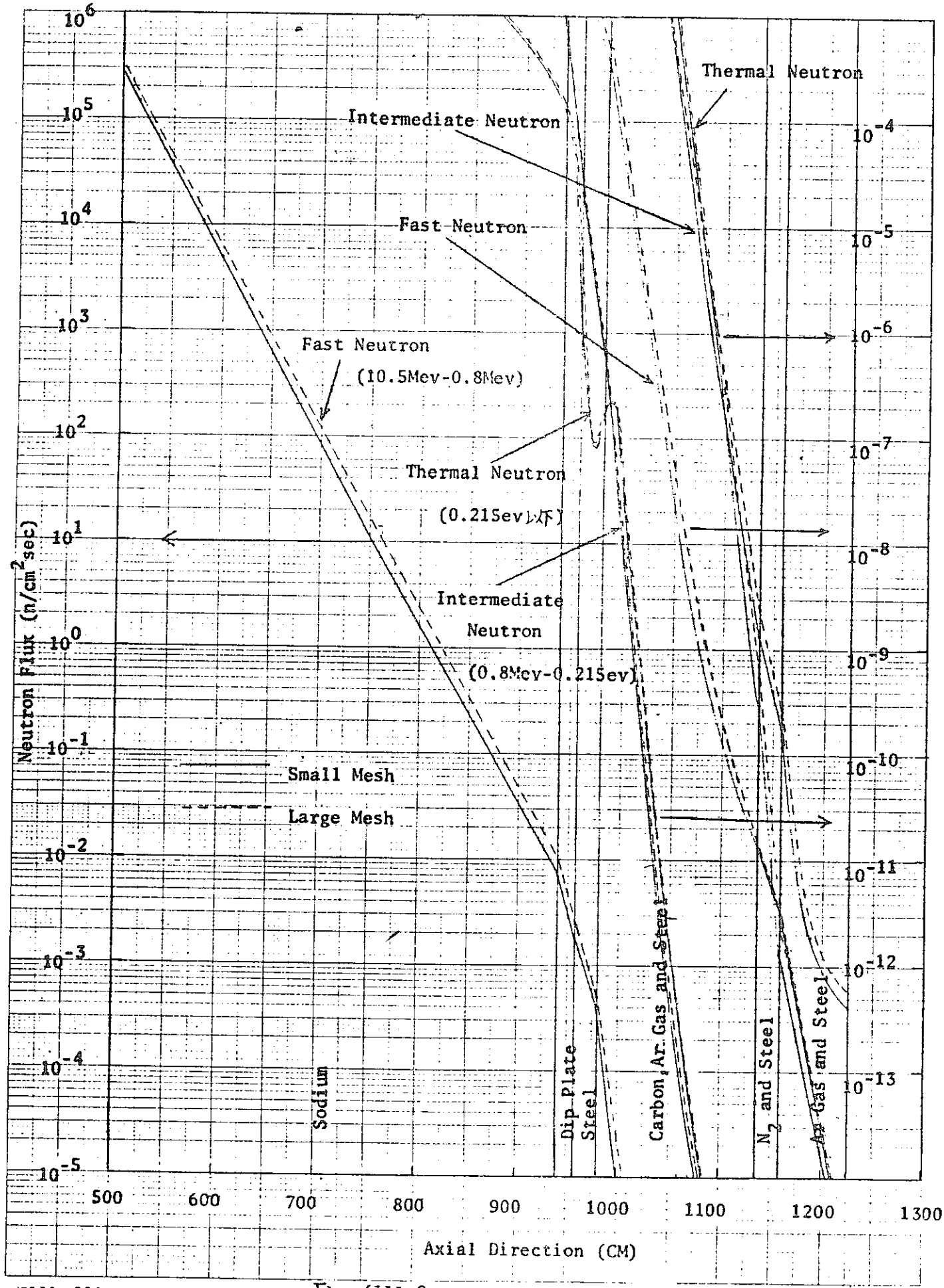

Fig. (III-6). Mesh Test Result (Z-Direction) (2)

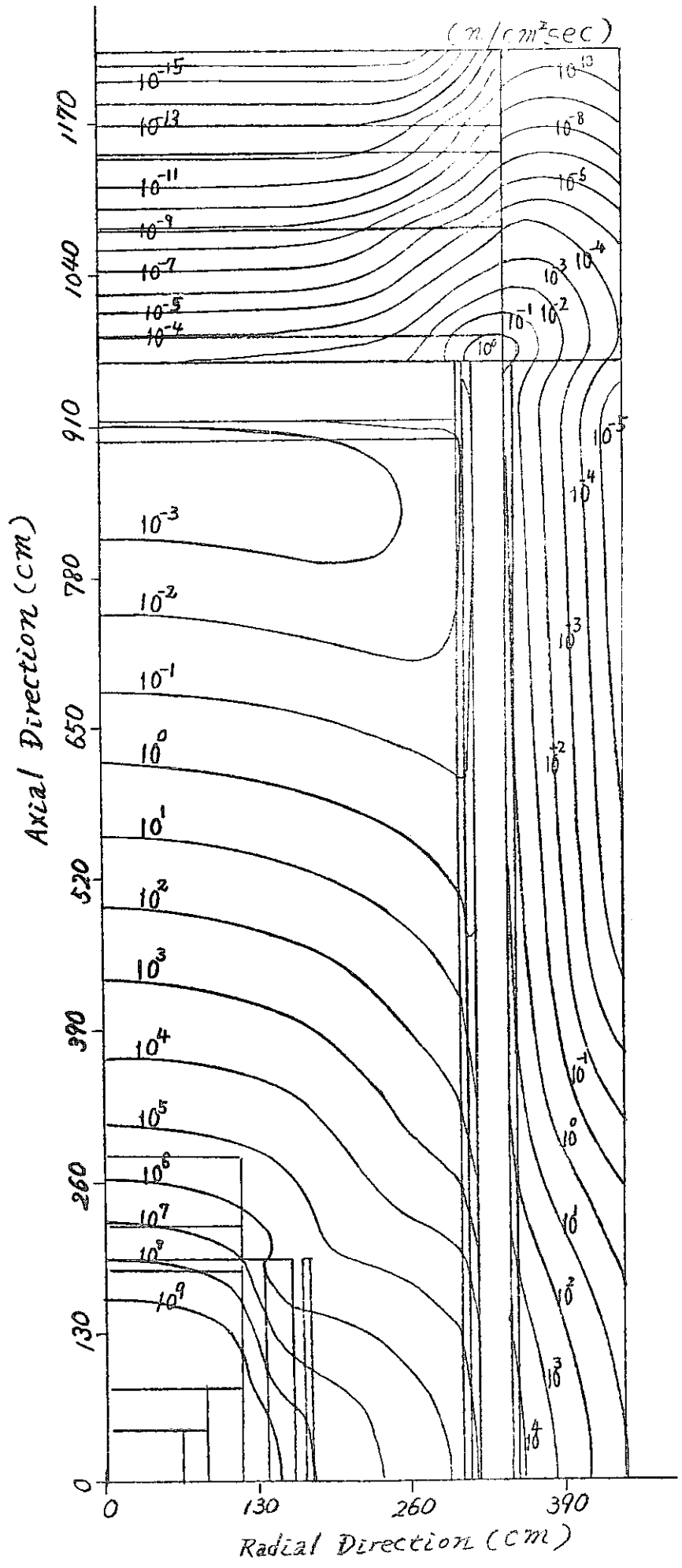

Fig. (Ⅲ-7) Neutron Contour Mapping 1 Group (10.5Mev-6.5Mev)

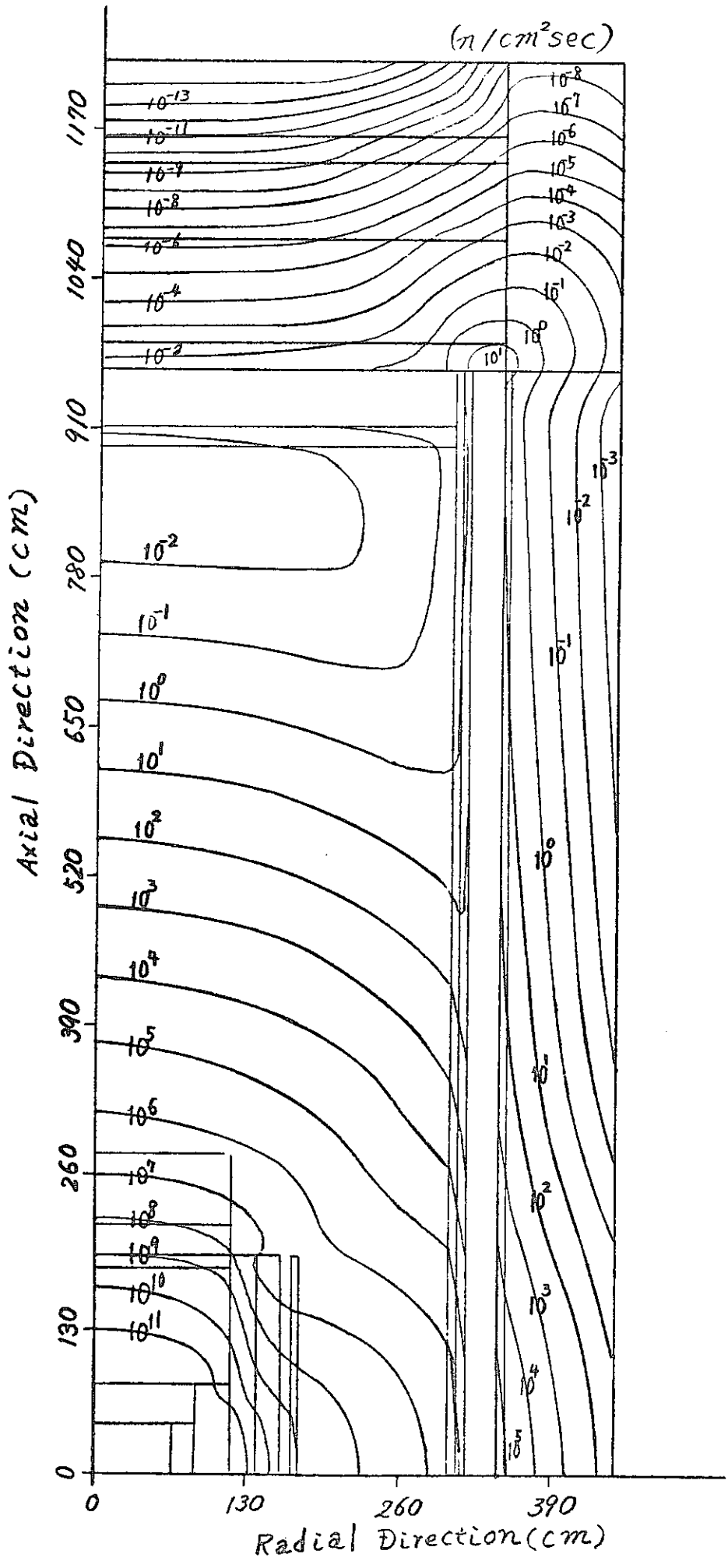

Fig(Ⅲ-8) Neutron Contour Mapping 2 Group (6.5Mev-2.5Mev)

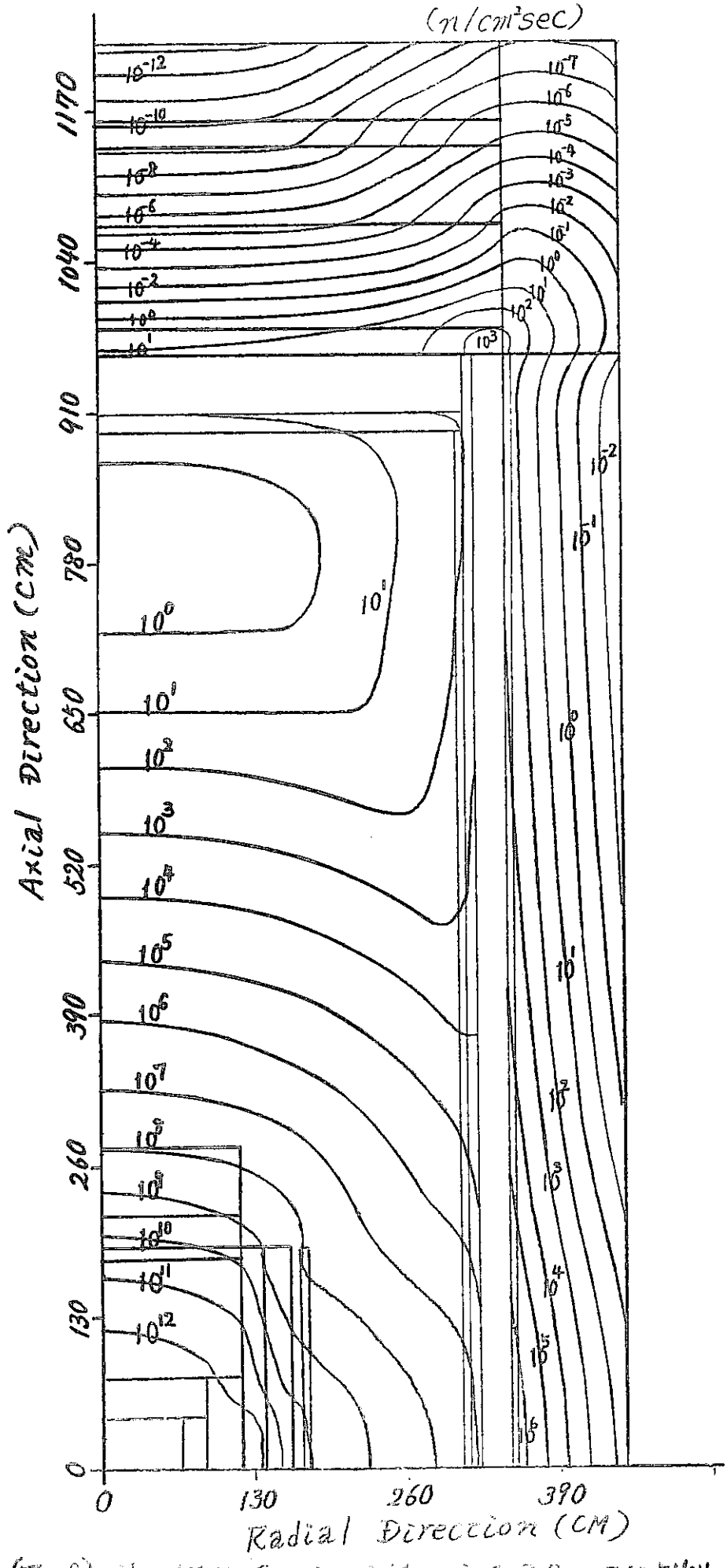

Fig.(III-9) Neutron Contour Mapping 3 Group (2.5MeV - 0.8MeV)

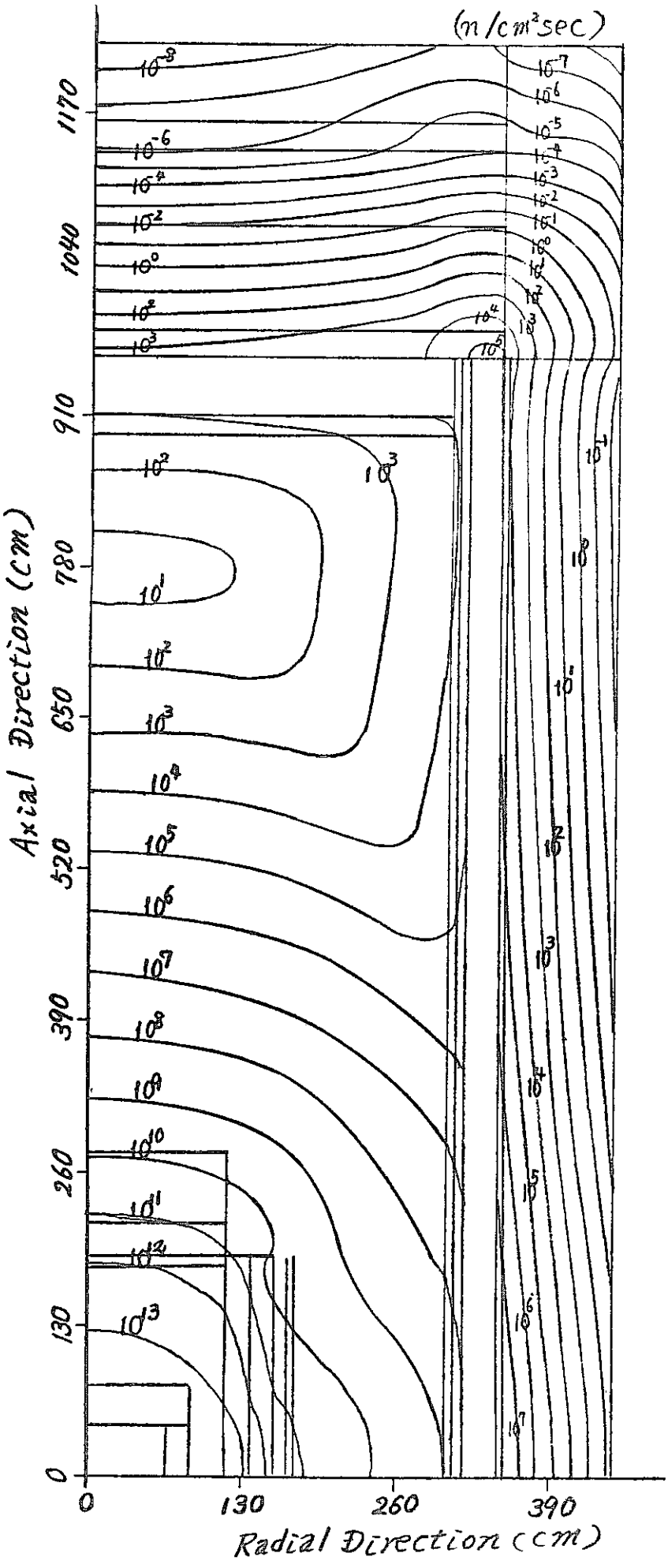

Fig. (Ⅲ-10) Neutron Contour Mapping 4 Group (0.8Mev-46.5Kev)

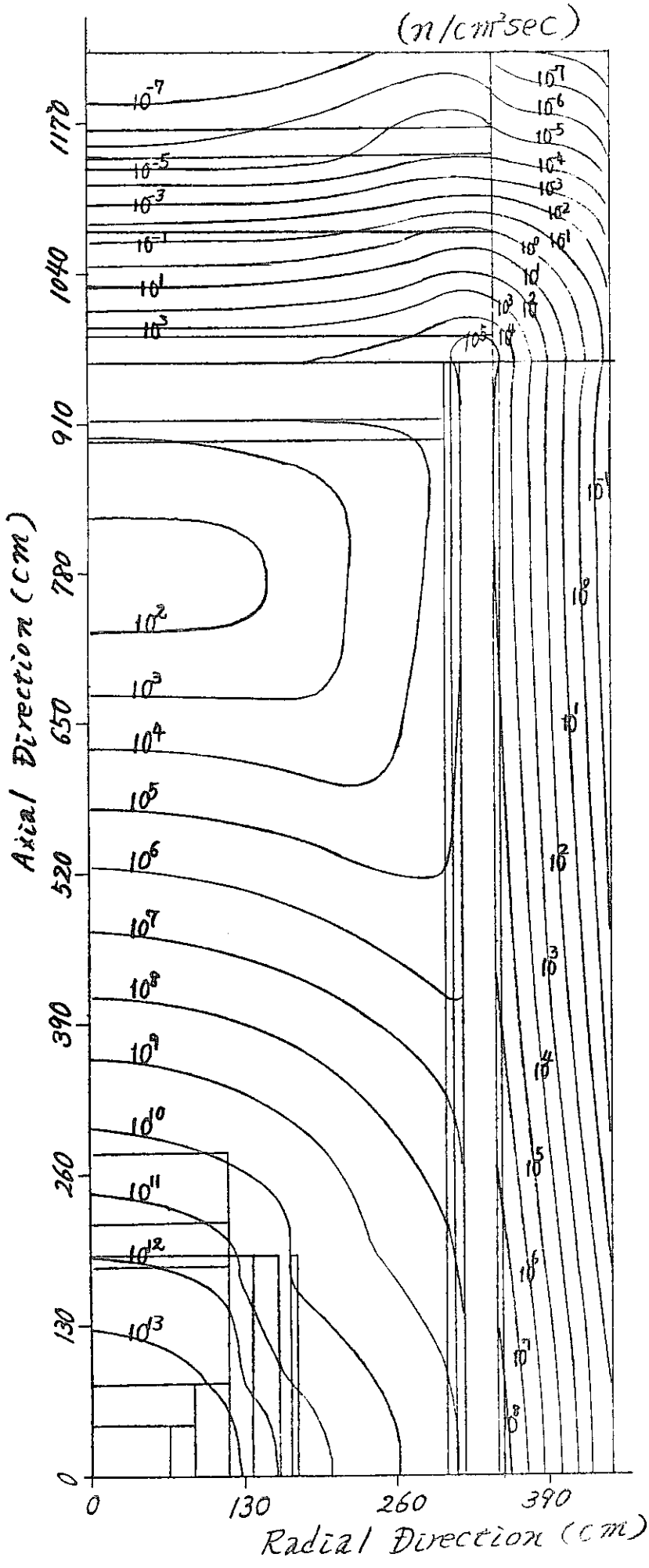

Fig.(Ⅲ-11) Neutron Contour Mapping 5 Group (46.5Kev-2.15Kev)

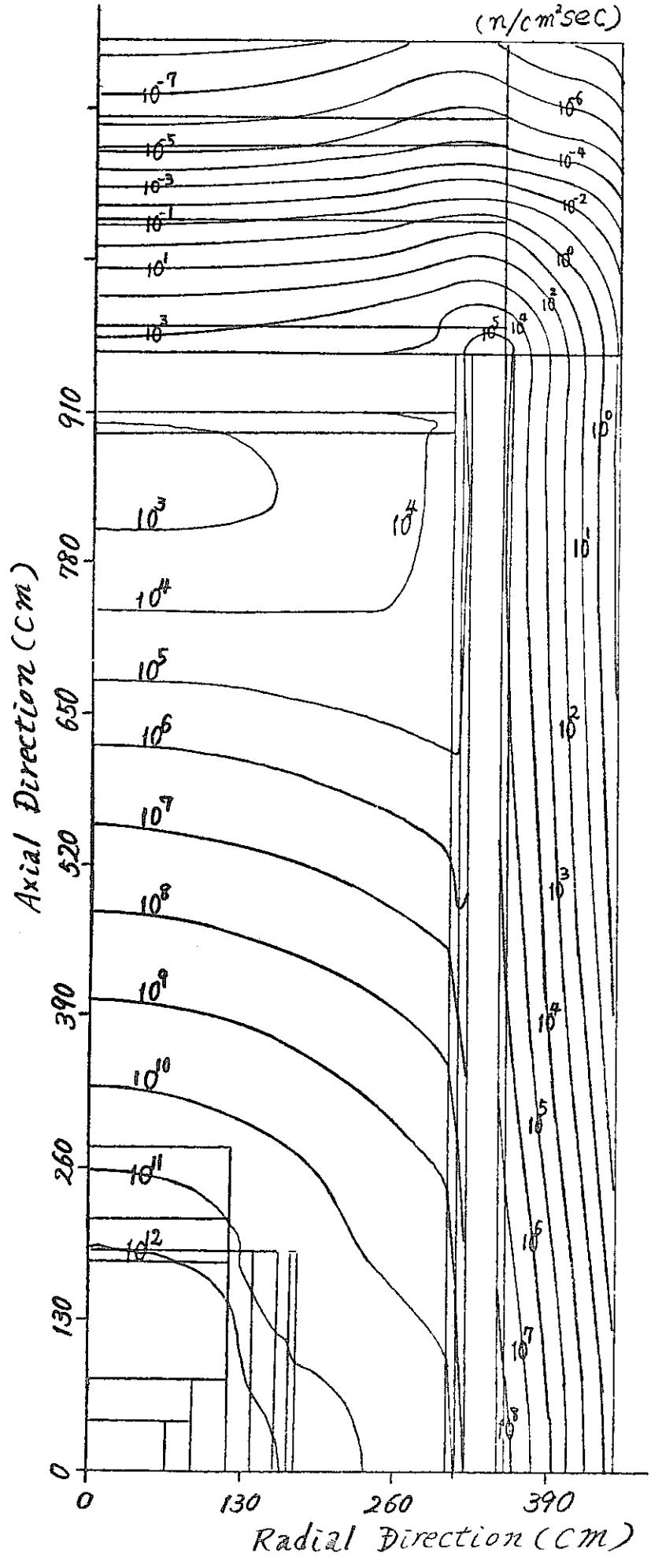

Fig.(Ⅲ-12) Neutron Contour Mapping 6 Group (2.15Kev-0.1Kev)

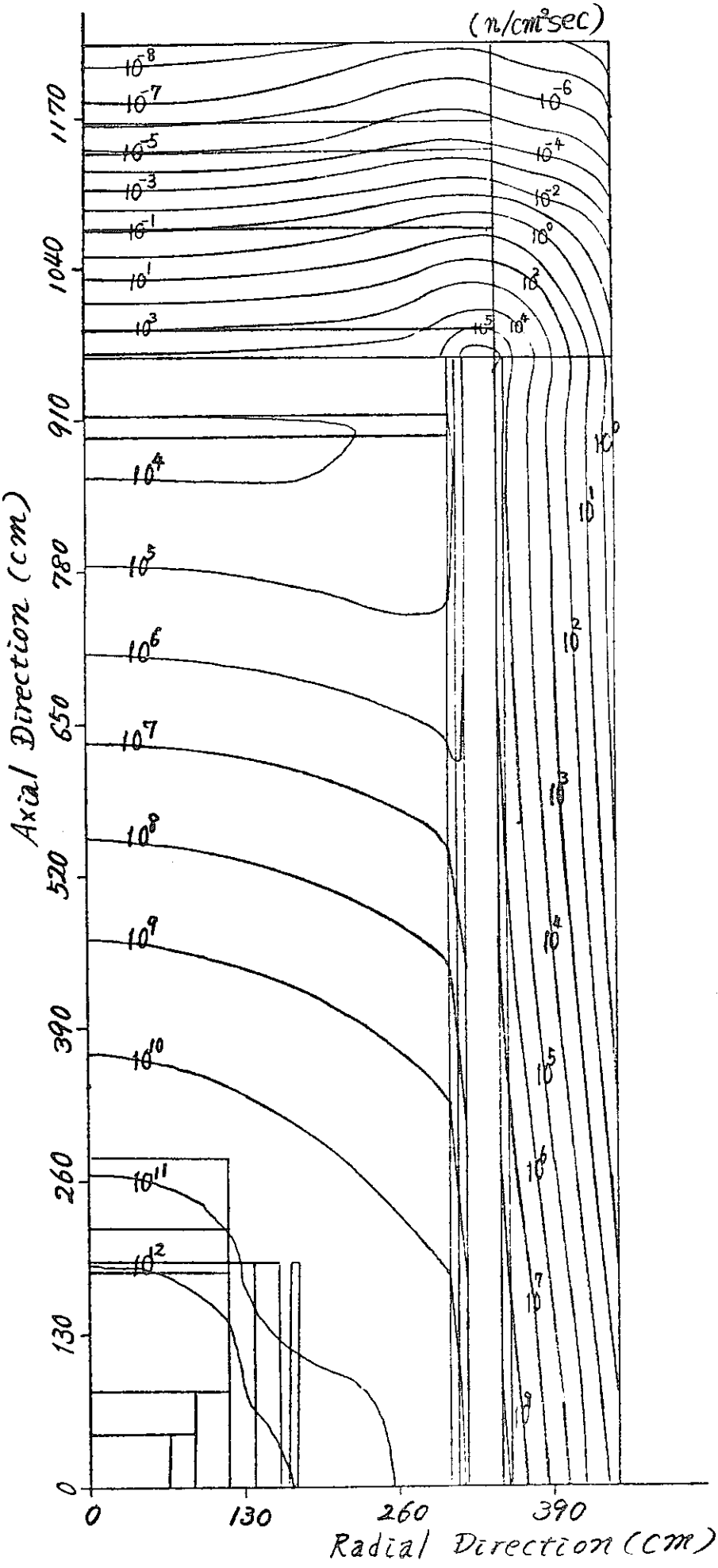

Fig.(Ⅲ-13) Neutron Contour Mapping 7 Group (0.1Kev-4.65ev)

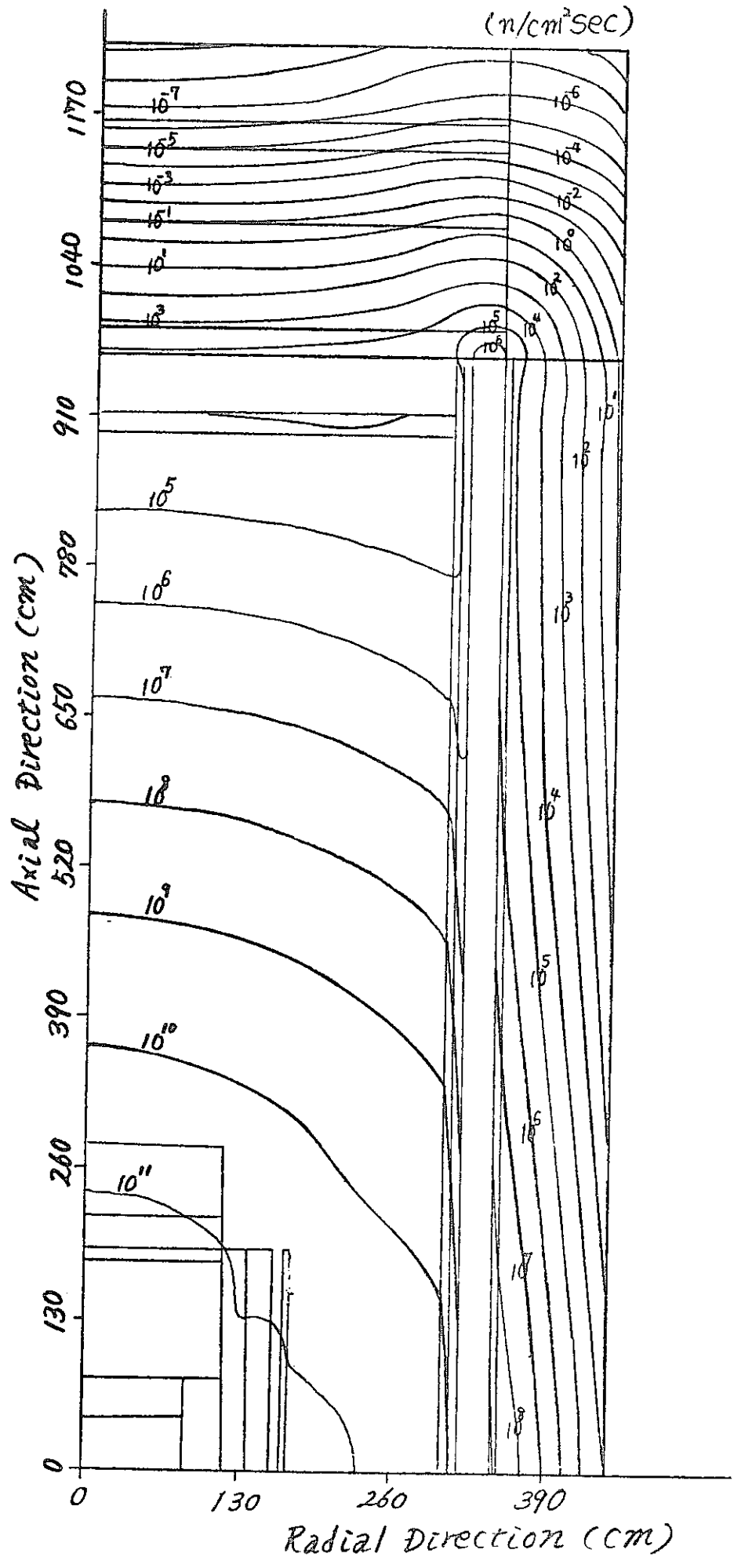

Fig.(Ⅲ-14) Neutron Contour Mapping 8Group(4.65ev-0.215ev)

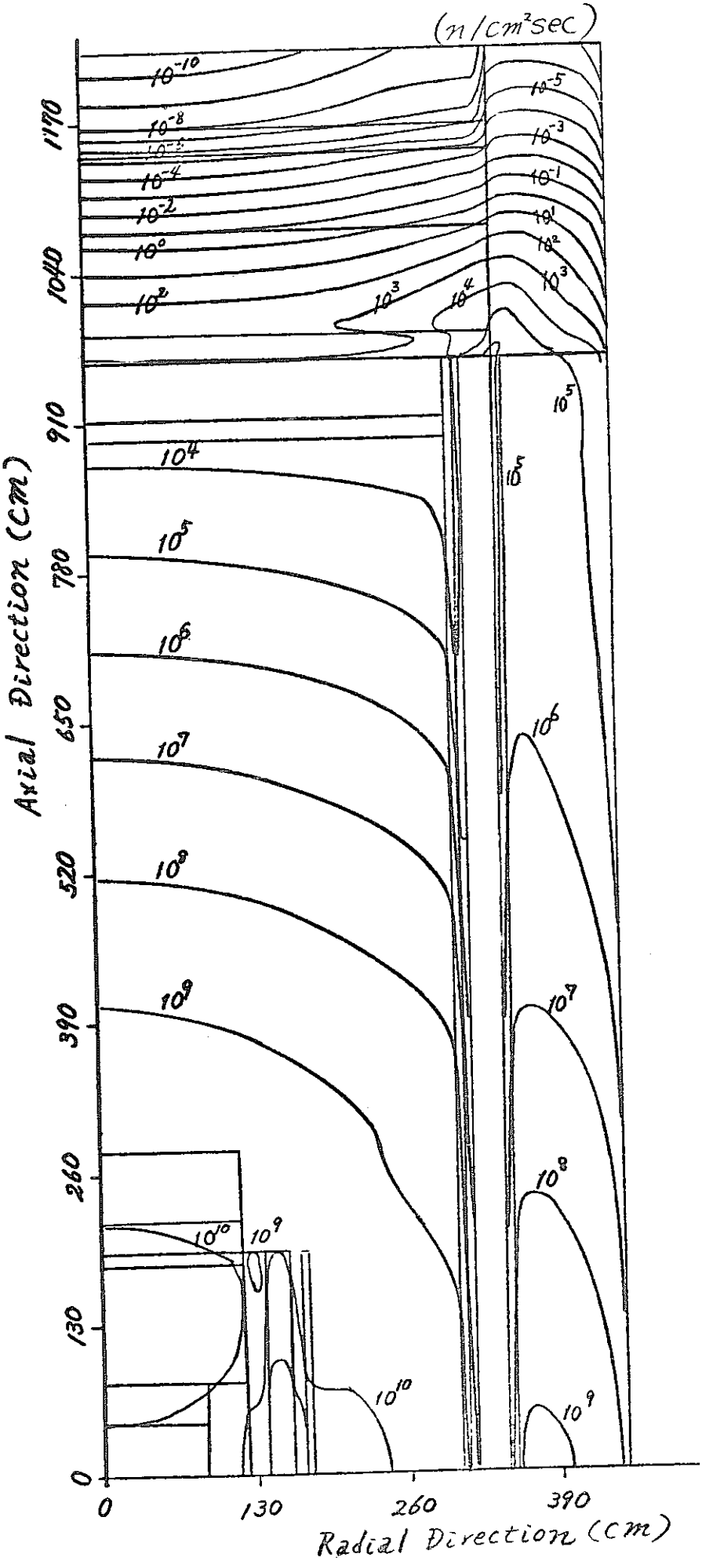

Fig.(III-15) Neutron Contour Mapping 9 Group (0.215eV >)

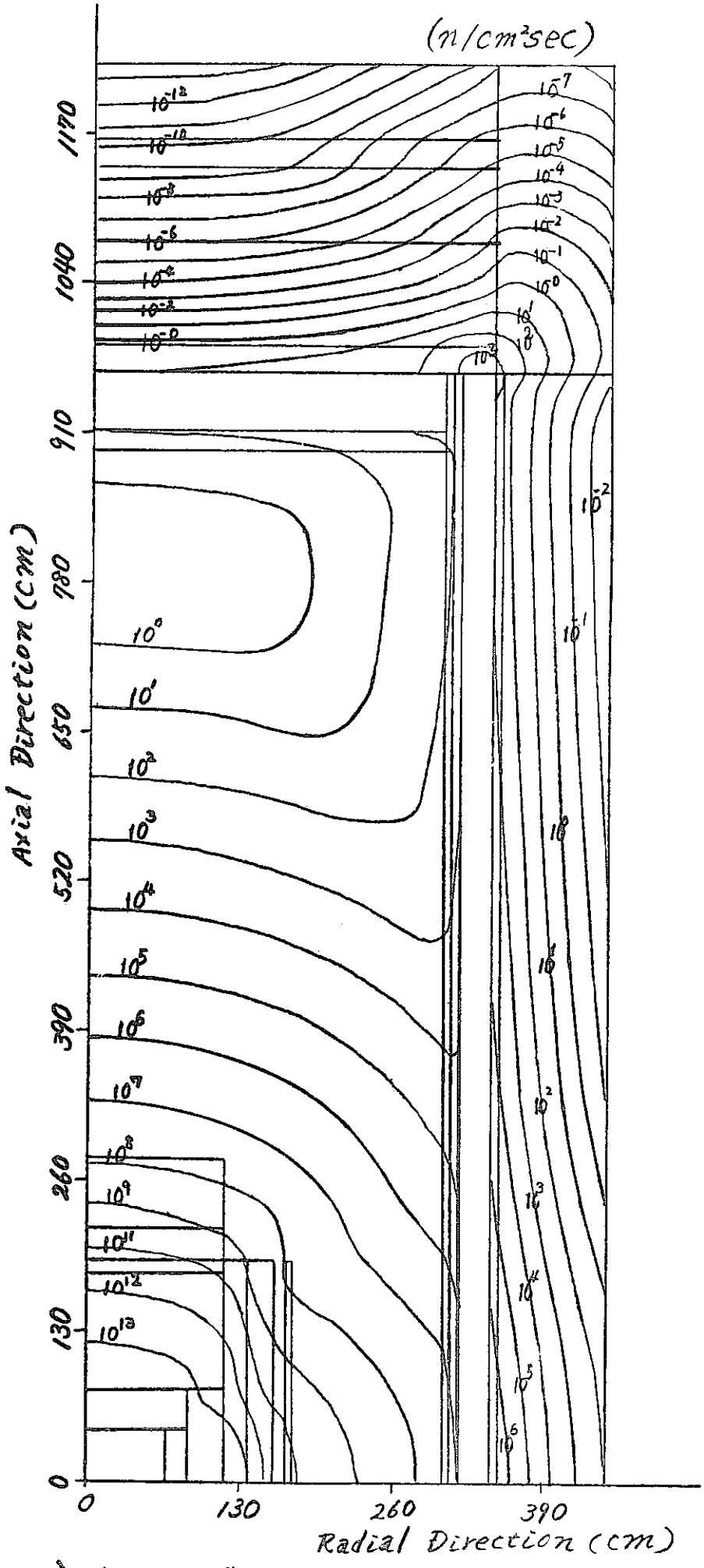

Fig.(Ⅲ-16) Neutron Contour Mapping Fast Neutron
(10.5MeV-0.8MeV)

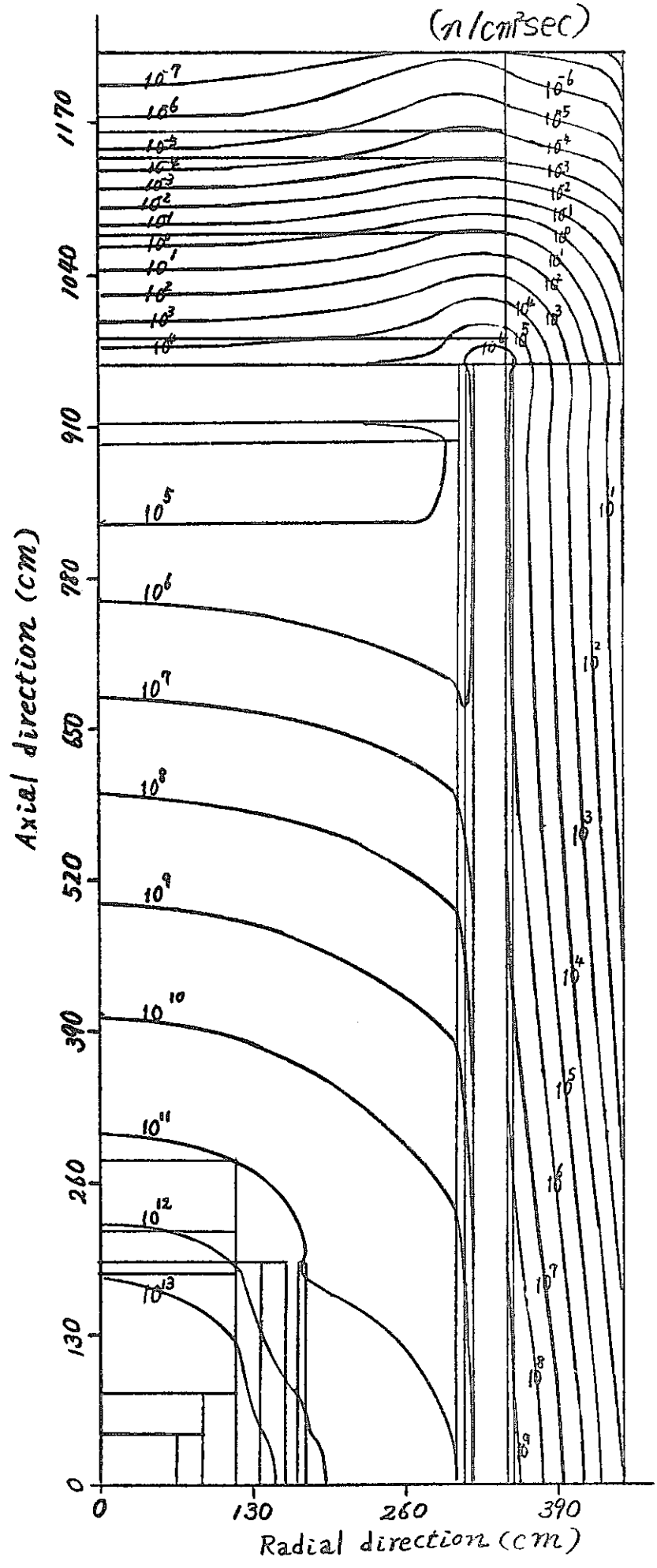

Fig(Ⅲ-17) Neutron Contour Mapping Intermediate Neutron (0.8 Mev - 0.215 eV)

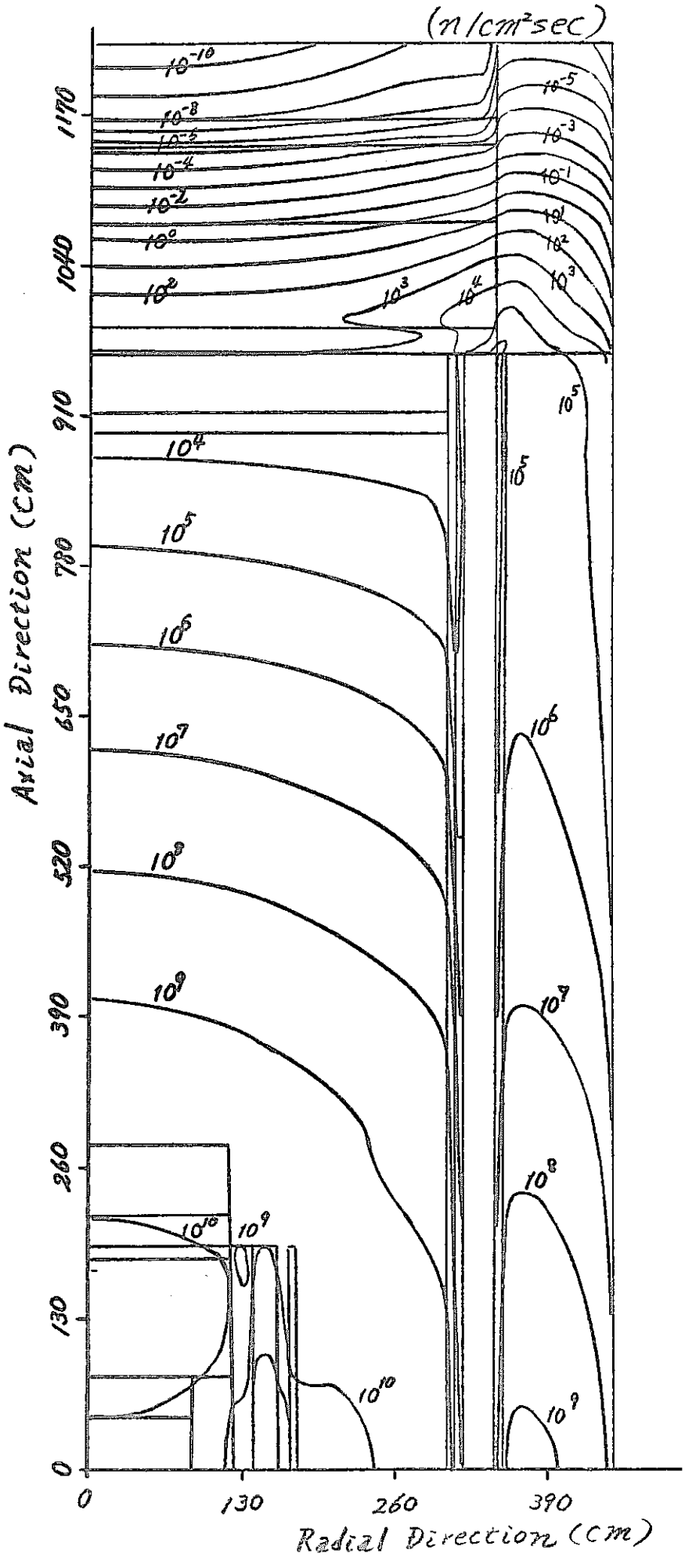

Fig.(III-18) Neutron Contour Mapping Thermal Neutron (0.215ev)

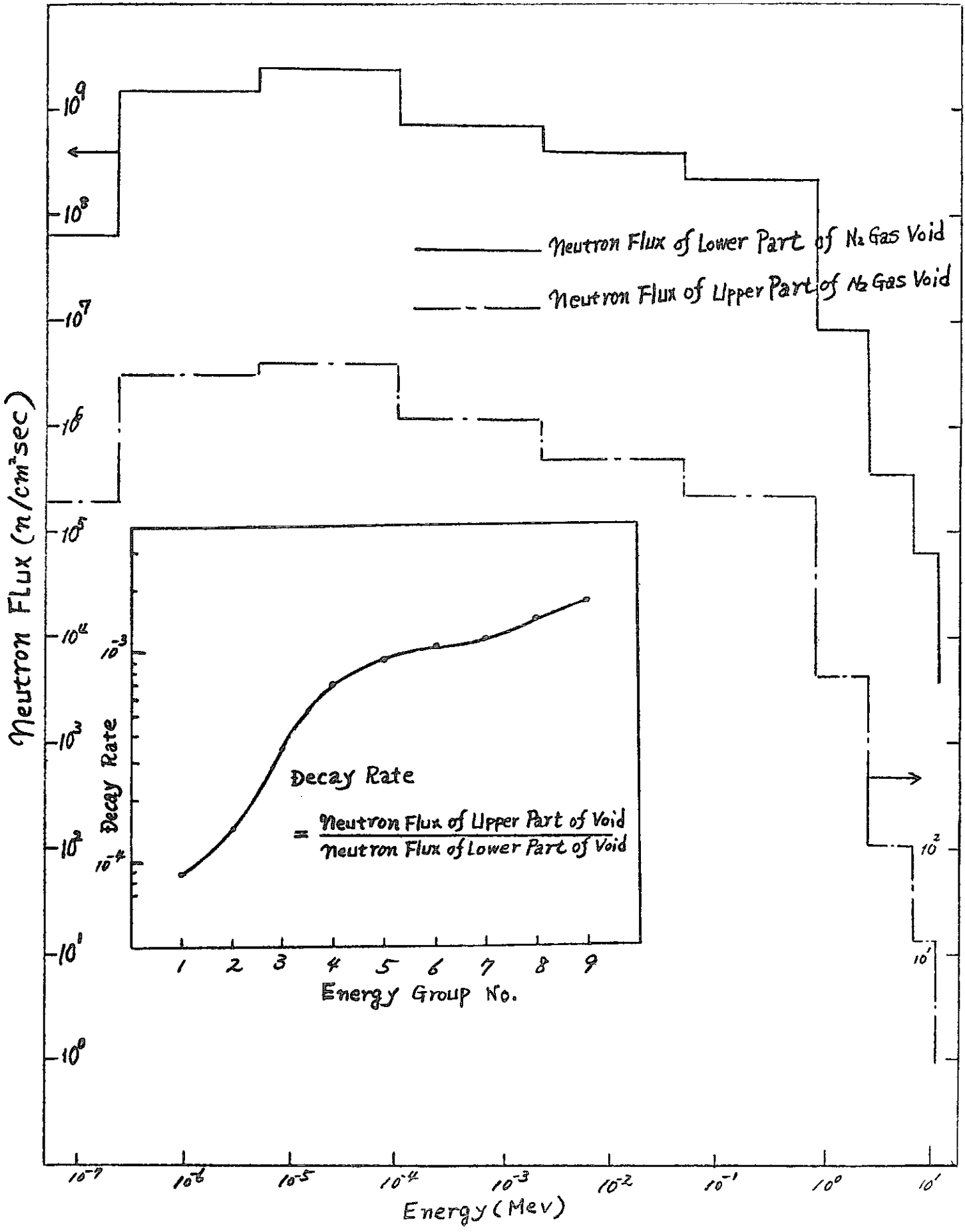

Fig.(Ⅲ-19) Comparison of Neutron Flux between at Lower Part of N_2 Gas Void and at Upper Part

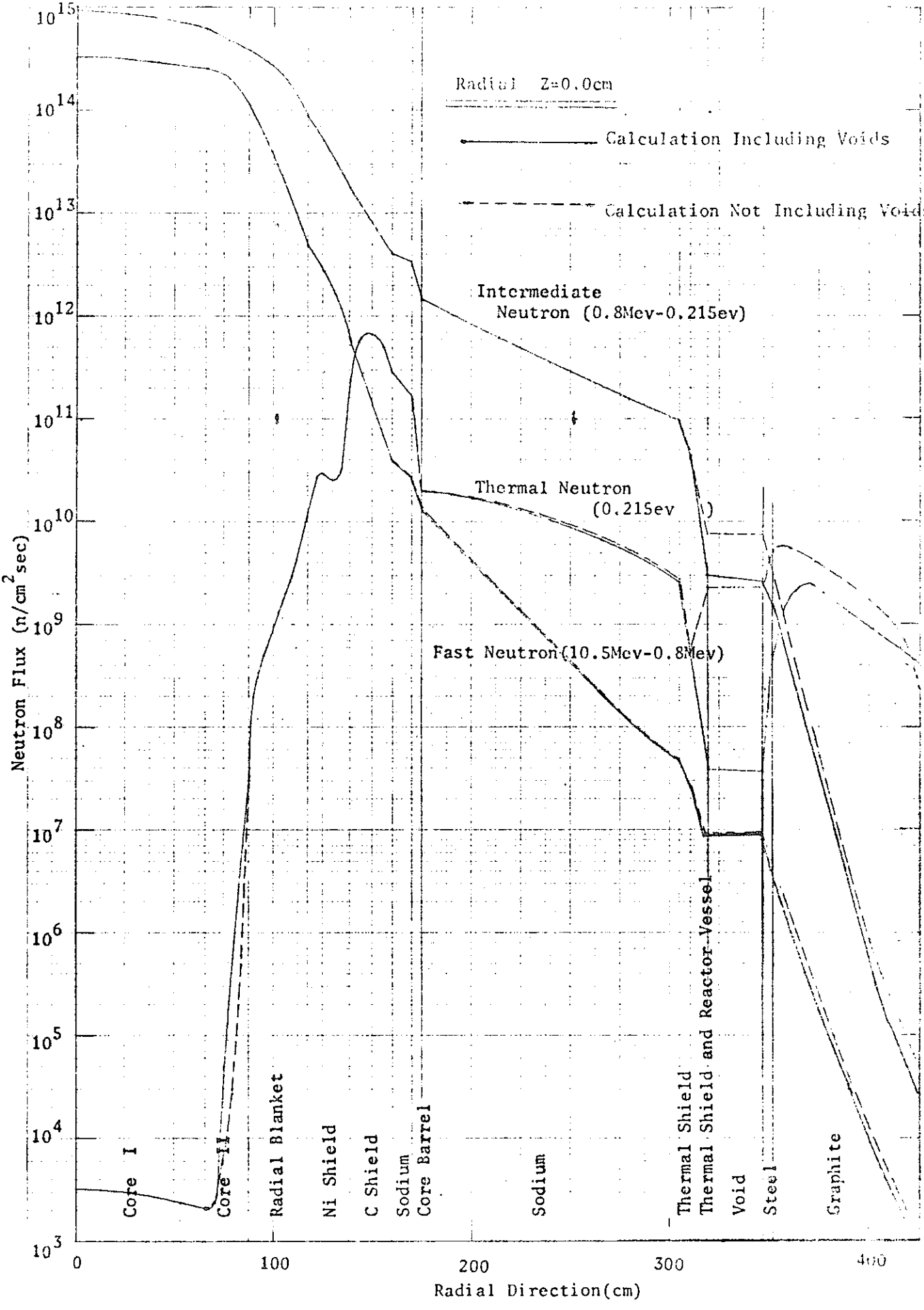

Fig.(III-20) Neutron Attenuation Distribution Z=0.0cm

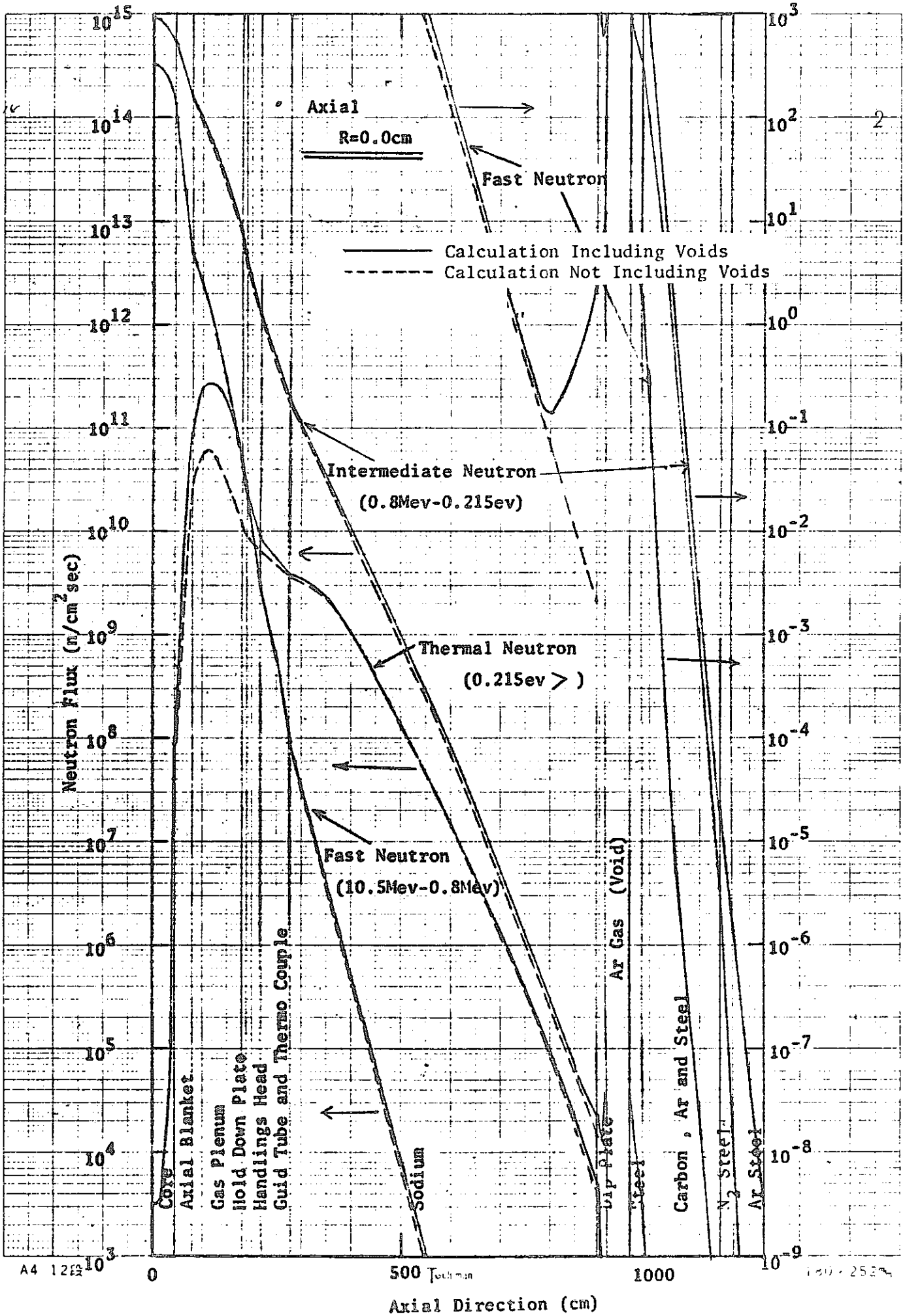

Fig. (II-21) Neutron Attenuation Distribution $r=0.0$

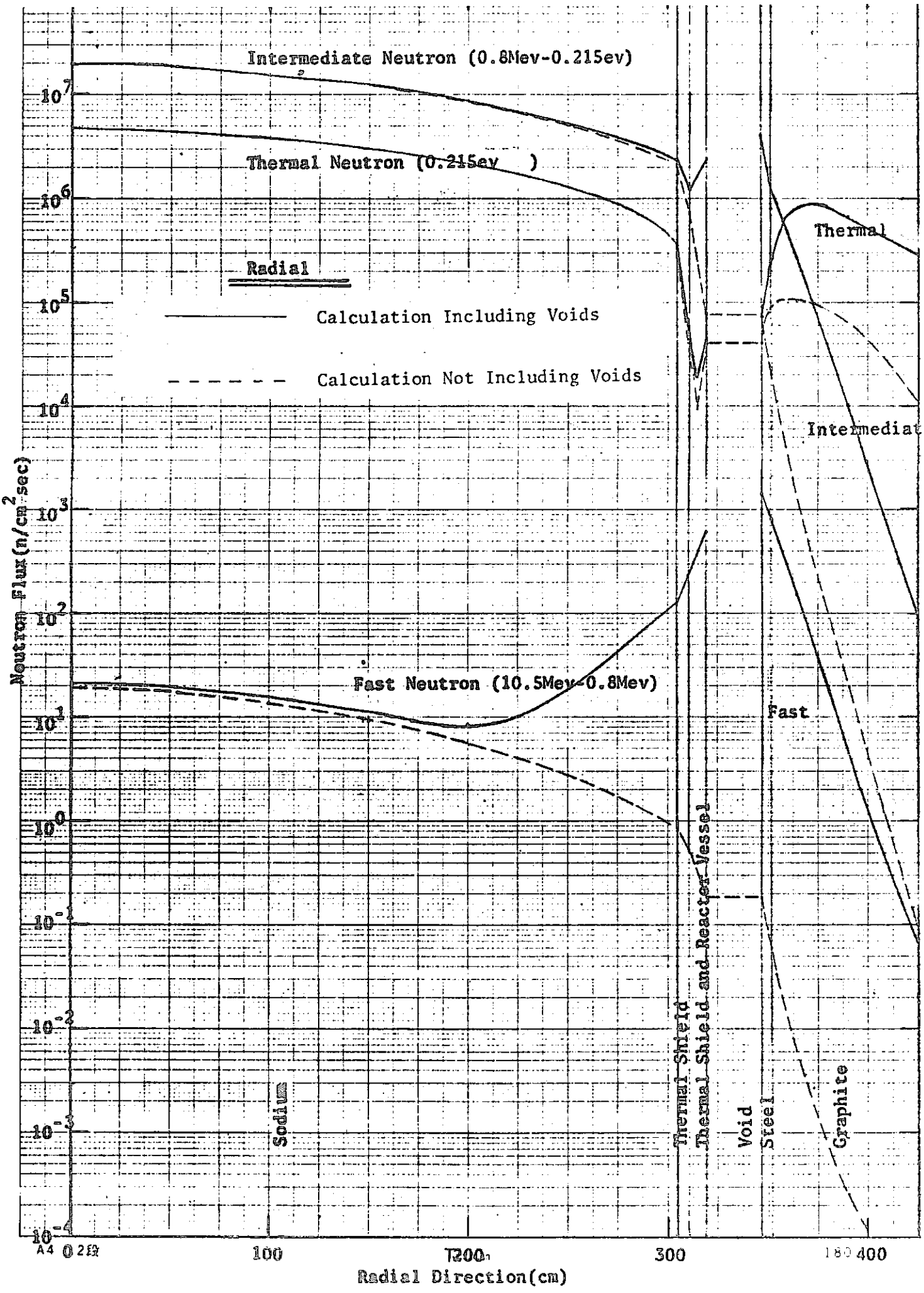

Fig. (III-22) Neutron Attenuation Distribution Z=~650cm

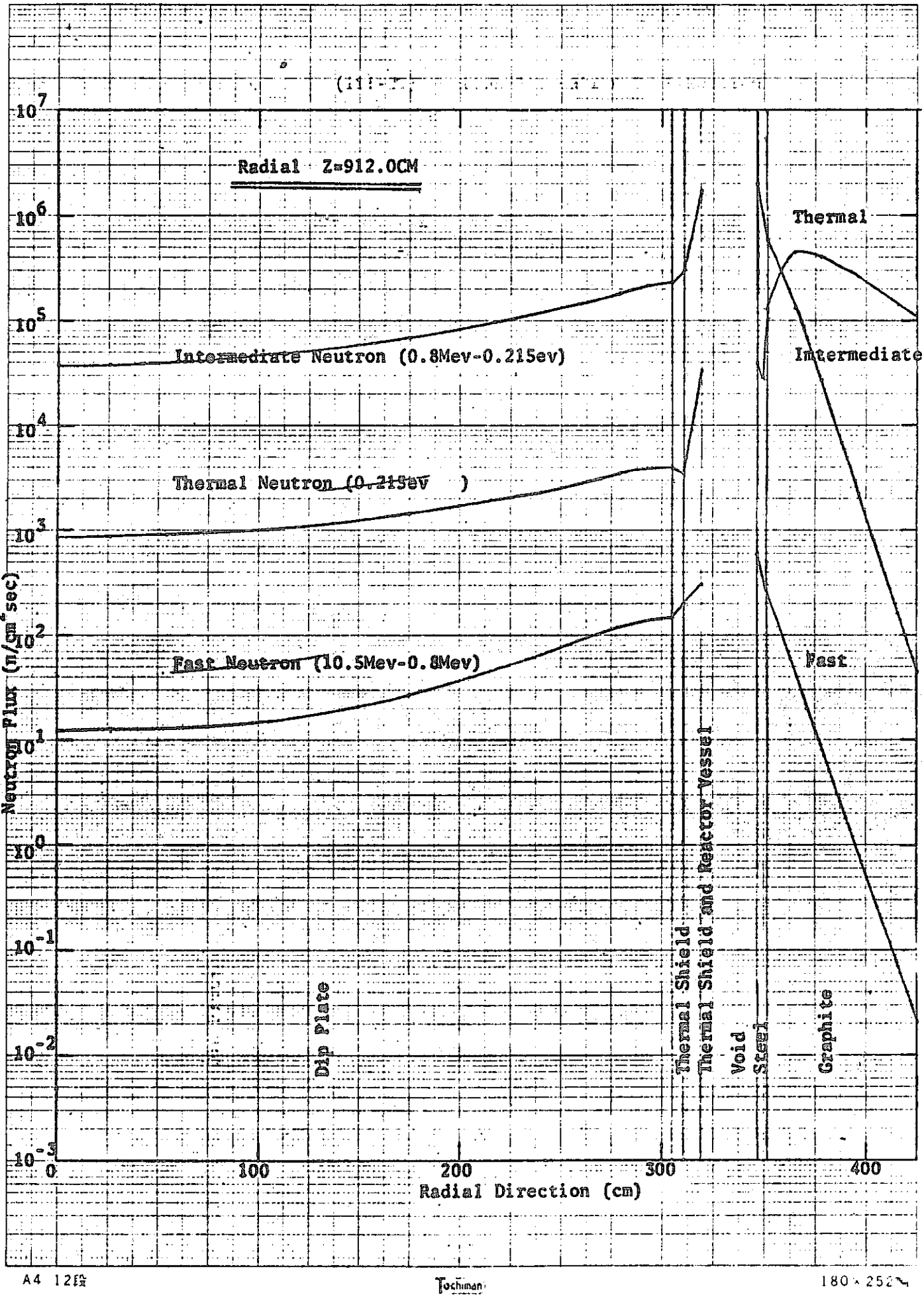

A4 12段 Tochiman 180×252

Fig.(II-23) Neutron Attenuation Distribution Z=912.0cm

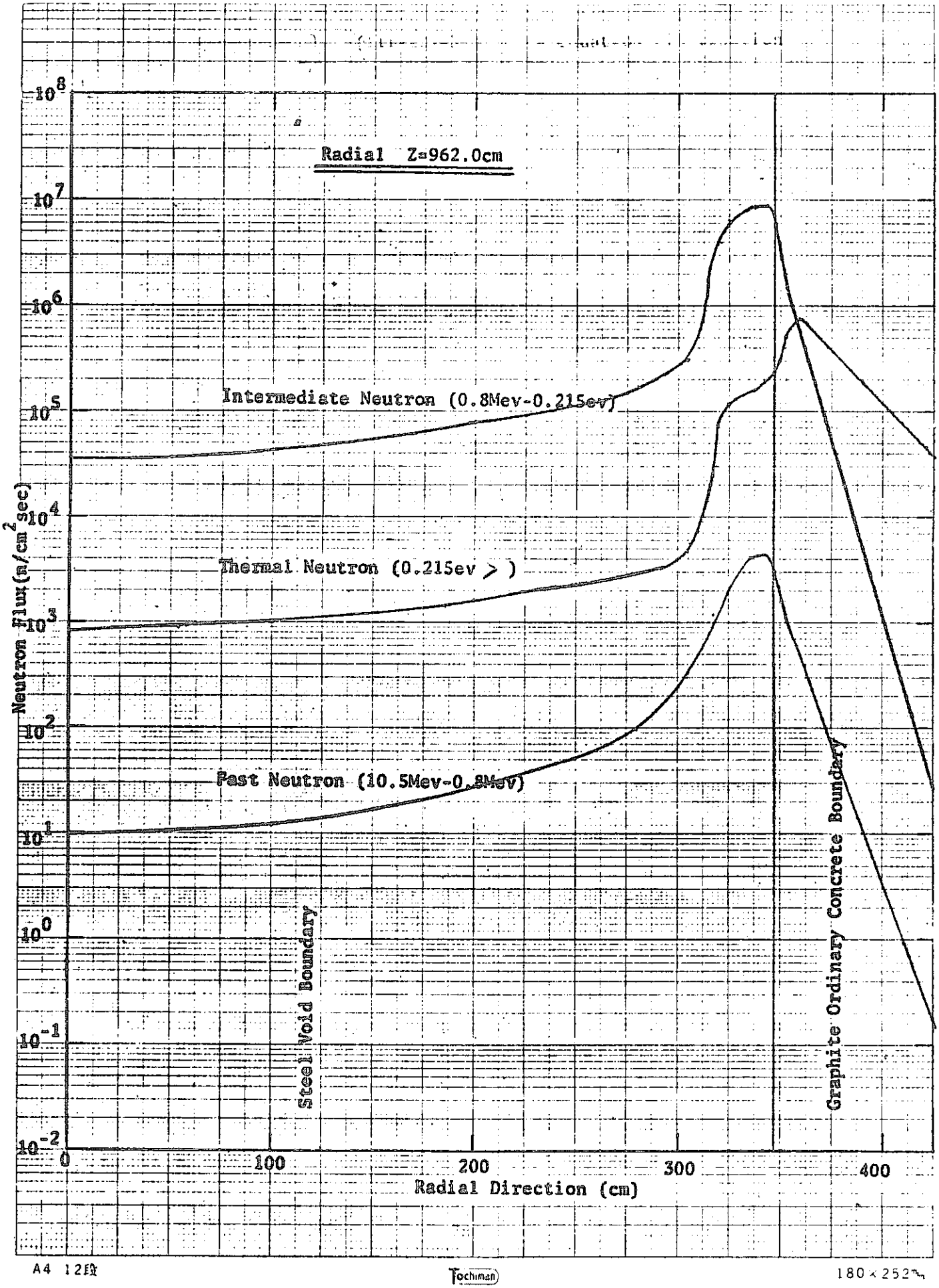

Fig. (Ⅲ-24) Neutron Attenuation Distribution Z=962.0cm

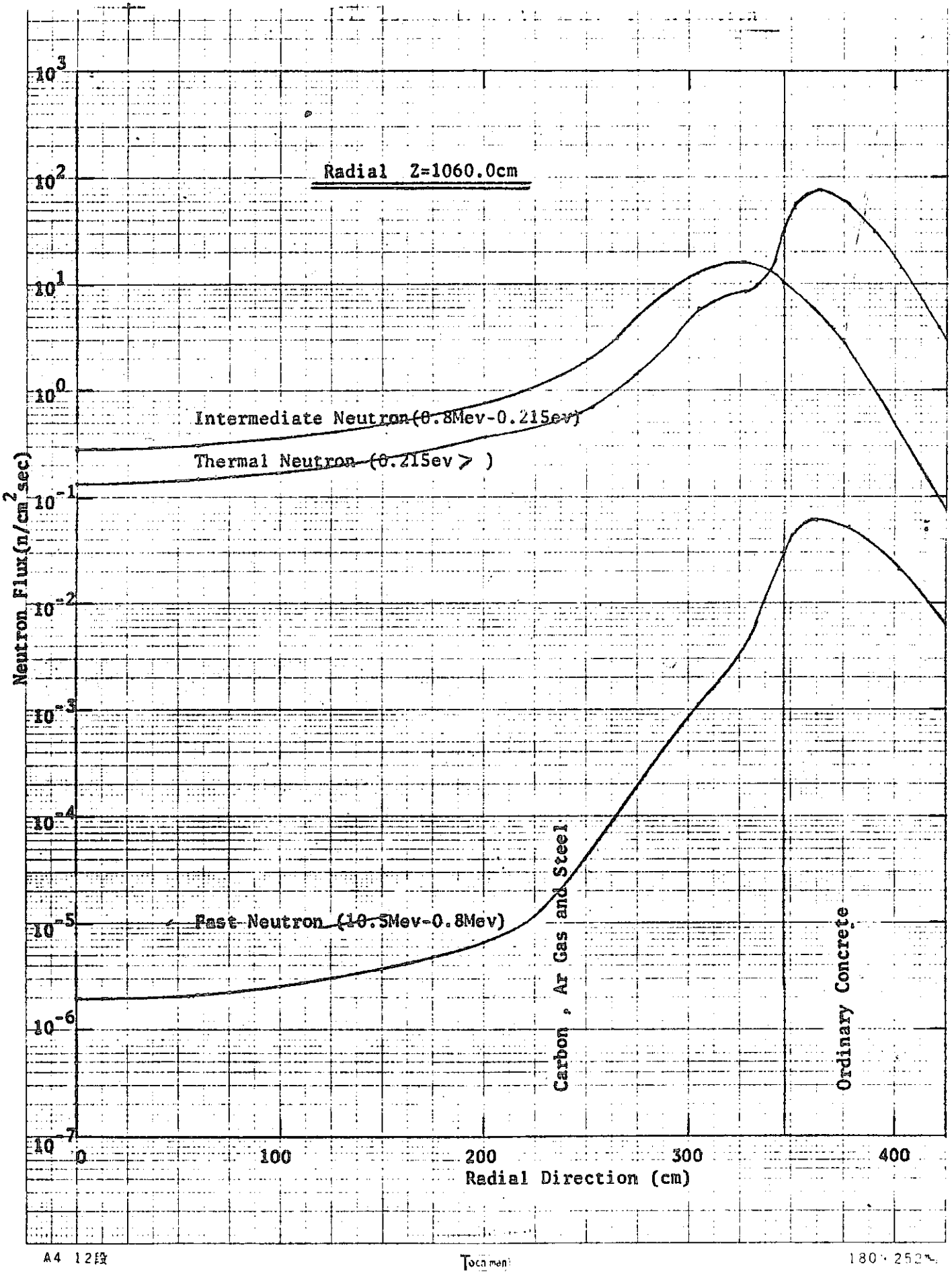

Fig. (Ⅲ-25) Neutron Attenuation Distribution Z=1060.0cm

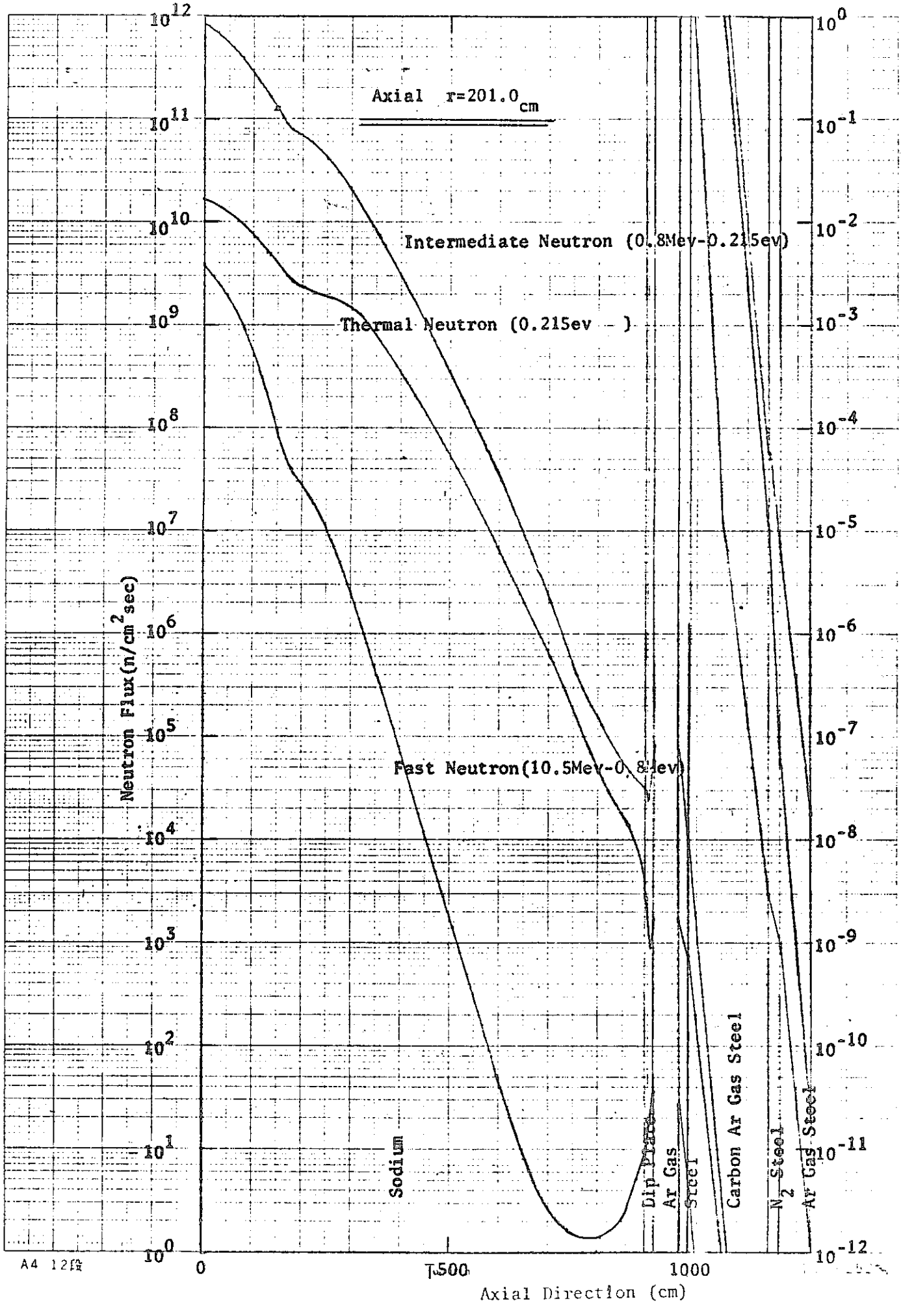

Fig.(Ⅲ-26) Neutron Attenuation Distribution r=201.0 cm

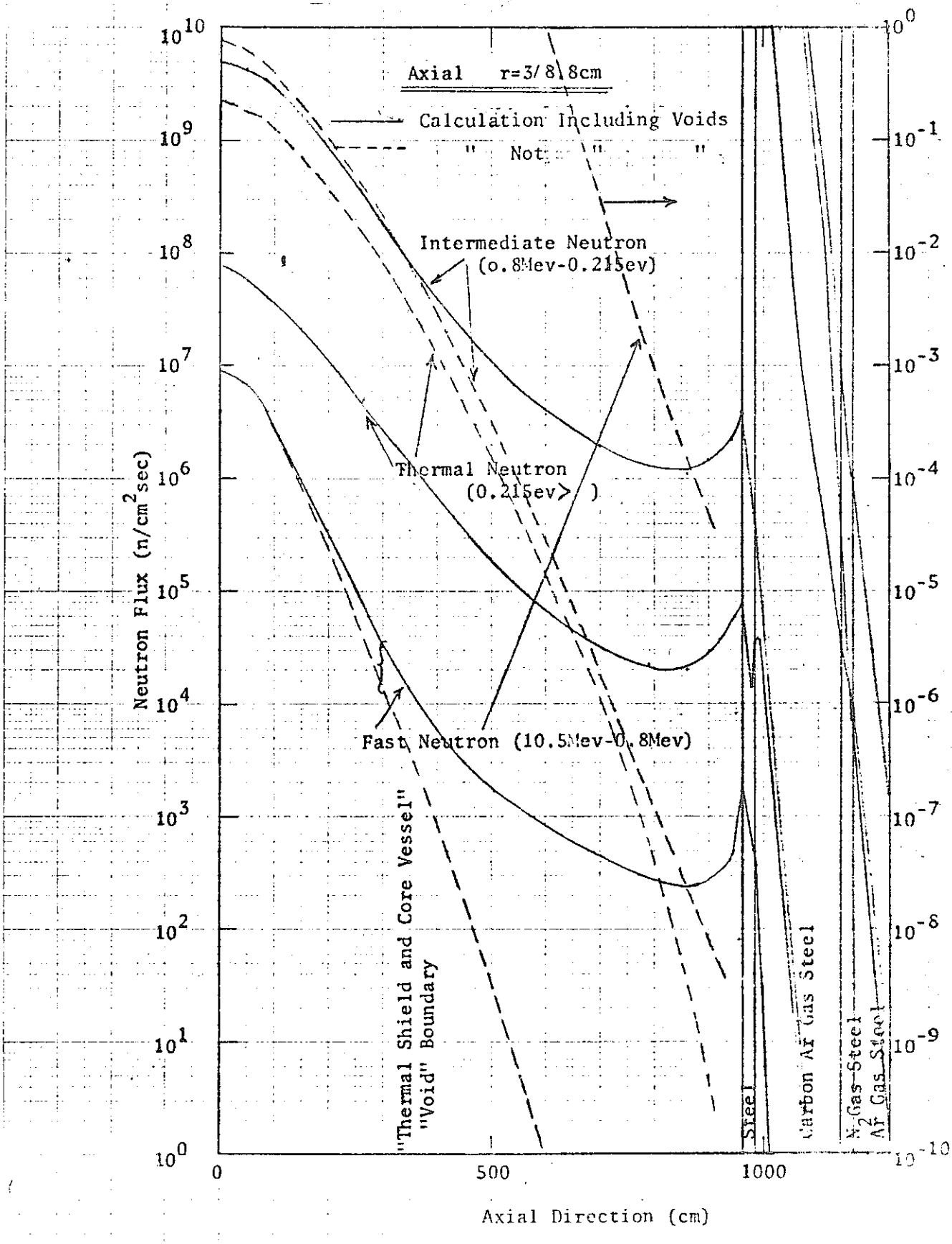

Fig.(III-27) Neutron Attenuation Distribution r=318.8cm

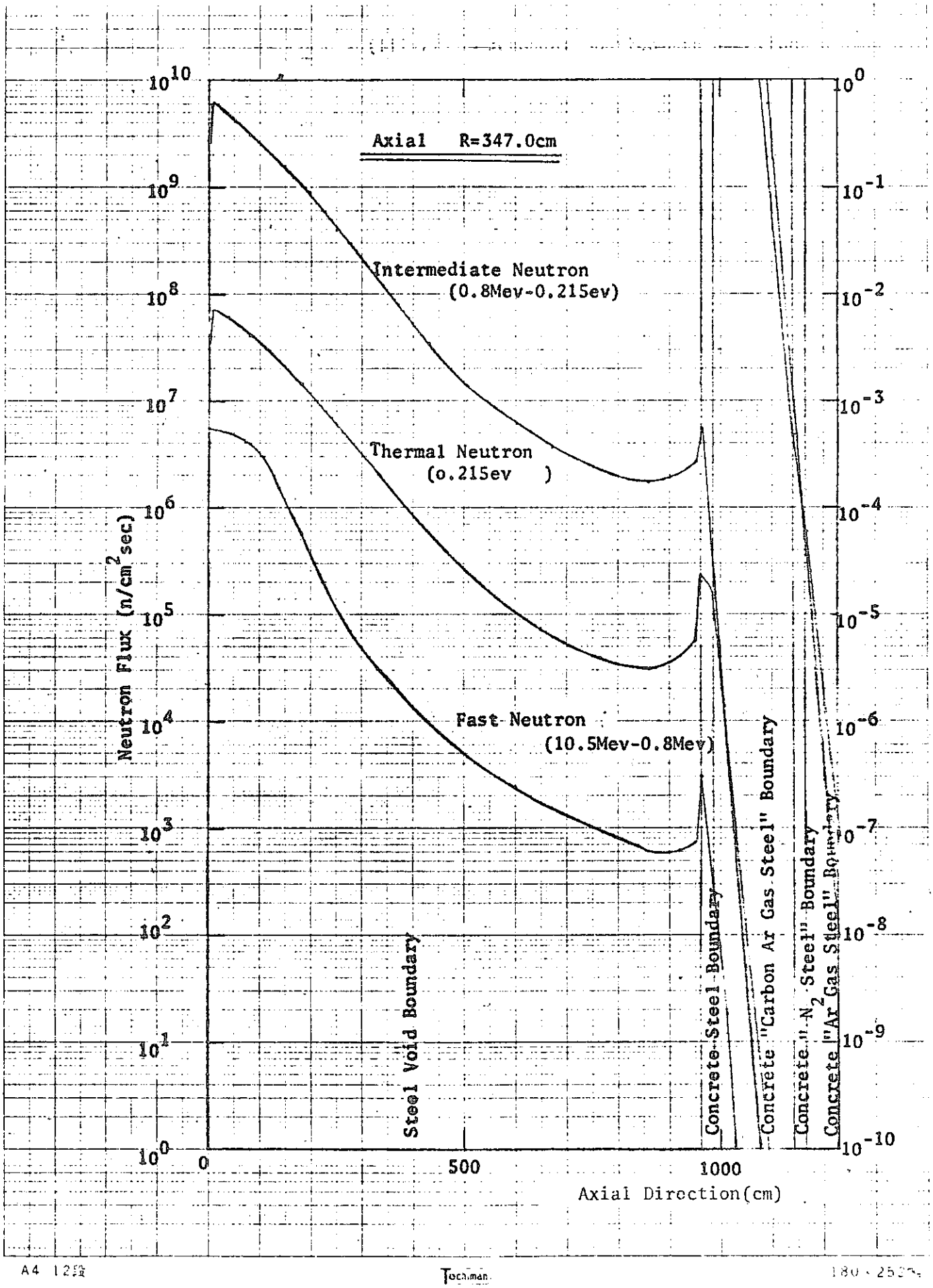

Fig.(Ⅲ-28) Neutron Attenuation Distribution r=347.0cm

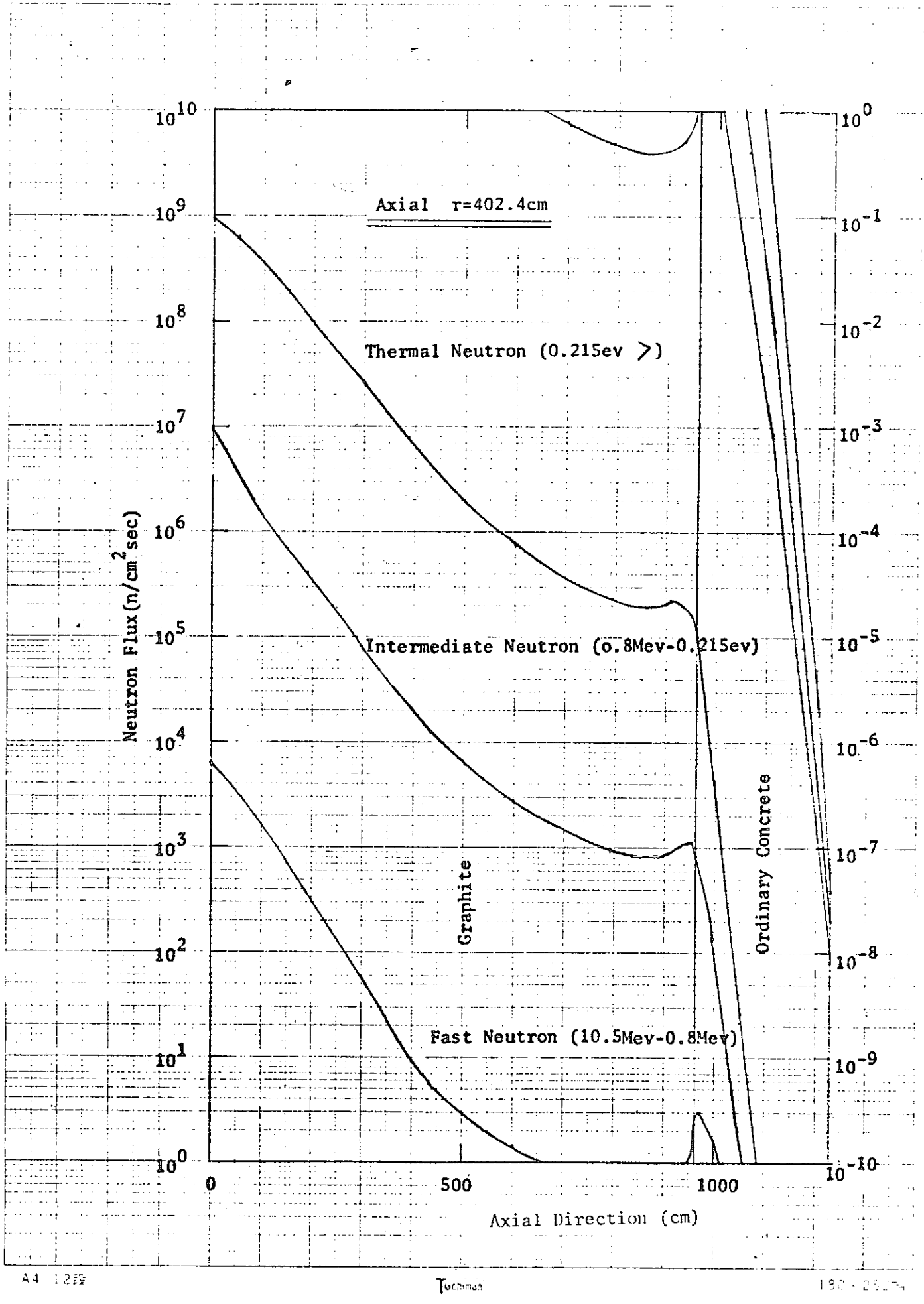

Fig.(Ⅲ-29) Neutron Attenuation Distribution r=402.4cm

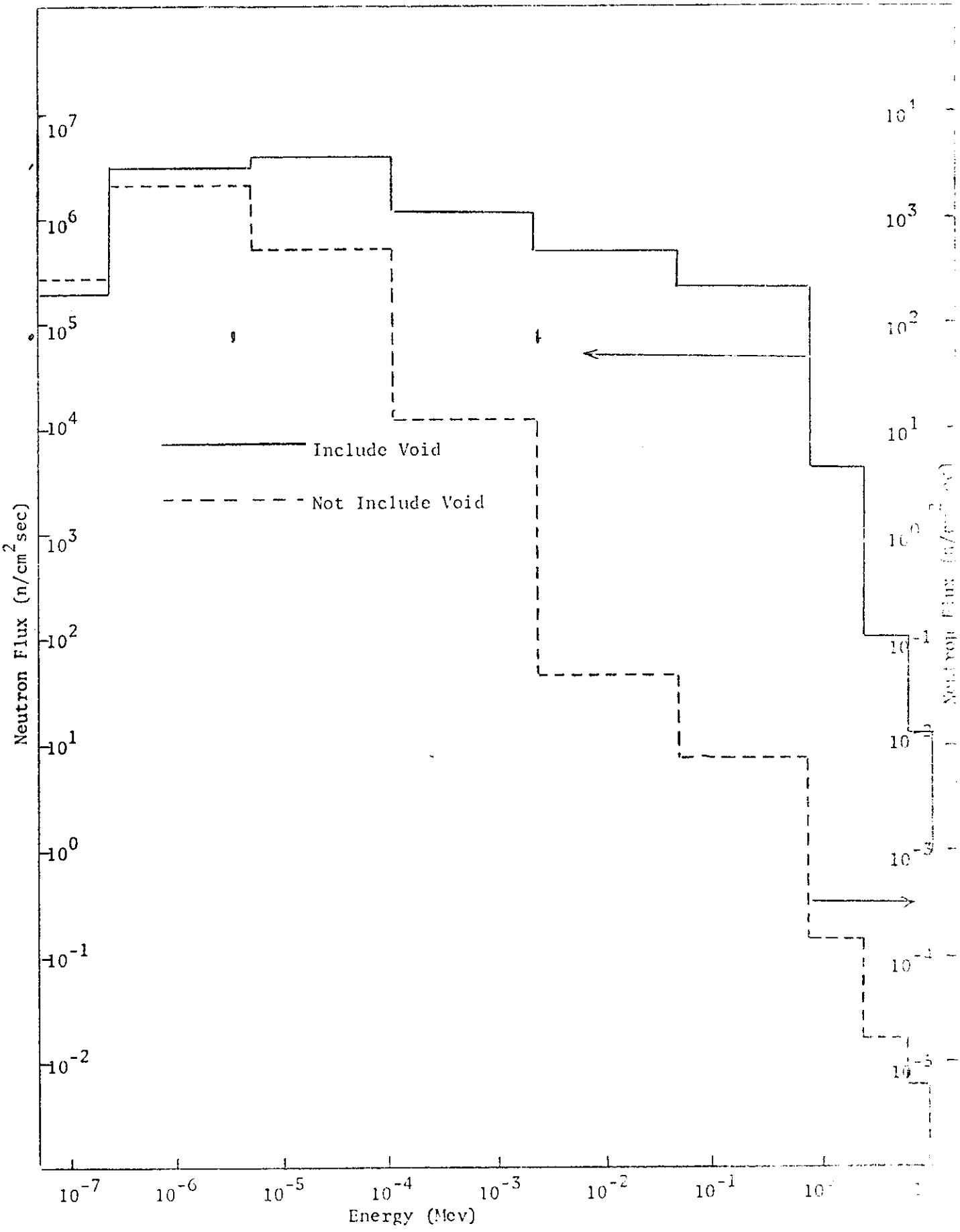

Fig.(III-30) Comparison of Neutron Flux between Calculation Including Void and Not Including Void

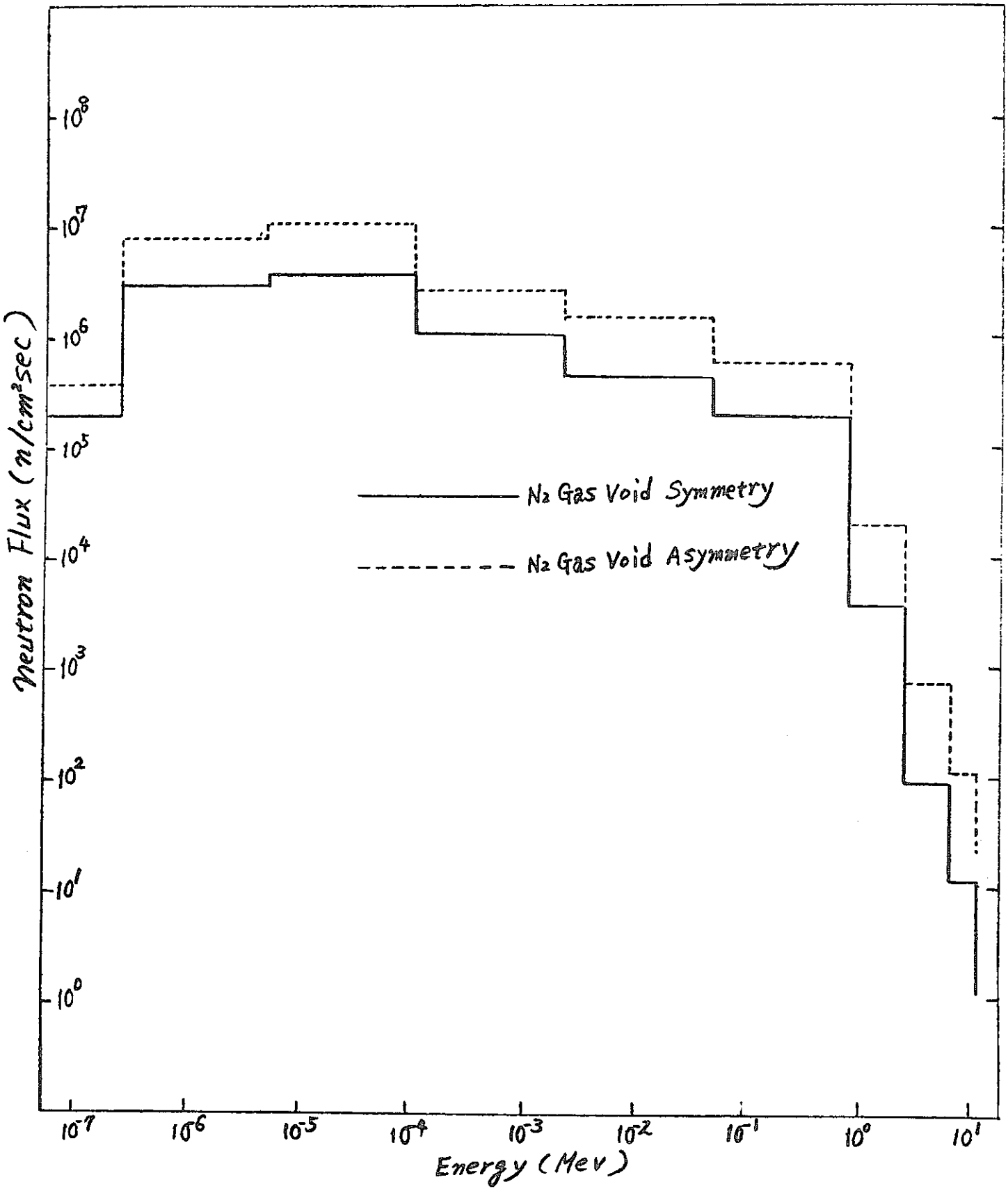

Fig. (Ⅲ-31) Difference of Void Boundary Condition

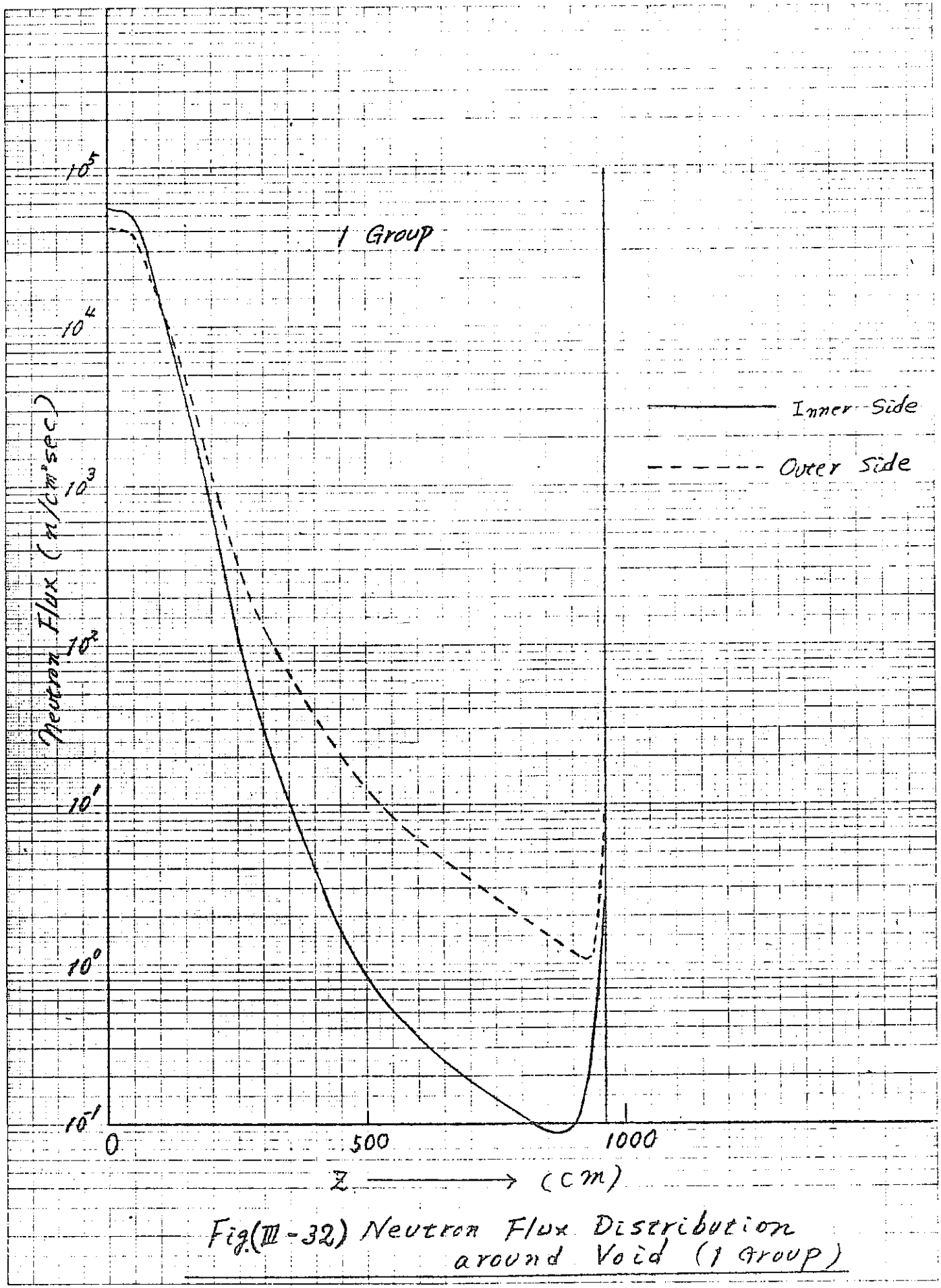

Fig.(Ⅲ-32) Neutron Flux Distribution around Void (1 Group)

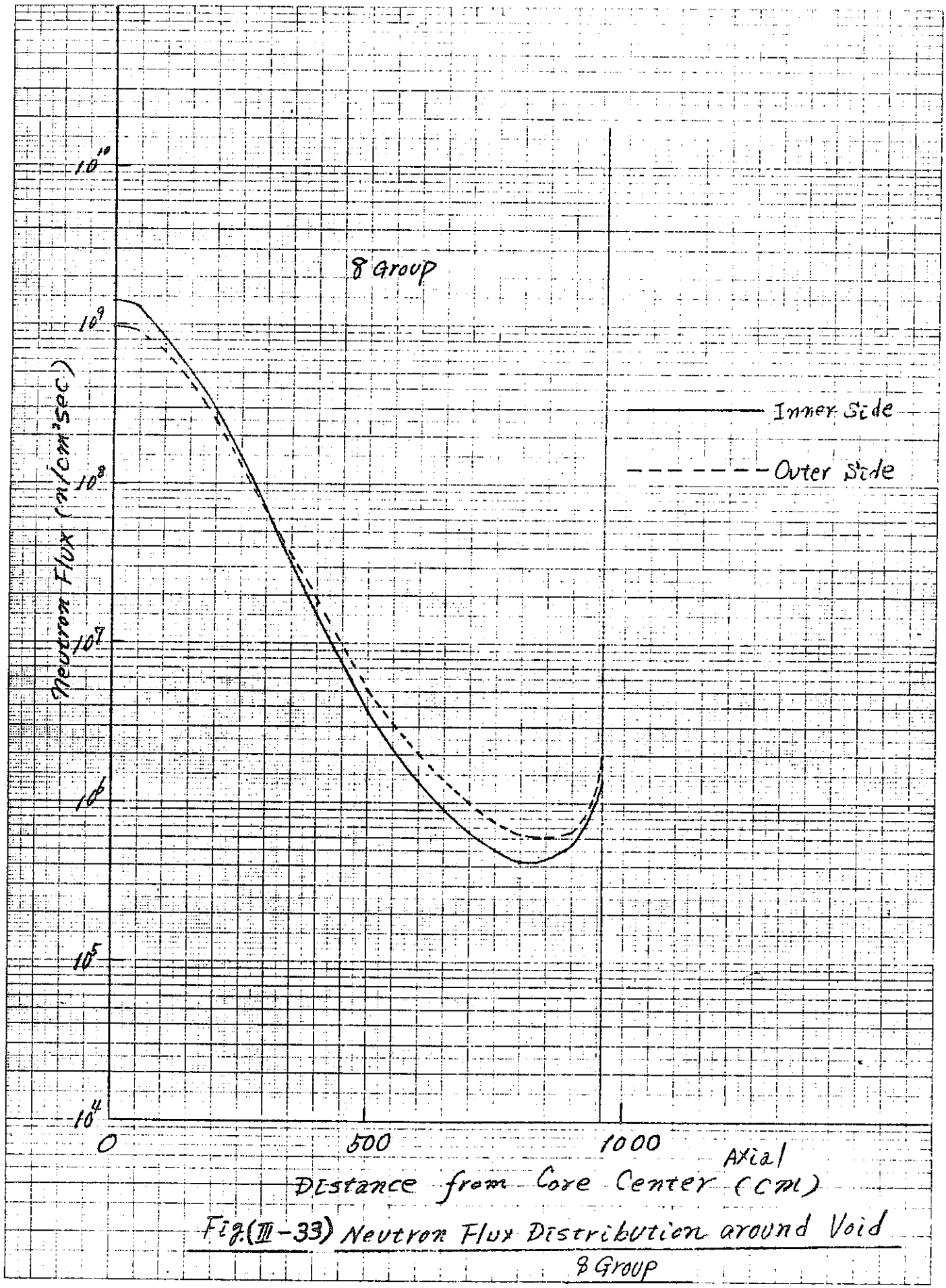

Fig.(Ⅲ-33) Neutron Flux Distribution around Void
8 Group

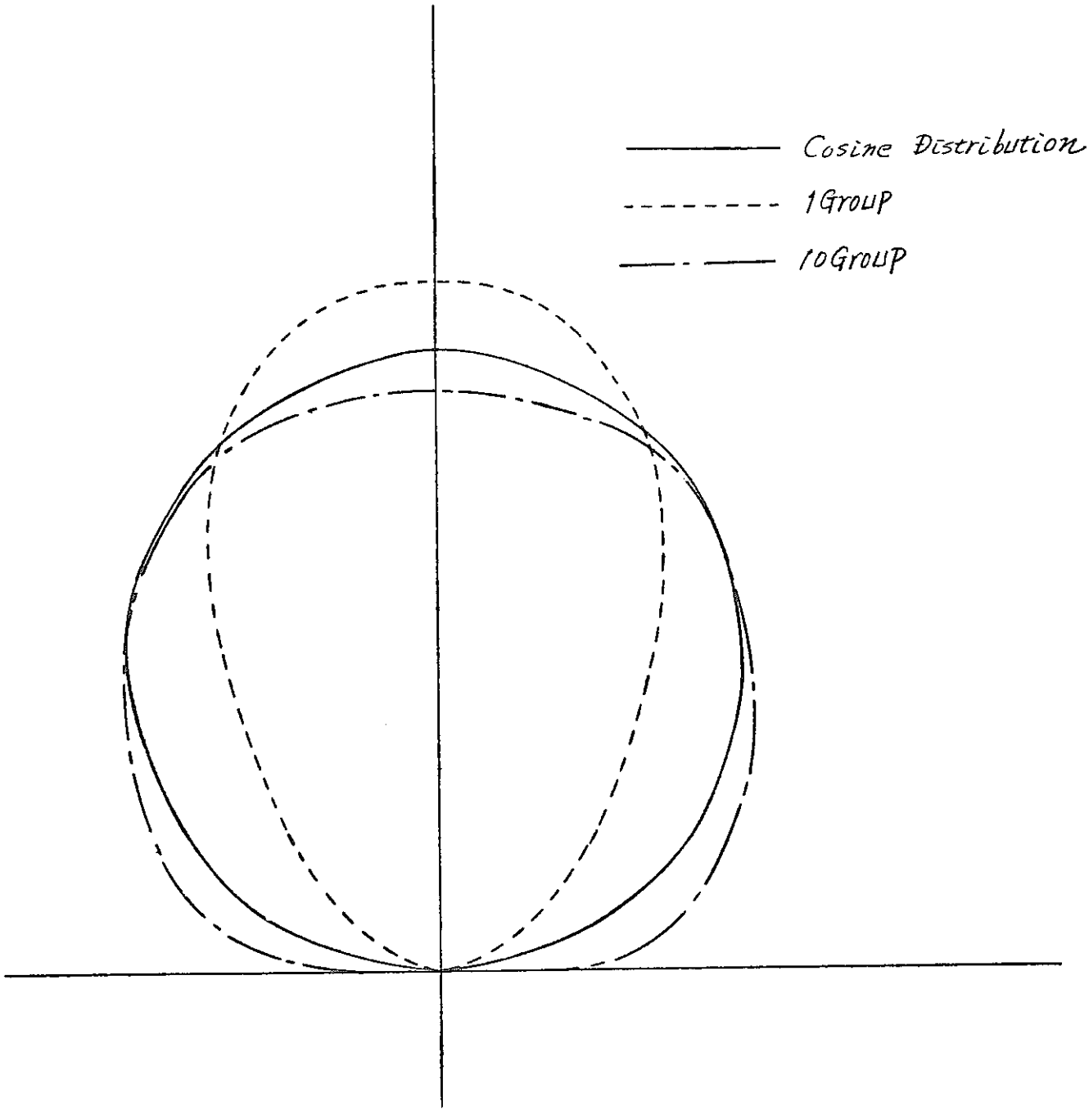

Fig.(Ⅲ-34) Angular Flux Distribution at Reactor Vessel of "Monju" by ANISN

IV. Summary

The following works have been performed as the research and development under contract for 1972:

1. In order to make possible the exact analysis of the geometries including voids, two-dimensional diffusion calculation code DIAC has been modified taking into account of the treatment of the axial symmetrical void geometry.

2. Unreasonable treatment of minus neutron current entering into void has been removed.

3. As an application example of the modified code, an analysis of the main shield of Fast Prototype Reactor "MONJU" including voids has been performed and the evaluation of void effect has been made. From this result, following points have been cleared.

a) Comparing the result not including voids (before previous analysis, there has been noted an increase of 3 ∿ 7 figures neutron flux level at the upper part of N_2 gas void (lowest part of top shield).

b) Comparing the result on the assumption that the neutrons enter into void from N_2 gas void lower surface on the radial central axis (previous analysis), there has been noted an decrease of ∿ 1 figure neutron flux level at the upper part of N_2 gas void.

c) That the neutron flux level at outer surface of N_2 gas void has been high than that at inner surface has been caused from the cosine angular distribution assumption of

neutron entering into void and from that the nutron current entering into void at inner void surface was greater than that at outer surface.

4. From the above works of 1 to 3, it has been found out that the presence of voids in the shield gives a conspicuous effect to the neutron flux distribution which could not be ignored from the standpoint of shield design. Future problems may be as follows:

a) Evaluation of diffusion approximation at high energy groups.

b) Evaluation of cosine angular distribution assumption of neutron entering into void.

c) Treatment of complex geometrical voids

d) Inprovement of the fitting method of the neutron transition probability within voids calculated by line of sight method.

V. Appreciation

This research work on "Applicability of Shielding Design Code" has been performed as follow up and further modification of those works of "Development of Two-Dimensional Shielding Design Code (I)--Evaluation of Two-Dimensional Analysis"-- in 1970, "Development of Two-Dimensional Shielding Design Code (II)--Group Constant Collapsing Method and Establishment of Core Boundary Connection Method--" in 1971, "Evaluation and Application Study of Fast Reactor's Two-Dimensional Shielding Code" in 1972, and "Improvement and Evaluation of Two-Dimensional Shielding Design Code" in 1973.

Taking this opportunity, we hereby wish to express our most sincere appreciation of the assistance and useful advice provided to us for this research work by Dr. Kobayashi, General Manager and other members of the Nuclear Research and Development Department of Kawasaki Heavy Industries, and Mr. Yoshiharu Higashihara, Director General of the Technical Development Headquarters of PNC.

VI. Reference

1) Y. Tanaka, I. Suzuki: Development of Two-Dimensional Shielding Design Code (I)--Code Manual--, J213 70 1-1 (1970).

2) Y. Tanaka, I. Suzuki: Development of Two-Dimensional Shielding Design Code(II)--Evaluation of Two-Dimensional Analysis--, J213 70 1-2 (1970).

3) Y. Tanaka, I. Suzuki and N. Ohtani: Development of Two-Dimensional Shielding Design Code (II)--Group Constant Collapsing Method and Establishment of Core Boundary Connection Method--, J213 71-02 (1971).

4) Y. Tanaka, I. Suzuki and N. Ohtani: Evaluation and Application Study of Fast Reactor's Two-Dimensional Shielding Design Code, J213 72-03-01 (1972).

5) Y. Tanaka, I. Suzuki and N. Ohtani: Evaluation and Application Study of Fast Reactor's Twp-Dimensional Shielding Design Code--Code Manual--, J213 72-03-02 (1972).

6) Y. Tanaka, I. Suzuki and M. Takemura: Improvement and Evaluation of Two-Dimensional Shielding Design Code, J213 73-01 (1973).

7) Von H. Vossebrecker: Two-dimensional shielding calculations using a combination of diffusion theory and line of sight method, Atomkernenergie (ATKE) Bd. 19 (1972).

VII. Appendix Code Manual of DIAC Code

1) Outline

As described in previous chapter, following two modification has been done in DIAC.

i) Line of sight calculation in axial symmetrical void geometry.

ii) Removement of minus neutron current at void surface.

Its elemental style has not been changed, so DIAC can be used in the same way as old two-dimensional calculation system of RASC-2D.

2) Calculation Flow

Fig. (VII-1) shows the Flow Diagram of DIAC code.

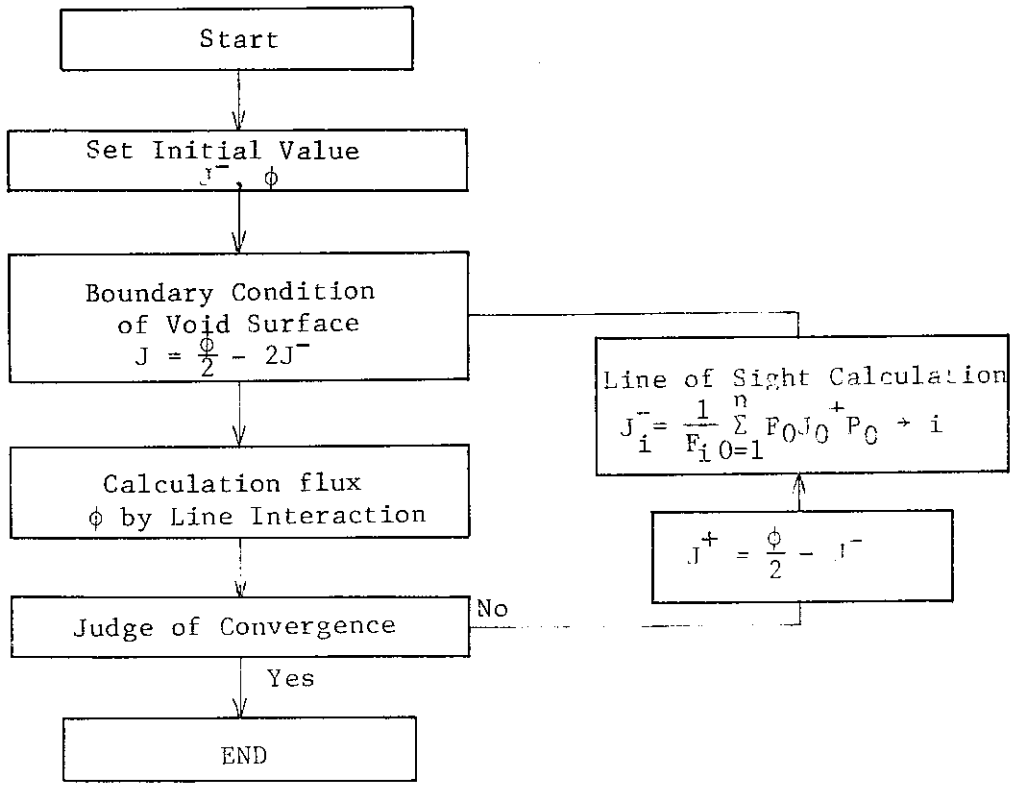

Fig. (VII-1) Flow Diagram of DIAC Code

4) Format of Input and Output

Table (VII-2) shows the Input Format of DIAC Code after Modification. Output format is same as previous one.

5) Test Calculation

Fig. (VII-2) shows the test calculation configuration of DIAC code. Table (VII-2) shows input data, and Table (VII-4) shows some of the output.

Probability Calculation	Gauss Division Points Approximate Polynomial Order	≦16 ≦14
Line of Sight Calculation	Void Mesh Number Void Number Void Geometry	≦85 ≦2 Cylinder, Cylindrical Shell
Diffusion Calculation	Mesh Number (P x Z) Region Number R Z Material Number Energy Group Number	≦10140 ≦16 ≦13 ≦26 ≦10

Table (VII-1) Limit Condition of DIAC Code

CONTROL DATA 3600 DATA INPUT FORM

Table (VII-2) DIAC Input Format (1)

TITLE(I),I=1,10			Title Card	FORMAT(10A8)
MATREGS(1)			MATREGS(1).....Put 8 characters as GEOMETRY.	FORMAT(A8)
MATREGS(1)			MATREGS(1).....Put 8 characters as bX-Ybbbb when xy geometry, or bR-Zbbbb when RZ geometry.	FORMAT(A8)
IGROUP		IG	IGRØUP.....Put 8 characters as GROUPSbb. IG .....Put maximum energy group number.	FORMAT(A8, 8X, I4)
MATREGS(I),I=1,2		MR	MATREGS(I).....Put 16 characters as MATERIALbbbbbbbb. MR .....Put maximum material number.	FORMAT(2A8,I4)
IACCUR	A1	A2	A3	FORMAT(A8,2X,3E10.3)
			IACCUR.....Put 8 characters as ACCURACY A1,A2,A3.....Put Convergence accuracy condition, (A1 > A2 > A3) final accuracy = A3.	
IOMEGA	W			FORMAT(A8,2X,3E10.3)
			IOMEGA.....Put 8 characters as OMEGAbbb. W .....Put Initial value of accerelation parameter.	
ICOUNT	IT	NIT	ICOUNT.....Put 8 characters as COUNTbbb. IT .....Put muximum iteration number. NIT .....Put iteration times with use same accerelation parameter.	FORMAT(A8,2X,2I5)

DATA DESCRIPTION _____ PREPARED BY _____

CRC Century Research Center Corporation

DATE _____ PAGE _____ OF _____

CONTROL DATA 3600 DATA INPUT FORM

Table (VII-2) DIAC Input Format (2)

ISOURCE(I),I=1,3					FORMAT(3A8)	
	ISOURCE(I)	Put 24 characters as when removal source is inputed				
		REMOVALbSOURCESbbbbbbbbb				
		or when removal source is not inputed				
		NObREMOVALbSOURCESbbbbbb				
ISOURCE(I),I=1,3	KGR	This card is necessary when removal source is inputed.				FORMAT(3A8,I6)
	ISOURCE(I)	Put 24 characters as				
		GRØUPSbOFbREMOVALbbbbbbb.				
	KGR	Put maximum energy group number of removal source (KGR≤30)				
MESH 1 = R(2)						
J = R(J+1)					FORMAT(1A8,i3,2X,F7.3)	
↓ = ↓						
* JME = R(JME+1)						
	MESH	Put 8 characters as MESHbbMR				
		on first card. On the second				
		card and thereafter, blank card is				
		desirable.				
		Put * on the last card from the first column.				
	J	Put mesh numbers in the boundaries of different				
		mesh width (begins from J=1).				
	R(J)	Put distance from the original point at J mesh number				
		(radial direction or horizontal direction) (cm).				
		R(2) proportionates with the original point.				
	JME	Put max. number of mesh point of radial or horizontal direction.				
It is easier understandable to put = in 13 column.						

DATA DESCRIPTION _____ PREPARED BY _____

DATE _____ PAGE _____ OF _____

CRC Century Research Center Corporation

CONTROL DATA 3600 DATA INPUT FORM

Table (VII-2) DIAC Input Format (3)

MESH	1 = Z(20	MESH	FORMAT(1A8,i3,2X,F7.2)
	I = Z(I+1)		
	↓ =		
*	IME =		
			Put 8 characters as bbbbbbMZ on first card.
			On the second card and thereafter, blank card is desirable.
			Put * on the last card from the first column.
		I	Put mesh numbers in the boundaries of different mesh width (begins from J=1)
		Z(I)	Put distance from original point at I mesh number (axial and horizontal direction)(cm).
			Z(2) proportionates with the original point.
		JME	Put max. number of mesh point axial and horizontal direction.
			It is easier understandable to put = in 13 column.
IZONE	MT		
		IZONE	FORMAT(1A8,i3)
			Put 8 characters as ZONEbbbb.
		MT	Put regional material number. Initially material designation is made in the entire region MT.
			By the following designation, the material in each region is put in.
IZONE	MT (I1, J1,	I2, J2)	FORMAT(1A8,I3,2X,4(i3,1X))
	↓ (, ,	,)	
	(, ,	,)	
	(, ,	,)	
		IZONE	Put blank. Put * on the last card from the first card.
		MT	Put regional material number. When MT=0, it is judged as voids (The void layer numbers are the input order).

DATA DESCRIPTION _____ PREPARED BY _____

CRC Century Research Center Corporation

DATE _____ PAGE _____ OF _____

CONTROL DATA 3600 DATA INPUT FORM

Table (VII-2) DIAC Input Format (4)

I1,J1 .....Put Each region's left lower corner mesh number.

J2,J2 .....Put Each region's right upper corner mesh number.

{I → Axial direction (perpendicular direction).
J → Radial direction (horizontal direction).}

JSOURCE(I)	I=1,2	K	JCH(I), I=1,2	NMS

FORMAT(2A8,I3,A8,A5,I3)

JSOURCE(I).....Put 16 characters as SOURCESbINbGRØUP
when internal source exists, and
as NObSOURCEbbbbbbb
when no internal source exists.

K (≤30) .....Put energy group of internal source.

JCH .....Put 16 character from 20th column as
BYbMATERIALS.

NMS (≤20) .....Put material number of internal source.

Unnecessay when NObSOURCE.

JSOURCE(1)	MTL(1)	TEMP2(1)	MTL(2)	TEMP2(2)			MTL(NMS)	TEMP2(NMS)

JSOURCE(1).....Put any 5 characters

MTL(M) .....Put material number in consideration of
internal source.

S(M) .....Put source intensity corresponding to material MTL(M).

FORMAT(3X,1A5,5(I5,
E10.3)/(8X,5(I5,E10.3)

Put in * the first column of the last card.

Provide to other energy if necessary.

DATA DESCRIPTION _____ PREPARED BY _____

DATE _____ PAGE _____ OF _____

CRC Century Research Center Corporation

CONTROL DATA 3600 DATA INPUT FORM

Table (VII-2) DIAC INPUT FORMAT (5)

IBOUNDS(1)	IBOUNDS(2)	IBOUNDS(3)	ID	*	IC	BV(1)	BV(2)
				*			
				*			
				*			

FORMAT(3A3,I1,2X,I3,2E10.2)

IBOUNDS(1).....Put 8 characters as BOUNDSbb in the first card for each energy. In other cases, blank is desirable.

IBOUNDS(2).....Put 8 characters in order from 9-th column as
- BRbLOWbb,
- BRbHIGHb,
- BZbLOWbb,
- BZbHIGHb,

IBOUNDS(3).....Put 8 characters selectively from 17th column as
- NONZEROb,
- ONEZEROb,
- TWOZEROb.

ID .....Put designation in providing boundary condition.

IC .....Put mesh number inthe boundary of the same condition.

BV(1),BV(2).....Put boundary condition values (as explained below

The boundary condition are generally given by

$$aD\frac{\partial\phi}{\partial n} + b\phi + C = 0$$

(1) NONZERØ	Give $\frac{b}{a}$, $\frac{c}{a}$ to BV(1) and BV(2). In this case, ID no needs to be given (blank)
(2) ONEZERØ	Designate $-\frac{c}{b}$, $\frac{c}{a}$, $\frac{b}{a}$ each to ID = 1, 2, 3 and give to BV(1).
(3) TWOZERØ	Give only IC. Unnecessary for ID, BV(1).

DATA DESCRIPTION _____ PREPARED BY _____

CRC Century Research Center Corporation

DATE _____ PAGE _____ OF _____

CRC DATA 3600 DATA INPUT FORM

Table (VII-2) DIAC Input Format (6)

IOUT	IO1		FORMAT (A8,2X,3I5)
		ICUT .....Put 8 characters as OUTPUTbb	
		IO1 .....0 write out the collapsed neutron flux.	
		1 write out the neutron flux of all groups.	
		2 write out the collapsed neutron flux and those of all groups.	
IDEGR	IGG		FORMAT (A8,2X,I5)
		IDEGR .....Put 8 characters as DE-GROUP.	
		IGG .....Put Energy collapsed group number.	
IGZ(1) IGZ(2)	IGZ(IGGH)		FORMAT(10I5)
		IGZ(N) .....Put collapsed energy group boundary number.	
		necessary only when it is IO1 = 1	
ILEAK	IBK		FORMAT (A8,2X,I5)
		ILEAK .....Put 8 characters as	
		when consider leak effect	
		LEAKbbbb	
		when not consider leak effect	
		NObLEAK.	
		IBK .....Put material number considering leak effect	
		necessary only cross-co-ordinate	

DATA DESCRIPTION _____ PREPARED BY _____

DATE _____ PAGE _____ OF _____

CRC Century Research Center Corporation

CONTROL DATA 3600 DATA INPUT FORM

Table (VII-2) DIAC Input Format (7)

MBK(1) | MBK(2) | ——→ MBK(IBK) — FORMAT(10I5)

MBK(I) .... Put designated number of material in consideration of leak.

BK1(1) | BK2(1) | BK3(1) — The leak effect is expressed by 2-degree formula as to perpendicular direction co-ordinate Z. — FORMAT(3E10.3)

↓ | ↓ | ↓

BK1(IBK) | BK2(IBK) | BK3(IBK)

Leak = BK1(MT)+BK2(MT)*Z+BK3(MT)*Z^2)*D(MT)

MT = designated material number.

D(MT) = diffusion constants.

VOID(I),I=1,4 — FORMAT(4A8)

VOID(I) .... Put 32 characters as VOIDbCALCULATIONbCONSTANTbbbbbbb.

GAUSS(I),I=1,3 — FORMAT(3A8)

GAUSS(I) .... Put 24 characters as GAUSSbDIVISIONbNUMBERbb

NION(1) | NICN(1) | NOCN(1) | NCIN(1) | NCON(1) — FORMAT(5I5)

↓ | ↓ | ↓ | ↓ | ↓

NION (NVOID) | NICN (NVOID) | NOCN (NVOID) | NCIN (NVOID) | NCON (NVOID)

NVOID .... Void number

Inner Side ↔ Outer Side

NION(N) .... Put gauss division — Inner Side ↔ Edge

NICN(N) .... number of Nth Void — Outer Side ↔ Edge

NOCN(N) .... for probability calculation — Outer Side ↔ Outer Side

NCIN(N) .... — Edge ↔ Edge

NCON(N) ....

DATA DESCRIPTION ______ PREPARED BY ______

CRC Century Research Center Corporation — DATE ______ PAGE ______ OF ______

CONTROL DATA 3600 DATA INPUT FORM

Table (VII-2) DIAC Input Format (8)

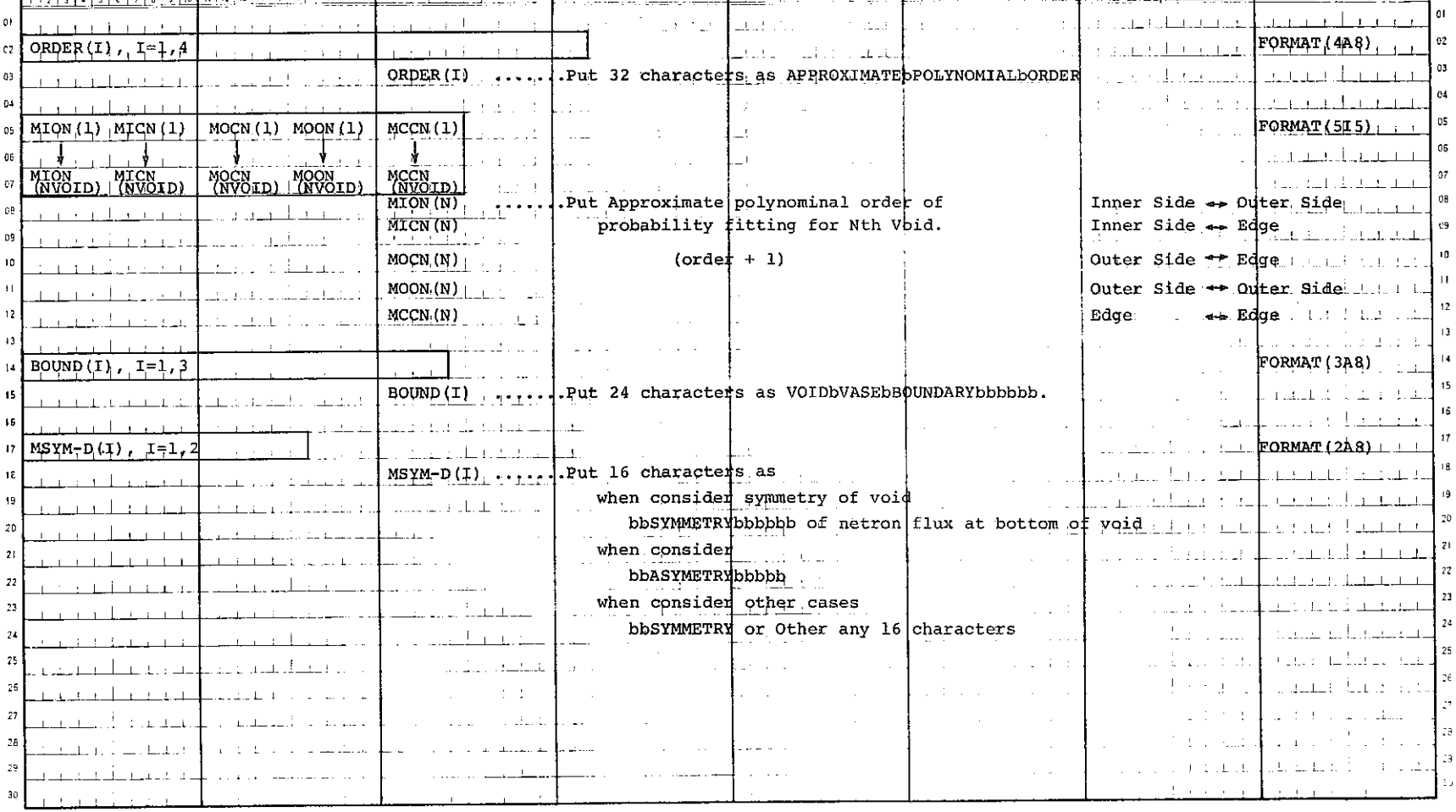

DATA DESCRIPTION _____ PREPARED BY _____

DATE _____ PAGE _____ OF _____

CRC Century Research Center Corporation

CONTROL DATA 3600 DATA INPUT FORM

Table (VII-2) DIAC Input Format (9)

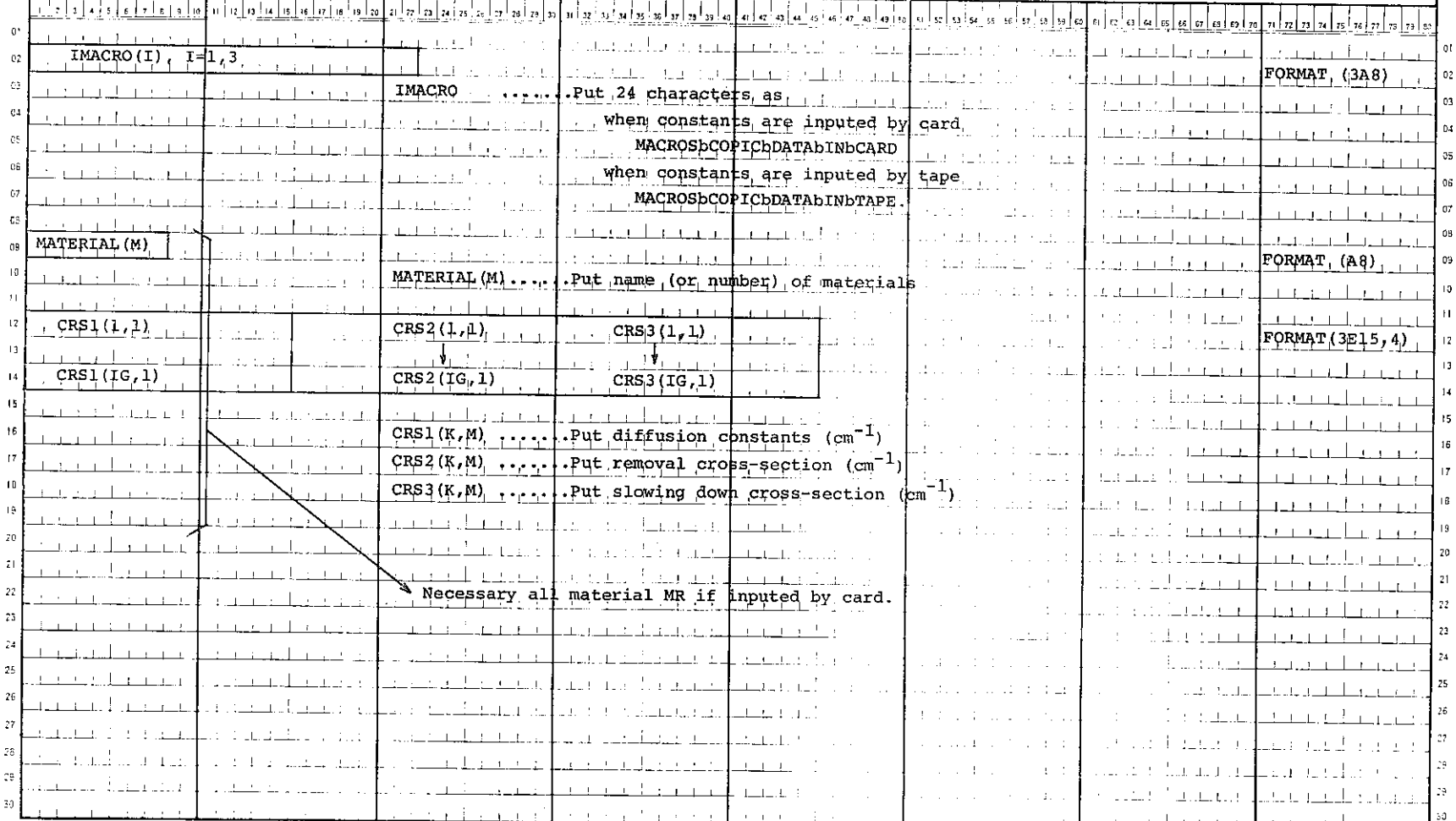

DATA DESCRIPTION _____ PREPARED BY _____

CRC Century Research Center Corporation DATE _____ PAGE _____ OF _____

Table(VII-3) Example of Diac Input

```
*** DIAC *** VOID SYST. [illegible] CALCULATION BY [illegible]. 48/12/24
GEOMETRY
 R-Z
GROUPS                   1
MATERIAL                 2
ACCURACY      0.1            0.01          0.001
OMEGA         1.3
COUNT        100
NO REMOVAL SOURCES
MESH   MR   1 =    0.0
*          21 = 100.0
       MZ   1 =    0.0
*          31 = 150.0
ZONE        2
            1 (  1,  1,  5,  4)
            0 ( 21,  1, 26, 11)
*           0 (  1, 12, 13, 17)
SOURCES IN GROUP  1BY MATERIALS   2
*      1     1.0+15     2      1.0 +0
BOUNDS  BR LOW  TWOZERO    * 21
        BR HIGH ONEZERO 2 * 21     0.5
        BZ LOW  TWOZERO    * 21
        BZ HIGH ONEZERO 3 * 21     0.5
OUTPUT            2    0    2
DE-GROUP          1
    1    1
VOID CALCULATION CONSTANT
 GAUSS DIVISION NUMBER
    4    4    4    4    4
    4    4    4    4    4
 APPROXIMATE POLYNOMIAL ORDER
    5    5    5    5   10
   12   12   12   12    4
VOID BASE BOUNDARY
  ASYMMETRY
  SYMMETRY
MACROSCOPIC DATA IN CARD
  101
   3.82             0.0743            0.0153
  102
  11.57             0.0744            0.0155
```

```
*** DIAC *** VOID SYSTEM TEST CALCULATION BY KHI.  48/11/24

  GEOMETRY
   R-Z

  GROUPS                1

  MATERIAL              2

  ACCURACY       .10E+00    .10E-01    .10E-02

  OMEGA          .15E+01

  COUNT          100     5

  NO REMOVAL SOURCES

  MESH  MR  1 =    0.00
  *        21 =  100.00

        MZ  1 =    0.00
  *        31 =  150.00

  ZONE      2
            1 (  1,  1,  5,  4)
            0 ( 21,  1, 26, 11)
  *         0 (  1, 13, 13, 17)

  RMESH
    0.000     5.000    10.000    15.000    20.000    25.000    30.000    35.000    40.000    45.000
   50.000    55.000    60.000    65.000    70.000    75.000    80.000    85.000    90.000    95.000
  100.000

  ZMESH
    0.000     5.000    10.000    15.000    20.000    25.000    30.000    35.000    40.000    45.000
   50.000    55.000    60.000    65.000    70.000    75.000    80.000    85.000    90.000    95.000
  100.000   105.000   110.000   115.000   120.000   125.000   130.000   135.000   140.000   145.000
  150.000
```

Table (VII-4) Example of DIAC Output (1)

Tabe (VII-4) Example of DIAC Output (2)

ZONES - (1,1) MESH AT BOTTOM LEFT -

2	2	2	2	2	2	2	2	2	2	2	2	2	2	2	2	2	2	2	2
2	2	2	2	2	2	2	2	2	2	2	2	2	2	2	2	2	2	2	2
2	2	2	2	2	2	2	2	2	2	2	2	2	2	2	2	2	2	2	2
2	2	2	2	2	2	2	2	2	2	2	2	2	2	2	2	2	2	2	2
2	2	2	2	2	2	2	2	2	2	2	2	2	2	2	2	2	2	2	2
0	0	0	0	0	0	0	0	0	0	2	2	2	2	2	2	2	2	2	2
0	0	0	0	0	0	0	0	0	0	2	2	2	2	2	2	2	2	2	2
0	0	0	0	0	0	0	0	0	0	2	2	2	2	2	2	2	2	2	2
0	0	0	0	0	0	0	0	0	0	2	2	2	2	2	2	2	2	2	2
0	0	0	0	0	0	0	0	0	0	2	2	2	2	2	2	2	2	2	2
2	2	2	2	2	2	2	2	2	2	2	2	2	2	2	2	2	2	2	2
2	2	2	2	2	2	2	2	2	2	2	2	2	2	2	2	2	2	2	2
2	2	2	2	2	2	2	2	2	2	2	2	2	2	2	2	2	2	2	2
2	2	2	2	2	2	2	2	2	2	2	2	2	2	2	2	2	2	2	2
2	2	2	2	2	2	2	2	2	2	2	2	2	2	2	2	2	2	2	2
2	2	2	2	2	2	2	2	2	2	2	2	2	2	2	2	2	2	2	2
2	2	2	2	2	2	2	2	2	2	2	2	2	2	2	2	2	2	2	2
2	2	2	2	2	2	2	2	2	2	2	2	2	2	2	2	2	2	2	2
2	2	2	2	2	2	2	2	2	2	2	2	0	0	0	0	2	2	2	2
2	2	2	2	2	2	2	2	2	2	2	2	0	0	0	0	2	2	2	2
2	2	2	2	2	2	2	2	2	2	2	2	0	0	0	0	2	2	2	2
2	2	2	2	2	2	2	2	2	2	2	2	0	0	0	0	2	2	2	2
2	2	2	2	2	2	2	2	2	2	2	2	0	0	0	0	2	2	2	2
2	2	2	2	2	2	2	2	2	2	2	2	0	0	0	0	2	2	2	2
2	2	2	2	2	2	2	2	2	2	2	2	0	0	0	0	2	2	2	2
2	2	2	2	2	2	2	2	2	2	2	2	0	0	0	0	2	2	2	2
1	1	1	2	2	2	2	2	2	2	2	2	0	0	0	0	2	2	2	2
1	1	1	2	2	2	2	2	2	2	2	2	0	0	0	0	2	2	2	2
1	1	1	2	2	2	2	2	2	2	2	2	0	0	0	0	2	2	2	2
1	1	1	2	2	2	2	2	2	2	2	2	0	0	0	0	2	2	2	2

Table (VIII-4) Example of DIAC Output (3)

```
SOURCES IN GROUP  1BY MATERIALS   2
*          1   .100E+16     2   .100E+10

BOUNDS   BR LOW   TWOZERO * * 31 -0.          -0.
         BR HIGH  ONEZERO 3 * 31    .50E+00 -0.
         BZ LOW   TWOZERO * * 21 -0.          -0.
         BZ HIGH  ONEZERO 3 * 21    .50E+00 -0.

OUTPUT          2     0     2

DE-GROUP        1

     1     1
```

Table (Ⅷ-4) Example of DIAC Output (4)

```
VOID CALCULATION CONSTANT

  GAUSS DIVISION NUMBER
                    4    4    4    4    4
                    4    4    4    4    4

  APPROXIMATE POLYNOMIAL ORDER
                    5    5    5    5   10
                   12   12   12   12    4

  VOID BASE BOUNDARY

    ASYMMETRY

    SYMMETRY
```

Table (VII-4) Example of DIAC Output (5)

MACROSCOPIC DATA IN CARD

MATERIAL	DIFF.COEF.	REM.C.S.	SL-DWN.C.S.
101	.3820E+01	.7430E-01	.1530E-01
102	.1157E+02	.3440E-01	.1550E-01

Table (VII-4) Table of DIAC Output (6)

	X(I)	X**K*LOG(Y)	ERROR	RESID**2
1	.125E+01	-.121E+02	-.800E-03	
2	.500E+01	-.121E+02	.477E-02	
3	.100E+02	-.120E+02	-.178E-01	
4	.150E+02	-.119E+02	.417E-01	
5	.200E+02	-.117E+02	-.585E-01	
6	.250E+02	-.115E+02	.386E-01	
7	.300E+02	-.113E+02	.192E-01	
8	.350E+02	-.111E+02	-.716E-01	
9	.400E+02	-.109E+02	.797E-01	
10	.450E+02	-.108E+02	-.514E-01	
11	.500E+02	-.108E+02	.208E-01	
12	.550E+02	-.112E+02	-.537E-02	
13	.588E+02	-.124E+02	.839E-03	
				.2193912E-05

P-FITTING

M= 12 L= 1 N= 13

	X(I)	X**K*LOG(Y)	ERROR	RESID**2
1	.125E+01	-.114E+02	-.682E-03	
2	.500E+01	-.114E+02	.407E-02	
3	.100E+02	-.113E+02	-.152E-01	
4	.150E+02	-.113E+02	.357E-01	
5	.200E+02	-.112E+02	-.501E-01	
6	.250E+02	-.110E+02	.331E-01	
7	.300E+02	-.109E+02	.162E-01	
8	.350E+02	-.107E+02	-.611E-01	
9	.400E+02	-.106E+02	.681E-01	
10	.450E+02	-.105E+02	-.440E-01	
11	.500E+02	-.106E+02	.178E-01	
12	.550E+02	-.110E+02	-.457E-02	
13	.588E+02	-.121E+02	.767E-03	
				.1603700E-05

P-FITTING

M= 12 L= 2 N= 13

	X(I)	X**K*LOG(Y)	ERROR	RESID**2
1	.125E+01	-.114E+02	-.675E-03	
2	.500E+01	-.114E+02	.402E-02	
3	.100E+02	-.113E+02	-.150E-01	
4	.150E+02	-.113E+02	.352E-01	
5	.200E+02	-.112E+02	-.494E-01	
6	.250E+02	-.110E+02	.326E-01	
7	.300E+02	-.109E+02	.162E-01	
8	.350E+02	-.107E+02	-.606E-01	
9	.400E+02	-.105E+02	.674E-01	
10	.450E+02	-.104E+02	-.435E-01	
11	.500E+02	-.103E+02	.176E-01	
12	.550E+02	-.106E+02	-.453E-02	
13	.588E+02	-.117E+02	.745E-03	
				.1569138E-05

Table(VII-4) Example of DIAC Output (7)

M= 10 L= 11 N= 11

	X(I)	X**K*LOG(Y)	ERROR	RESID**2
1	.125E+01	-.107E+02	-.385E-05	
2	.500E+01	-.107E+02	.104E-04	
3	.100E+02	-.106E+02	.125E-04	
4	.150E+02	-.105E+02	-.136E-03	
5	.200E+02	-.104E+02	.376E-03	
6	.250E+02	-.102E+02	-.585E-03	
7	.300E+02	-.100E+02	.593E-03	
8	.350E+02	-.982E+01	-.383E-03	
9	.400E+02	-.968E+01	.165E-03	
10	.450E+02	-.960E+01	-.448E-04	
11	.488E+02	-.961E+01	.958E-05	
				.1018867E-09

P-FITTING

M= 12 L= 1 N= 13

	X(I)	X**K*LOG(Y)	ERROR	RESID**2
1	.125E+01	-.915E+01	-.426E-04	
2	.500E+01	-.924E+01	.230E-03	
3	.100E+02	-.949E+01	-.105E-02	
4	.150E+02	-.984E+01	.349E-02	
5	.200E+02	-.102E+02	-.705E-02	
6	.250E+02	-.106E+02	.773E-02	
7	.300E+02	-.110E+02	-.203E-02	
8	.350E+02	-.114E+02	-.651E-02	
9	.400E+02	-.118E+02	.105E-01	
10	.450E+02	-.121E+02	-.801E-02	
11	.500E+02	-.124E+02	.362E-02	
12	.550E+02	-.127E+02	-.102E-02	
13	.588E+02	-.129E+02	.162E-03	
				.3570359E-07

P-FITTING

M= 12 L= 2 N= 13

	X(I)	X**K*LOG(Y)	ERROR	RESID**2
1	.125E+01	-.924E+01	.258E-04	
2	.500E+01	-.931E+01	-.145E-03	
3	.100E+02	-.950E+01	.496E-03	
4	.150E+02	-.979E+01	-.108E-02	
5	.200E+02	-.102E+02	.146E-02	
6	.250E+02	-.106E+02	-.105E-02	
7	.300E+02	-.110E+02	-.367E-04	
8	.350E+02	-.113E+02	.980E-03	
9	.400E+02	-.117E+02	-.115E-02	
10	.450E+02	-.120E+02	.730E-03	
11	.500E+02	-.124E+02	-.301E-03	
12	.550E+02	-.127E+02	.561E-04	
13	.588E+02	-.129E+02	-.354E-04	
				.7582590E-09

Table(Ⅶ-4) Example of DIAC Output(8)

	X(I)	X**K*LOG(Y)	ERROR	RESID**2
1	.125E+01	-.760E+01	.232E-05	
2	.500E+01	-.769E+01	.270E-04	
3	.100E+02	-.790E+01	-.273E-03	
4	.150E+02	-.821E+01	.103E-02	
5	.200E+02	-.857E+01	-.223E-02	
6	.250E+02	-.897E+01	.311E-02	
7	.300E+02	-.936E+01	-.291E-02	
8	.350E+02	-.975E+01	.184E-02	
9	.400E+02	-.101E+02	-.766E-03	
10	.450E+02	-.105E+02	.210E-03	
11	.488E+02	-.107E+02	-.341E-04	
				.2827319E-08

P-FITTING

M= 10 L= 2 N= 11

	X(I)	X**K*LOG(Y)	ERROR	RESID**2
1	.125E+01	-.769E+01	-.168E-05	
2	.500E+01	-.776E+01	.395E-04	
3	.100E+02	-.794E+01	-.273E-03	
4	.150E+02	-.822E+01	.937E-03	
5	.200E+02	-.857E+01	-.194E-02	
6	.250E+02	-.895E+01	.263E-02	
7	.300E+02	-.933E+01	-.242E-02	
8	.350E+02	-.972E+01	.151E-02	
9	.400E+02	-.101E+02	-.625E-03	
10	.450E+02	-.104E+02	.170E-03	
11	.488E+02	-.107E+02	-.268E-04	
				.2020598E-08

P-FITTING

M= 10 L= 3 N= 11

	X(I)	X**K*LOG(Y)	ERROR	RESID**2
1	.125E+01	-.790E+01	-.957E-05	
2	.500E+01	-.794E+01	.718E-04	
3	.100E+02	-.807E+01	-.334E-03	
4	.150E+02	-.828E+01	.965E-03	
5	.200E+02	-.856E+01	-.181E-02	
6	.250E+02	-.890E+01	.232E-02	
7	.300E+02	-.927E+01	-.204E-02	
8	.350E+02	-.964E+01	.123E-02	
9	.400E+02	-.100E+02	-.499E-03	
10	.450E+02	-.104E+02	.133E-03	
11	.488E+02	-.106E+02	-.207E-04	
				.1566137E-08

P-FITTING

M= 10 L= 4 N= 11

Table (VII-4) Example of DIAC Output (9)

P-FITTING

M= 5 L= 1 N= 6

	X(I)	X**K*LOG(Y)	ERROR	RESID**2
1	.125E+01	-.101E+02	-.465E+00	
2	.500E+01	-.102E+02	.170E+01	
3	.100E+02	-.103E+02	-.291E+01	
4	.150E+02	-.107E+02	.300E+01	
5	.200E+02	-.113E+02	-.167E+01	
6	.238E+02	-.127E+02	.468E+00	
				.2352807E-02

P-FITTING

M= 5 L= 2 N= 6

	X(I)	X**K*LOG(Y)	ERROR	RESID**2
1	.125E+01	-.101E+02	-.465E+00	
2	.500E+01	-.102E+02	.170E+01	
3	.100E+02	-.103E+02	-.291E+01	
4	.150E+02	-.106E+02	.299E+01	
5	.200E+02	-.113E+02	-.167E+01	
6	.238E+02	-.126E+02	.467E+00	
				.2350398E-02

P-FITTING

M= 5 L= 3 N= 6

	X(I)	X**K*LOG(Y)	ERROR	RESID**2
1	.125E+01	-.101E+02	-.464E+00	
2	.500E+01	-.101E+02	.169E+01	
3	.100E+02	-.103E+02	-.290E+01	
4	.150E+02	-.106E+02	.299E+01	
5	.200E+02	-.112E+02	-.167E+01	
6	.238E+02	-.126E+02	.467E+00	
				.2343189E-02

P-FITTING

M= 5 L= 4 N= 6

	X(I)	X**K*LOG(Y)	ERROR	RESID**2
1	.125E+01	-.101E+02	-.463E+00	
2	.500E+01	-.101E+02	.169E+01	
3	.100E+02	-.102E+02	-.289E+01	
4	.150E+02	-.105E+02	.298E+01	
5	.200E+02	-.111E+02	-.166E+01	

Table(VII-4) Example of DIAC Output (O)

	X(I)	X**K*LOG(Y)	ERROR	RESID**2
1	.125E+01	-.114E+02	.577E-04	
2	.500E+01	-.115E+02	-.322E-03	
3	.100E+02	-.116E+02	.137E-02	
4	.150E+02	-.117E+02	-.413E-02	
5	.200E+02	-.118E+02	.782E-02	
6	.250E+02	-.119E+02	-.831E-02	
7	.300E+02	-.121E+02	.242E-02	
8	.350E+02	-.122E+02	.606E-02	
9	.400E+02	-.123E+02	-.991E-02	
10	.450E+02	-.124E+02	.758E-02	
11	.500E+02	-.126E+02	-.340E-02	
12	.550E+02	-.127E+02	.969E-03	
13	.588E+02	-.128E+02	-.135E-03	
				.3600592E-07

P-FITTING

M= 12 L= 2 N= 13

	X(I)	X**K*LOG(Y)	ERROR	RESID**2
1	.125E+01	-.115E+02	-.174E-03	
2	.500E+01	-.115E+02	.102E-02	
3	.100E+02	-.116E+02	-.397E-02	
4	.150E+02	-.117E+02	.103E-01	
5	.200E+02	-.118E+02	-.170E-01	
6	.250E+02	-.119E+02	.164E-01	
7	.300E+02	-.120E+02	-.493E-02	
8	.350E+02	-.122E+02	-.938E-02	
9	.400E+02	-.123E+02	.152E-01	
10	.450E+02	-.124E+02	-.113E-01	
11	.500E+02	-.125E+02	.496E-02	
12	.550E+02	-.127E+02	-.133E-02	
13	.588E+02	-.128E+02	.254E-03	
				.1179838E-06

P-FITTING

M= 12 L= 3 N= 13

	X(I)	X**K*LOG(Y)	ERROR	RESID**2
1	.125E+01	-.116E+02	-.405E-03	
2	.500E+01	-.116E+02	.214E-02	
3	.100E+02	-.116E+02	-.934E-02	
4	.150E+02	-.117E+02	.300E-01	
5	.200E+02	-.118E+02	-.593E-01	
6	.250E+02	-.119E+02	.633E-01	
7	.300E+02	-.120E+02	-.128E-01	
8	.350E+02	-.121E+02	-.605E-01	
9	.400E+02	-.123E+02	.931E-01	
10	.450E+02	-.124E+02	-.703E-01	
11	.500E+02	-.125E+02	.317E-01	
12	.550E+02	-.126E+02	-.878E-02	
13	.588E+02	-.127E+02	.155E-02	

Table(VII-4) Example of DIAC Output (II)

	X(I)	X**K*LOG(Y)	ERROR	RESID**2
1	.125E+01	-.128E+02	-.425E-04	
2	.500E+01	-.128E+02	.255E-03	
3	.100E+02	-.127E+02	-.952E-03	
4	.150E+02	-.127E+02	.222E-02	
5	.200E+02	-.126E+02	-.307E-02	
6	.250E+02	-.126E+02	.192E-02	
7	.300E+02	-.125E+02	.124E-02	
8	.350E+02	-.124E+02	-.404E-02	
9	.400E+02	-.123E+02	.439E-02	
10	.450E+02	-.123E+02	-.280E-02	
11	.500E+02	-.122E+02	.113E-02	
12	.550E+02	-.121E+02	-.289E-03	
13	.588E+02	-.120E+02	.377E-04	
				.6532871E-08

P-FITTING

M= 4 L= 1 N= 5

	X(I)	X**K*LOG(Y)	ERROR	RESID**2
1	.125E+01	-.129E+02	.390E+00	
2	.500E+01	-.125E+02	-.119E+01	
3	.100E+02	-.123E+02	.162E+01	
4	.150E+02	-.122E+02	-.119E+01	
5	.187E+02	-.122E+02	.390E+00	
				.5732252E-03

P-FITTING

M= 4 L= 2 N= 5

	X(I)	X**K*LOG(Y)	ERROR	RESID**2
1	.125E+01	-.125E+02	.232E+00	
2	.500E+01	-.122E+02	-.706E+00	
3	.100E+02	-.121E+02	.959E+00	
4	.150E+02	-.120E+02	-.706E+00	
5	.187E+02	-.120E+02	.232E+00	
				.2021633E-03

P-FITTING

M= 4 L= 3 N= 5

	X(I)	X**K*LOG(Y)	ERROR	RESID**2
1	.125E+01	-.123E+02	.169E+00	
2	.500E+01	-.121E+02	-.517E+00	
3	.100E+02	-.120E+02	.701E+00	
4	.150E+02	-.120E+02	-.517E+00	
5	.187E+02	-.119E+02	.169E+00	
				.1081745E-03

P-FITTING

Table (VII-4) Example of DIAC Output (12)

ITERATION PARAMETERS FOR GROUP 1

RESIDUAL	LAMBDA	OMEGA	DIFF	PRODIF	THE PROPORTIONAL DIFFERENCE CRITERION IS SATISFIED AS FAR AS MESH LINE.....		
.1824390E+17	.3816810E+00	1.500000000	.1637367E+16	.9958554E+00	0	0	0
.9093266E+16	.4984277E+00	1.500000000	.3649363E+15	.7872491E+00	0	0	0
.5785027E+16	.6361440E+00	1.500000000	.2919330E+15	.7203373E+00	0	0	0
.3196195E+16	.5524944E+00	1.500000000	.1672903E+15	.6336648E+00	0	0	0
.2509962E+16	.7852782E+00	1.500000000	.1815062E+15	.5331325E+00	0	0	0
.1556278E+16	.6200553E+00	1.546781178	.4883282E+14	.4322495E+00	0	0	0
.1018128E+16	.6542070E+00	1.546781178	.1669177E+14	.3398014E+00	0	0	0
.6415736E+15	.6301502E+00	1.546781178	.1620144E+14	.2488395E+00	0	0	0
.3999100E+15	.5609802E+00	1.546781178	.5687634E+13	.1679761E+00	0	0	0
.2168054E+15	.6023877E+00	1.546781178	.3712971E+13	.1034504E+00	0	0	0
.1231536E+15	.5688376E+00	1.548991140	.2067030E+13	.5858732E-01	31	0	0
.7023644E+14	.5703320E+00	1.548991140	.1503074E+13	.3158435E-01	31	0	0
.3437849E+14	.4994541E+00	1.548991140	.6087220E+12	.1648307E-01	31	0	0
.1946840E+14	.5662966E+00	1.548991140	.3150507E+12	.7958058E-02	31	31	0
.1131348E+14	.5811199E+00	1.548991140	.1657544E+12	.3340814E-02	31	31	0
.6266781E+13	.5538865E+00	1.549756167	.8803896E+11	.1330692E-02	31	31	0
.3728265E+13	.5949630E+00	1.549756167	.4840635E+11	.6806722E-03	31	31	31

Table (VII-4) Example of DIAC Output (13)

FLUXES IN GROUP 1 FOR COLUMNS 1 TO 10

	Z / R	0.00	5.00	10.00	15.00	20.00	25.00	30.00	35.00	40.00	45.00
1	0.00	.889E+16	.841E+16	.678E+16	.338E+16	.213E+16	.137E+16	.907E+15	.610E+15	.417E+15	.290E+15
2	5.00	.874E+16	.827E+16	.668E+16	.331E+16	.208E+16	.134E+16	.888E+15	.598E+15	.410E+15	.285E+15
3	10.00	.819E+16	.777E+16	.630E+16	.311E+16	.194E+16	.125E+16	.832E+15	.563E+15	.388E+15	.272E+15
4	15.00	.680E+16	.647E+16	.533E+16	.269E+16	.168E+16	.110E+16	.741E+15	.508E+15	.354E+15	.251E+15
5	20.00	.349E+16	.334E+16	.284E+16	.195E+16	.132E+16	.907E+15	.628E+15	.440E+15	.311E+15	.224E+15
6	25.00	.215E+16	.205E+16	.177E+16	.135E+16	.987E+15	.711E+15	.510E+15	.367E+15	.265E+15	.194E+15
7	30.00	.135E+16	.129E+16	.114E+16	.926E+15	.716E+15	.539E+15	.401E+15	.297E+15	.219E+15	.163E+15
8	35.00	.867E+15	.837E+15	.754E+15	.636E+15	.513E+15	.401E+15	.308E+15	.234E+15	.177E+15	.134E+15
9	40.00	.569E+15	.553E+15	.506E+15	.439E+15	.366E+15	.295E+15	.233E+15	.182E+15	.141E+15	.109E+15
10	45.00	.381E+15	.371E+15	.344E+15	.305E+15	.260E+15	.216E+15	.175E+15	.139E+15	.110E+15	.864E+14
11	50.00	.258E+15	.253E+15	.237E+15	.213E+15	.186E+15	.157E+15	.130E+15	.106E+15	.850E+14	.678E+14
12	55.00	.177E+15	.174E+15	.164E+15	.150E+15	.133E+15	.114E+15	.962E+14	.796E+14	.651E+14	.527E+14
13	60.00	.123E+15	.121E+15	.115E+15	.106E+15	.950E+14	.830E+14	.710E+14	.597E+14	.495E+14	.406E+14
14	65.00	.861E+14	.849E+14	.811E+14	.754E+14	.683E+14	.604E+14	.523E+14	.446E+14	.375E+14	.311E+14
15	70.00	.608E+14	.600E+14	.576E+14	.539E+14	.492E+14	.440E+14	.386E+14	.333E+14	.283E+14	.238E+14
16	75.00	.432E+14	.427E+14	.412E+14	.387E+14	.357E+14	.322E+14	.285E+14	.248E+14	.214E+14	.182E+14
17	80.00	.310E+14	.307E+14	.297E+14	.281E+14	.260E+14	.236E+14	.211E+14	.186E+14	.161E+14	.138E+14
18	85.00	.225E+14	.223E+14	.216E+14	.205E+14	.191E+14	.175E+14	.158E+14	.140E+14	.122E+14	.106E+14
19	90.00	.166E+14	.164E+14	.160E+14	.152E+14	.142E+14	.131E+14	.119E+14	.106E+14	.935E+13	.815E+13
20	95.00	.125E+14	.124E+14	.121E+14	.116E+14	.109E+14	.100E+14	.914E+13	.821E+13	.727E+13	.636E+13
21	100.00	.988E+13	.979E+13	.953E+13	.912E+13	.858E+13	.795E+13	.726E+13	.654E+13	.583E+13	.511E+13
22	105.00	0.	0.	0.	0.	0.	0.	0.	0.	0.	0.
23	110.00	0.	0.	0.	0.	0.	0.	0.	0.	0.	0.
24	115.00	0.	0.	0.	0.	0.	0.	0.	0.	0.	0.
25	120.00	0.	0.	0.	0.	0.	0.	0.	0.	0.	0.
26	125.00	.527E+13	.523E+13	.511E+13	.491E+13	.465E+13	.431E+13	.392E+13	.347E+13	.298E+13	.245E+13
27	130.00	.385E+13	.382E+13	.374E+13	.359E+13	.340E+13	.316E+13	.287E+13	.255E+13	.220E+13	.183E+13
28	135.00	.284E+13	.281E+13	.275E+13	.265E+13	.251E+13	.233E+13	.212E+13	.189E+13	.164E+13	.139E+13
29	140.00	.211E+13	.210E+13	.205E+13	.197E+13	.187E+13	.174E+13	.159E+13	.142E+13	.124E+13	.106E+13
30	145.00	.161E+13	.160E+13	.156E+13	.150E+13	.143E+13	.133E+13	.122E+13	.109E+13	.959E+12	.827E+12
31	150.00	.127E+13	.126E+13	.123E+13	.119E+13	.113E+13	.105E+13	.961E+12	.864E+12	.761E+12	.658E+12

Table (VII-4) Example of DIAC Output (14)

FLUXES IN GROUP 1 FOR COLUMNS 11 TO 20

	Z / R	50.00	55.00	60.00	65.00	70.00	75.00	80.00	85.00	90.00	95.00
1	0.00	.205E+15	.148E+15	.105E+15	0.	0.	0.	.515E+14	.404E+14	.312E+14	.245E+14
2	5.00	.203E+15	.148E+15	.113E+15	0.	0.	0.	.560E+14	.413E+14	.313E+14	.245E+14
3	10.00	.195E+15	.144E+15	.112E+15	0.	0.	0.	.563E+14	.413E+14	.310E+14	.242E+14
4	15.00	.181E+15	.135E+15	.106E+15	0.	0.	0.	.547E+14	.402E+14	.302E+14	.235E+14
5	20.00	.163E+15	.123E+15	.967E+14	0.	0.	0.	.519E+14	.383E+14	.288E+14	.225E+14
6	25.00	.143E+15	.109E+15	.860E+14	0.	0.	0.	.482E+14	.357E+14	.270E+14	.211E+14
7	30.00	.123E+15	.942E+14	.746E+14	0.	0.	0.	.438E+14	.327E+14	.248E+14	.194E+14
8	35.00	.103E+15	.796E+14	.633E+14	0.	0.	0.	.391E+14	.293E+14	.223E+14	.175E+14
9	40.00	.842E+14	.660E+14	.527E+14	0.	0.	0.	.342E+14	.257E+14	.197E+14	.155E+14
10	45.00	.679E+14	.538E+14	.431E+14	0.	0.	0.	.292E+14	.221E+14	.170E+14	.134E+14
11	50.00	.540E+14	.432E+14	.348E+14	0.	0.	0.	.241E+14	.184E+14	.143E+14	.113E+14
12	55.00	.425E+14	.342E+14	.277E+14	0.	0.	0.	.191E+14	.148E+14	.117E+14	.934E+13
13	60.00	.331E+14	.266E+14	.209E+14	.168E+14	.154E+14	.146E+14	.139E+14	.114E+14	.925E+13	.750E+13
14	65.00	.256E+14	.209E+14	.170E+14	.141E+14	.124E+14	.113E+14	.102E+14	.867E+13	.720E+13	.591E+13
15	70.00	.198E+14	.164E+14	.136E+14	.114E+14	.990E+13	.874E+13	.771E+13	.662E+13	.557E+13	.461E+13
16	75.00	.153E+14	.128E+14	.108E+14	.913E+13	.783E+13	.681E+13	.593E+13	.509E+13	.430E+13	.359E+13
17	80.00	.116E+14	.998E+13	.844E+13	.716E+13	.616E+13	.532E+13	.459E+13	.394E+13	.333E+13	.276E+13
18	85.00	.908E+13	.775E+13	.660E+13	.564E+13	.483E+13	.416E+13	.357E+13	.305E+13	.258E+13	.216E+13
19	90.00	.703E+13	.603E+13	.516E+13	.442E+13	.379E+13	.325E+13	.279E+13	.238E+13	.201E+13	.169E+13
20	95.00	.547E+13	.473E+13	.404E+13	.347E+13	.297E+13	.255E+13	.218E+13	.186E+13	.157E+13	.131E+13
21	100.00	.424E+13	.369E+13	.317E+13	.273E+13	.234E+13	.200E+13	.171E+13	.145E+13	.123E+13	.102E+13
22	105.00	.336E+13	.293E+13	.253E+13	.216E+13	.185E+13	.158E+13	.135E+13	.114E+13	.964E+12	.803E+12
23	110.00	.286E+13	.241E+13	.204E+13	.174E+13	.148E+13	.126E+13	.107E+13	.904E+12	.761E+12	.633E+12
24	115.00	.246E+13	.202E+13	.168E+13	.141E+13	.119E+13	.101E+13	.851E+12	.718E+12	.603E+12	.501E+12
25	120.00	.216E+13	.171E+13	.139E+13	.115E+13	.963E+12	.809E+12	.682E+12	.574E+12	.480E+12	.399E+12
26	125.00	.187E+13	.144E+13	.116E+13	.945E+12	.783E+12	.654E+12	.548E+12	.460E+12	.385E+12	.319E+12
27	130.00	.147E+13	.117E+13	.943E+12	.770E+12	.636E+12	.530E+12	.443E+12	.371E+12	.309E+12	.256E+12
28	135.00	.114E+13	.933E+12	.761E+12	.624E+12	.516E+12	.429E+12	.358E+12	.299E+12	.250E+12	.207E+12
29	140.00	.892E+12	.739E+12	.610E+12	.504E+12	.418E+12	.347E+12	.290E+12	.242E+12	.202E+12	.167E+12
30	145.00	.701E+12	.587E+12	.488E+12	.406E+12	.337E+12	.281E+12	.235E+12	.196E+12	.164E+12	.136E+12
31	150.00	.560E+12	.471E+12	.393E+12	.327E+12	.272E+12	.227E+12	.190E+12	.159E+12	.132E+12	.110E+12

FLUXES IN GROUP 1 FOR COLUMNS 21 TO 21

	Z / R	1J0.00
1	0.00	.201E+14
2	5.00	.200E+14
3	10.00	.198E+14
4	15.00	.193E+14
5	20.00	.184E+14
6	25.00	.173E+14
7	30.00	.159E+14
8	35.00	.143E+14
9	40.00	.127E+14
10	45.00	.110E+14
11	50.00	.928E+13
12	55.00	.765E+13
13	60.00	.614E+13
14	65.00	.484E+13
15	70.00	.378E+13
16	75.00	.293E+13
17	80.00	.227E+13
18	85.00	.176E+13
19	90.00	.137E+13
20	95.00	.107E+13
21	100.00	.837E+12
22	105.00	.657E+12
23	110.00	.518E+12
24	115.00	.410E+12
25	120.00	.327E+12
26	125.00	.261E+12
27	130.00	.210E+12
28	135.00	.169E+12
29	140.00	.137E+12
30	145.00	.111E+12
31	150.00	.898E+11

Table (VII-4) Example of DIAC Output (5)

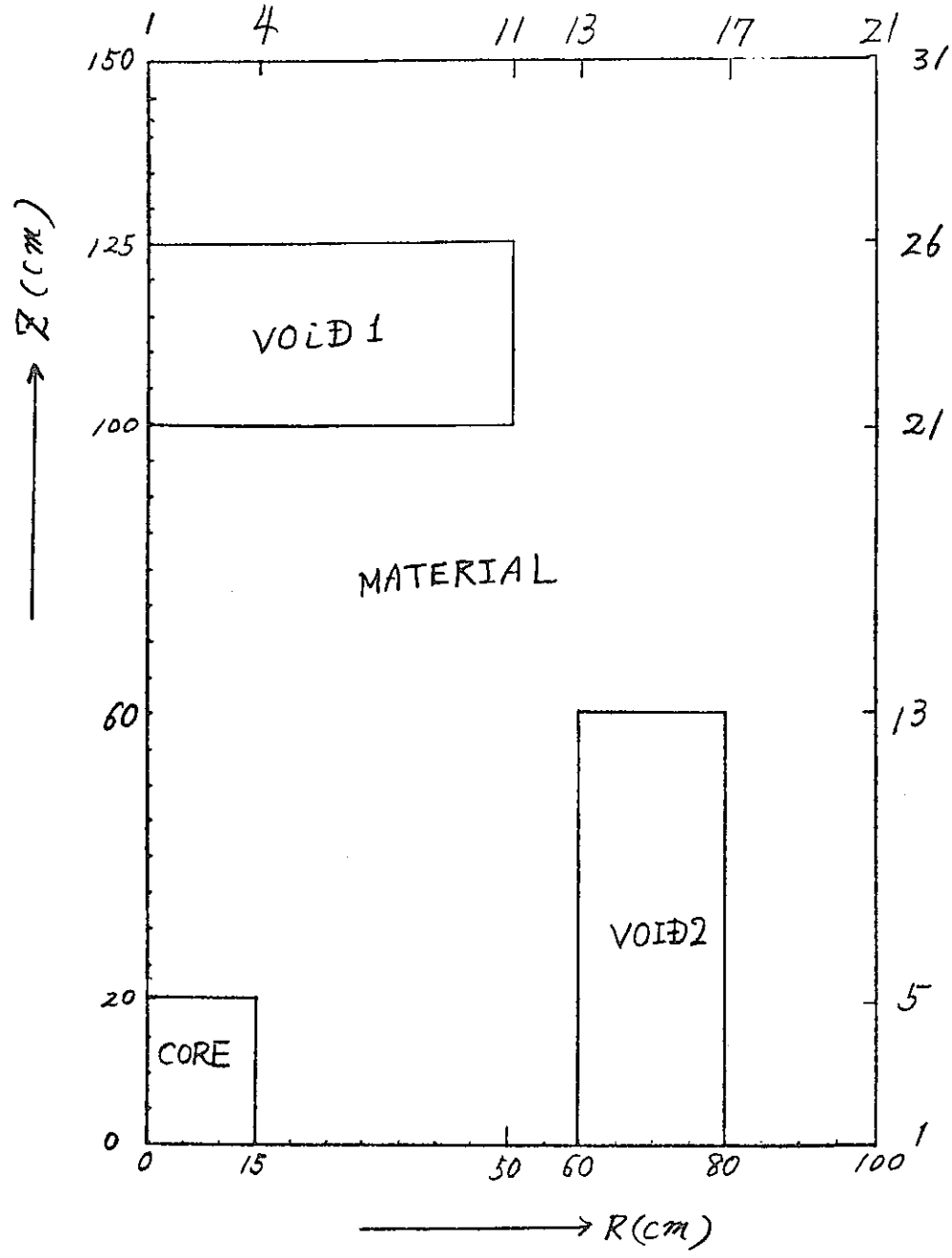

	Diffusion Constant	Absorbtion Cross-section	Slowing-Down Cross-section
CORE	3.82	0.0143	0.0153
MATERIAL	11.57	0.0344	0.0155

Fig VII-2 Geometry of DiAC Test Calculation